Shale Reservoir Simulation in Basins with High Pore Pressure and Small Differential Stress

Thesis by

Daniela Andrea Arias Ortiz

In Partial Fulfillment of the Requirements

For the Degree of

Master of Science

King Abdullah University of Science and Technology

Thuwal, Kingdom of Saudi Arabia

August, 2020

EXAMINATION COMMITTEE PAGE

The thesis of Daniela Andrea Arias Ortiz is approved by the examination committee

Committee Chairperson: Dr. Hussein Hoteit
Committee Members: Dr. Tadeusz W. Patzek, Dr. Thomas Finkbeiner,
Dr. Lukasz Klimkowski

ABSTRACT

Shale Reservoir Simulation in Basins with High Pore Pressure and Small Differential Stress

Daniela Andrea Arias Ortiz

Hydrocarbon production from mudrock ("shale") reservoirs is fundamental in the global energy supply. Extracting commercial amounts of hydrocarbons from shale plays requires a combination of horizontal well drilling, hydraulic fracturing, and multi-stage completions. This technology creates conductive hydrofractures that may interact with pre-existing natural fractures and bedding planes. Microseismic studies and field pilots have uncovered evidence of complex hydrofracture geometries that can lead to unsatisfactory wellbore flow performance.

This study examines the effects of three hydrofracture geometries ("scenarios") on wellbore production in overpressured shale oil reservoirs using a commercial reservoir simulator (CMG IMEX). The first scenario is our reference case. It comprises idealized and vertical hydrofractures. The second scenario has an orthogonal hydrofracture network made up of vertical hydrofractures with perpendicular secondary fractures. The third scenario has vertical hydrofractures with horizontal bedding plane fractures. We generated additional simulation models that aim to capture the effect on hydrocarbon production of different fracture properties, such as natural fracture orientation and spacing, number of hydrofractures per stage, number of perpendicular secondary fractures and horizontal fractures, and fracture closure mechanism. The results show that ideal planar fractures are an oversimplification of the hydrofracture geometry in anisotropic shale plays. They fail to represent the complex geometry in reservoir simulation and lead to unexpected hydrocarbon production forecasting. They also show that the generation of unpropped horizontal fractures harms hydrocarbon productivity, while perpendicular secondary fractures enhance initial reservoir

fluid production.

The generation of horizontal hydrofractures is a particular scenario that may occur in reservoirs with high pore pressure and transitional strike-slip to reverse faulting regime. These conditions have been reported in unconventional source rock plays, like the Marcellus shale in northeast Pennsylvania and southwest Virginia, and the Tuwaiq Mountain formation in the Jafurah Basin in Saudi Arabia. Our findings reveal that the presence of horizontal hydrofractures might reduce the cumulative hydrocarbon production by 20%, and the initial hydrocarbon production by 55% compared to the reference case. Our work shows unique reservoir simulations that enable us to assess the impact of different variables on wellbore production performance and understand the effects of varied hydrofracture geometries on hydrocarbon production.

ACKNOWLEDGEMENTS

I want to express my gratitude to my advisor Professor Tadeusz W. Patzek, and Ph.D. Thomas Finkbeiner, for their great support and encouragement. I was honored to work with them while pursuing my Masters degree in Energy Resources and Petroleum Engineering at KAUST University, Saudi Arabia.

I would like to thank Ph.D. Lukasz Klimkowski for his help and guidance during this time. I especially want to thank him for taking the time to discuss technical details, share his knowledge in CMG reservoir simulator, and for his advice to improve this work. I should also thank Ph.D. student Wardana Saputra for sharing his knowledge and experience in Matlab, LaTeX, and shale reservoirs.

Finally, I would like to thank my colleagues at Ali I. Al-Naimi Petroleum Engineering Research center.

TABLE OF CONTENTS

Examination Committee Page **2**

Copyright **3**

Abstract **4**

Acknowledgements **6**

Table of Contents **7**

List of Figures **9**

List of Tables **14**

1 Introduction **16**

1.1 Objectives, Motivation and Approach 18

1.2 Thesis Organization 20

2 Shale Reservoirs **22**

2.1 General Properties 23

2.2 Horizontal Wells and Multi-stage Hydraulic Fracturing 25

2.2.1 Fracturing methods 26

2.2.2 Fracturing fluids 27

2.2.3 Proppant 29

2.3 Interactions between Hydraulic Fractures and Pre-existing Discontinuities 31

3 Hydraulic Fracture Propagation Direction **34**

3.1 Hydraulic Fracture Geometry 34

3.2 Evidence of Horizontal Hydraulic Fractures 37

3.3 Geological Parameters Affecting Hydraulic Fracture Propagation . . 38
3.4 Operational Parameters Affecting Hydraulic Fracture Propagation . 41
3.5 Proppant Transport in a Complex Fracture Network 43

4 Shale Oil Reservoir Modeling 46
4.1 Naturally Fractured Reservoir Modelling 47
4.2 Hydraulic Fracture Modeling 50

5 Application: Simulation of Shale Oil Reservoirs by Varying the Hydraulic Fracture Geometry 54
5.1 Numerical Simulation Model Description 54
5.2 Basic Numerical Simulation Case: Vertical, Planar, Symmetrical Hydraulic Fractures with Reactivated Secondary Fractures. 63
5.2.1 Comparison between the multi-stage model and the single-stage model 65
5.2.2 The effect of natural fracture network density 66
5.2.3 The effect of natural fracture orientation 70
5.2.4 Geomechanics effect in natural fractures 72
5.2.5 Geomechanics effect in hydraulic fractures 77
5.2.6 The effect of number of clusters per stage 80
5.3 Second Case: Vertical Hydraulic Fractures with Perpendicular Secondary Fractures 85
5.3.1 The geomechanics effect of secondary fractures 86
5.3.2 The effect of the number of perpendicular secondary fractures 88
5.4 Third Case: Vertical Hydraulic Fractures with Horizontal Bedding Plane Fractures. 91
5.4.1 The effect of bedding plane fracture closure 93
5.4.2 The effect of horizontal bedding plane fracture position 95
5.4.3 The effect of number of horizontal bedding plane fractures 98
5.4.4 The effect of loss in vertical hydraulic fracture conductivity 101

6 Discussion 104

7 Conclusions 112

References 116

Appendices 131

LIST OF FIGURES

2.1 Shale oil and shale gas resources worldwide. This map was taken from the U.S. Energy Information Administration (EIA)'s report of 2014. The map has significant omissions, including Saudi Arabia shale resources, which at that time were prospectives. 22
2.2 Idealized sketch of the horizontal wellbore along with multi-stage hydraulic fracturing (Cross-view along the wellbore). The vertical hydraulic fractures (red lines) are shown within the target zone, but they may grow out of the zone. 26
2.3 Fracturing fluid design. 28
2.4 Schematic diagram of hydraulic fractures and natural fractures interaction when using slick water fracturing fluid. 28
2.5 Schematic diagram of hydraulic fractures generated during the injection of cross-linked gel fluid. 29
2.6 Different proppant types. (a) White sand, (b) Resin-coated sand, and (c) Ceramic proppant. 31
2.7 Sketch of hydraulic fracture interaction with discontinuities such as natural fractures and bedding planes. 32

3.1 Diagram illustrating the complex hydraulic fracture geometry. 34
3.2 Diagram illustrating a primary hydraulic fracture with four bedding plane fractures. 36
3.3 Sketch of proppant distribution in a vertical hydraulic fracture. 45

4.1 Idealized naturally fractured system. 46
4.2 Schematic figure of the connectivity between fractures and matrix blocks for the dual-porosity model. 48
4.3 Schematic figure of the connectivity between fractures and matrix blocks for the dual-permeability model. 48
4.4 Multiple-interacting continua (MINC) nested rings division. 49

4.5 Schematic figure of the connectivity between fractures and matrix blocks for the MINC model. 49
4.6 Comparison between the gridding used in the MINC model and the LS-LR-DK model (map view). 52
4.7 Diagram of a planar hydraulic fracture in the simulation model. . . . 53

5.1 Reservoir model (CMG-IMEX). 54
5.2 Comparison between the multi-stage model (including 22 stages) and the single-stage model. 55
5.3 Water-Oil relative permeability curves. (a) Rock matrix relative permeability curves: solid curves represent the target zone and dashed curves the upper and lower zone (Up&Down). (b) Fractures relative permeability curves: solid curves represent the hydraulic fractures (HF), and dashed curves represent secondary fractures (SF). 57
5.4 Schematic figure of an orthogonal natural fracture system. 59
5.5 Natural fracture network in the reservoir simulation model. 60
5.6 Hydraulic fracture system (map view). 60
5.7 Compaction curves for the propped (blue line) and the unpropped (red line) zone of the hydraulic fractures, (a) Porosity multipliers and (b) Permeability multipliers. 61
5.8 Basic numerical simulation case model (Cross-view along the wellbore). 64
5.9 Basic numerical simulation case model (map view). 64
5.10 15 years of reservoir fluid production for the single-stage simulation model and the multi-stage simulation model (22 stages). 66
5.11 Three different scenarios varying the natural fracture (NF) spacing . 67
5.12 15 years of reservoir fluid production obtained by varying the natural fracture spacing from 6m (20 ft) to 12 m (40 ft). The black curves show the production of a reservoir with no natural fractures. 68
5.13 Three different scenarios with varying natural fracture orientation. . . 70
5.14 15 years of reservoir fluid production obtained by varying the natural fracture orientation. The black curves show the production of a reservoir with no natural fractures. 72
5.15 Compaction curves applied to the natural fractures to simulate the natural fracture closure mechanism. The curves have different stress sensitivity coefficient (C_{frac}). (a) Porosity multipliers and (b) Permeability multipliers. 74

5.16 15 years of reservoir fluid production obtained by varying the compaction curves applied to the natural fractures to simulate the closure mechanism. The black curves represent the wellbore flow performance of a reservoir that lacks natural fractures. 76
5.17 On the left, a map view of three vertical hydraulic fractures with the propped region (green area) and unpropped region (red area). On the right, the compaction curves assigned to the propped region (green line) and unpropped region (red line). 77
5.18 15 years of reservoir fluid production obtained by varying the compaction tables applied to the principal hydraulic fractures. The compaction curves model the fracture closure mechanism. The black line represents the scenario that lacks compaction curves. The red line is the scenario where the unpropped and propped zone has the same closure rate. The blue line represents the scenario that assigns two compaction curves to the hydrofractures. 79
5.19 The three scenarios with a varying number of clusters per stage (Cross-view along the wellbore). 80
5.20 15 years of reservoir fluid production obtained by varying the number of clusters per stage. Each of the clusters has a fracturing fluid volume of 190 m^3 (1200 bbls). 82
5.21 Net present value (NPV) at different oil prices for three different scenarios where the number of clusters per stage varies from two to five. The net present values were calculated at: (a) 5% discount rate and (b) 10% discount rate. 84
5.22 Orthogonal fracture network. 85
5.23 Vertical hydraulic fractures with perpendicular secondary fractures. a) Cross-view of the model along the wellbore and b) map view of the model. 86
5.24 15 years of reservoir fluid production obtained by varying the compaction curves applied to the secondary fractures. The reference case only has vertical, symmetrical and planar fractures (ideal case). . . . 87
5.25 The three scenarios with varying numbers of secondary hydraulic fractures (map view).The red lines are the unpropped fractures and the green lines are the propped fractures. 88

5.26 15 years of reservoir fluid production obtained by varying the number of perpendicular secondary fractures. The reference case only has vertical, symmetrical and planar fractures (ideal case). 90
5.27 Horizontal bedding plane fractures. 91
5.28 Vertical hydraulic fractures with bedding plane fractures. a) Cross-view of the model along the wellbore and b) map view of the model. . 92
5.29 Different compaction curves applied to the bedding plane fractures to simulate fracture closure. (a) Porosity multipliers and (b) permeability multipliers. 93
5.30 15 years of reservoir fluid production obtained by varying the compaction curves assigned to the horizontal bedding plane fractures. The reference case only comprises vertical and planar hydraulic fractures. The blue curves illustrate a case with highly compressible horizontal fractures while the red lines describe a case with less compressible horizontal fractures. 94
5.31 Three different scenarios with varied bedding plane fracture positions (Cross-view along the wellbore). 96
5.32 15 years of reservoir fluid production obtained by varying the horizontal bedding plane fracture (BPF) position. All the scenarios have the horizontal fractures in the upward wing of the hydraulic fractures. The first scenario has a bedding plane fracture near the wellbore and the other one far from the wellbore (red line). The second scenario has horizontal fractures near the wellbore (green line). The last scenario has the horizontal fractures (BPF) far from the wellbore (blue line). The reference case only has vertical and planar hydraulic fractures. . 97
5.33 Three different scenarios, each consisting of a varied number of bedding plane fractures (Cross-view along the wellbore). 98
5.34 15 years of reservoir fluid production obtained by varying the number of horizontal bedding plane fractures. The reference case only has three vertical and planar hydraulic fractures. 99
5.35 15 years of reservoir fluid production obtained by varying the vertical hydraulic fracture (HF) permeability. The reference case only has three vertical and planar hydraulic fractures. 102

6.1 Map view of three hydrofracture geometries (scenarios). The first scenario is the reference case, which only has three vertical hydraulic fractures. The second scenario comprises three vertical hydraulic fractures and eight perpendicular secondary fractures. The last scenario has 3 vertical hydraulic fractures and 2 horizontal bedding plane fractures. 105

6.2 15 years of reservoir fluid production obtained by varying the hydraulic fracture geometry. The first scenario is the reference case, which only has three vertical hydraulic fractures (black line). The second scenario has three vertical hydraulic fractures and eight perpendicular secondary fractures (red line). The last scenario has three vertical hydraulic fractures and two horizontal bedding plane fractures (blue line). All the scenarios have equal vertical hydraulic fracture permeability (2000 mD). 109

6.3 15 years of reservoir fluid production obtained by varying the hydraulic fracture geometry. The first scenario is the reference case, which only has three vertical hydraulic fractures (black line). The second scenario has three vertical hydraulic fractures and eight perpendicular secondary fractures (red line). The last scenario has three vertical hydraulic fractures and two horizontal bedding plane fractures (blue line). The scenario with only vertical hydraulic fractures and the scenario with additional reactivated natural fractures have a vertical hydraulic fracture permeability of 2000 mD. The scenario with horizontal fractures has a vertical hydraulic fracture permeability reduced by 90% (200 mD). 110

LIST OF TABLES

5.1 Properties of the horizons of the reservoir simulation model. 56
5.2 PVT reservoir fluid properties. 56
5.3 Initial reservoir conditions. 58
5.4 Natural Fracture Network Properties. 59
5.5 Hydraulic fracture properties of the reference simulation case. 61
5.6 Comparison between the scenarios with high, medium and low natural fracture network (NFN) density and the scenario with no natural fractures 69
5.7 Comparison between the proposed scenarios and the case with no natural fractures. The scenarios are: the first scenario has natural fractures (NF) oriented parallel and perpendicular to the well, the second scenario has natural fractures parallel to the well, and the last scenario has natural fractures perpendicular to the wellbore. 71
5.8 Stress sensitivity coefficient values assigned to the natural fracture system. 73
5.9 Comparison between the four scenarios in which the stress sensitivity coefficient (C_{frac}) varies and the scenario with no natural fractures. . . 75
5.10 Comparison between the scenario with two compaction curves, the scenario with the same fracture closure rate and the scenario that lacks compaction curves. 78
5.11 Hydraulic fracturing treatment data. 80
5.12 Comparison between the scenario with five and two clusters against the scenario with three clusters. 81
5.13 Parameters to calculate the net present value. 83
5.14 Comparison between the scenarios with 14, 8 and 6 secondary fractures and the scenario with only vertical hydraulic fractures (reference case). 89
5.15 Comparison between the scenarios with different compaction curves and the scenario with only vertical and planar fractures (Reference case). 95

5.16 Comparison between the scenarios with three, two and one horizontal fractures and the scenario with only vertical hydraulic fractures. . . . 100
5.17 Comparison between the scenarios with varied vertical hydrofracture (HF) permeability and the scenario with only vertical hydraulic fractures. 103

6.1 Comparison between the scenarios with secondary fractures, horizontal bedding plane fractures, and the reference case (only vertical hydraulic fractures) when all the scenarios have the same vertical hydraulic fracture permeability (2000 mD). 107
6.2 Comparison between the scenarios with secondary fractures, horizontal bedding plane fractures, and the reference case (only vertical hydraulic fractures) when the scenario with horizontal bedding plane fractures considers 90% reduction in the vertical hydraulic fracture permeability. 108

Chapter 1

Introduction

Conventional reservoirs have been unable to supply the increasing global demand for energy, prompting a recent industrial shift to ultra-low permeability reservoirs such as mudrock (shale) plays [1]. The development of these reservoirs consists of a combination of multi-stage completions with hydraulic fracturing stimulation along horizontal wells that have one or two miles in length. Hydraulic fracturing generates dominant flow conduits with much higher permeability than the rock matrix, to accelerate hydrocarbon production [2].

In hydraulic fracturing design, traditional hydrofracture geometry is elliptical, vertical with symmetrical bi-wings, and propagation direction aligned to the maximum horizontal principal stress [3, 4]. However, discontinuities such as natural fractures and bedding planes alter the hydrofracture geometry in shale plays. Geological factors like the pore pressure and the present-day in-situ stress magnitudes determine the complexity of the hydraulic fracture system. Therefore, it is critical to understand the fracture initiation and propagation mechanisms before estimating the initial production and ultimate recovery factor.

Several researchers developed experimental, theoretical, and numerical models to study the factors that influence the complexity of the hydrofracture geometry in shale plays. Blanton [5, 6] showed the crossing and diversion interaction between the hydrofractures and pre-existing discontinuities in the rock. He identified the horizontal differential stress and the interaction angle as the most critical factors that control the hydrofracture propagation. Other researchers validated this finding years later through tri-axial laboratory experiments [7, 8, 9, 10]. These experiments also showed that pre-existing discontinuities could arrest hydrofracture propagation.

Experimental studies also identified operational parameters such as the fracturing fluid viscosity, pumping rate, and treating pressure as critical factors altering the hydrofracture propagation and resulting geometry [11, 10, 12, 13]. In 1994, Renshaw et al. [14] found that idealized planar fractures occur in rocks with high horizontal differential stress conditions. Additional studies [13, 9], subsequently confirmed this finding. Tan et al. [15] identified the non-planar fracture geometry in strike-slip stress conditions through tri-axial tests in Logmaxi shale cores.

Numerical simulation is also a practical method used to study hydraulic fracture geometry in shale plays. Different three-dimensional models have been developed to study natural fractures and bedding plane effects on hydrofracture propagation [16, 17, 18]. These models captured the primary physical mechanisms that determine the complexity of hydrofracture systems.

Previous findings revealed that hydraulic fracture propagation mechanisms had not been fully understood. However, experimental and theoretical studies have shown that shale reservoir properties such as rock stiffness, pore pressure, present-day in-situ stress magnitudes, and rock discontinuities are crucial parameters that determine the hydraulic fracture geometry and its complexity [13]. Additionally, the operational parameters can alter these reservoir properties and the hydraulic fracture system [13, 19, 20]. The hydrofracture complexity is likely to increase in shale reservoirs with high pore pressure and small differential stress. Microseismic studies and field pilots have uncovered evidence of complex hydrofracture geometries that includes horizontal hydrofractures generation and can lead to unsatisfactory wellbore flow performance [21, 22, 23]. At present, the studies assess the hydrofracture propagation and shape, but they do not integrate the fracture geometry into reservoir simulation analyses. Consequently, studies lack in understanding the impact of complex hydrofracture systems on reservoir fluid production.

1.1 Objectives, Motivation and Approach

The main objective of this study was to analyze the impact of different hydraulic fracture geometries on the productivity of a horizontal, multi-fractured well in shale oil reservoirs with high pore pressure and low differential effective stresses.

To accomplish this objective, we:

- studied the effects of natural fracture geometry and connectivity, such as fracture spacing, orientation, and closure;
- examined the impact of increasing the number of clusters per stage on production;
- investigated the effect of increasing the number of secondary fractures and generated horizontal bedding plane fractures on water and hydrocarbon production;
- compared the geomechanics-related causes of the different types of fractures, such as natural fractures, vertical hydraulic fractures, secondary fractures, and bedding plane fractures.

This study's motivation is the massive fracturing treatments that many operators apply to stimulate shale reservoirs and obtain economic production. In 2020, the expected mean value (P50) of fracturing fluid injected into U.S. shale plays, is about 60,600 m^3 (380,000 bbls) for the mean (P50) wellbore lengths of 2,500 m (8,000 ft) [24]. The mean proppant mass injected is 7,500 tons (15 MM lbs) [24]. Similarly, the stimulation treatments in the Jafurah Basin in Saudi Arabia require huge fracturing fluid volume and amount of proppant. The fracturing fluid volume injected per cluster is 190 m^3 (1200 bbls) combined with 40 tons (80,000 lbs) of proppant [25, 26]. Horizontal wellbores have about 30 stages, with an average of 3 clusters per stage [27, 26]. The average horizontal wellbore length in the Jafurah basin is about 1500 m (5,000 ft) [26, 28]. From the published data, we can infer that the total fracturing fluid volume and mass proppant per wellbore are about 18,000 m^3 (113,000 bbls) and 3,600 tons (7.2 MM lbs), respectively. The large volume of fracturing fluid indicates a significant fluid leak-off into the discontinuities and the formation of complex hydraulic fracture geometries.

In this study, we propose three hydraulic fracture geometries (”scenarios”) found in naturally fractured reservoirs. We assess these fracture geometries and examine their effect on wellbore flow performance using a commercial reservoir simulator (CMG IMEX). The first scenario is our reference case. It includes only vertical, ideal hydraulic fractures. The second scenario has the same vertical hydrofractures, but with additional hydraulically stimulated natural fractures. The third scenario has vertical hydrofractures and horizontal bedding plane fractures. This last scenario is a distinct case that may occur in shale plays with high pore pressure and small differential stress. Such conditions often exist in transitional strike-slip to reverse faulting environments that have been reported in some shale plays, such as Marcellus shale in southern West Virginia and the Tuwaiq Mountain formation in the Jafurah Basin (Saudi Arabia) [21, 29, 30]. Our findings show that the presence of horizontal bedding plane fractures harms hydrocarbon production. These fractures might decrease the initial hydrocarbon production by about 55%, and the cumulative hydrocarbon production by 20%, compared to the reference case.

This research is a parametric investigation that assumes idealized natural fracture networks and hydraulic fracture systems. Despite this, it presents unique reservoir simulations that enable us to understand the impact of hydraulic fracture geometry on hydrocarbon production. We conclude that the planar, bi-wing fracture shape is an oversimplification of the hydrofracture geometry in shale plays. They fail to represent the complex geometry in reservoir simulation and lead to unexpected initial hydrocarbon production and ultimate oil recovery. Shale oil reservoir simulation that uses a more realistic hydraulic fracture geometry yields more reliable hydrocarbon production forecasting results.

1.2 Thesis Organization

The thesis is composed of five chapters. Chapter 2 introduces the general properties of shale reservoirs and the parameters required to describe hydraulic fracturing design. This chapter also discusses the interactions between primary hydraulic fractures and pre-existing reservoir discontinuities.

In Chapter 3, we examine the hydraulic fracture propagation, and geometry in shale plays at different stress conditions. This chapter comprises a summary of the hydraulic fracture geometries reported in the literature. It also presents evidence of the development of horizontal hydraulic fractures in shale plays worldwide. We also review in detail the geological and operational parameters that affect hydraulic fracture geometry. Finally, there is a discussion of proppant transport in complex hydraulic fracture networks.

Chapter 4 summarizes the different models applied to simulate fluid storage and flow characteristics of naturally fractured reservoirs. The models discussed are the dual-porosity and dual-permeability model, the multiple interacting continua, and the discrete fracture model. This chapter also presents an overview of the methods implemented to model the hydraulic fractures generated in the reservoir matrix. There are three standard methods: Explicit Hydraulic Fracture modeling, Stimulated Reservoir Volume, and logarithmically spaced-locally refined-dual permeability (LS-LR-DK) model.

Chapter 5 shows the conceptual numerical models built and run in a commercial black oil simulator (CMG IMEX). This chapter discusses the effects of the hydraulic fracture geometries presented in Chapter 3 on the reservoir fluid production. We show the effects of high pore pressure and small differential stresses in shale oil reservoirs.

Hydraulic stimulation under such reservoir conditions may result in the generation of horizontal bedding plane fractures that harm hydrocarbon production. We propose two more fracture geometries and compare them with the scenario that includes horizontal fractures. Lastly, we present a discussion and key conclusions of the analyses performed in Chapter 5.

Chapter 2

Shale Reservoirs

Mudrock ("shale") plays are unconventional reservoir rocks that act as both source and reservoir rocks [31]. The fundamental properties of these reservoirs are the nano-Darcy permeability and the micro and mesoporosity. Therefore, hydrocarbon generation and accumulation occur under high-pore pressure, while ultra-low permeability limits the hydrocarbon migration to short-distances [32].

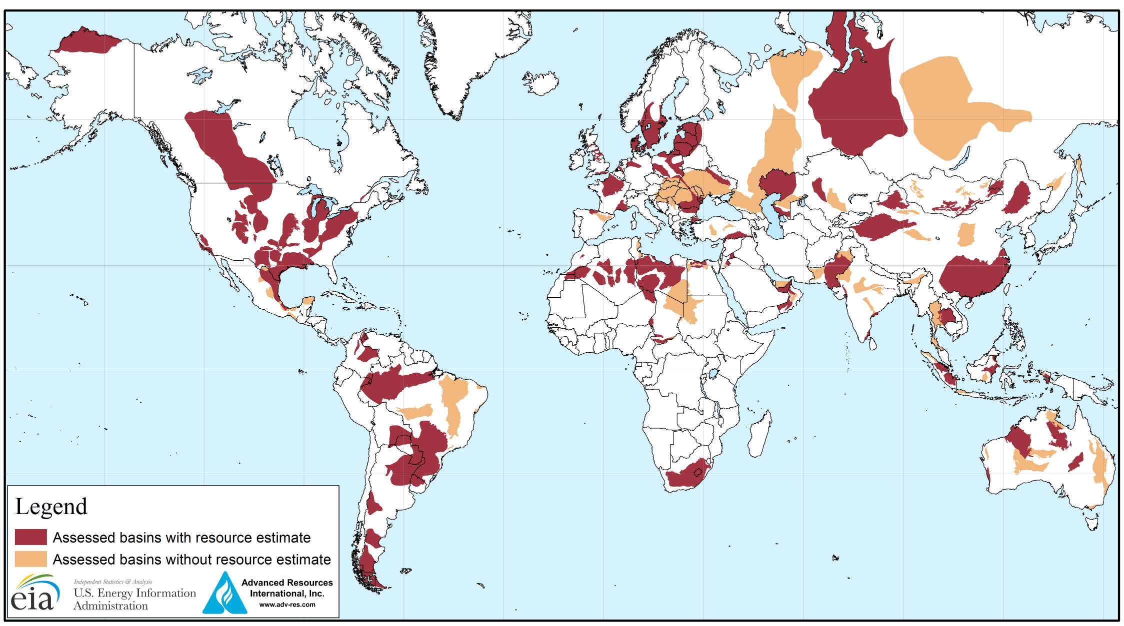

Figure 2.1: Shale oil and shale gas resources worldwide. This map was taken from the U.S. Energy Information Administration (EIA)'s report of 2014. The map has significant omissions, including Saudi Arabia shale resources, which at that time were prospectives.

Shale matrix composition is principally clay and silt-sized minerals with calcite and quartz cement, and a significant volume of organic content (more than 3% TOC). Matrix composition diverges from one shale formation to another and within the source rock itself [33]. Shale plays also comprise discontinuities such as natural fractures and laminations that are important for economic hydrocarbon production [34]. The natural fracture systems are often sealed by precipitated minerals such as calcite [35, 36]. The laminations can be organic matter, clastic, or carbonate filled [32].

These reservoirs are geologically distinct from conventional reservoirs [31]. Therefore, the use of specialized techniques such as horizontal wellbores, hydraulic fracturing, and multi-stage completions to make them profitable is necessary. [34]. The interaction between the hydraulic fractures and the discontinuities generates permeable flow conduits that accelerate the hydrocarbons production [34]. These fine-grained sedimentary rocks contribute to global oil and gas production significantly. The U.S Energy Information Administration (EIA, 2013) reported shale oil and shale gas resources in 42 countries worldwide (Figure 2.1). According to the EIA, more than 63% of U.S. oil production came from tight plays in 2019.

2.1 General Properties

Shale reservoir rocks are deposited as sedimentary layers with varying rock matrix composition, organic content, and rock fabric [37]. Major shale reservoirs in the United States share standard features such as high total organic content (TOC), clay content of less than 40%, and over 5% porosity [38]. However, they differ geologically due to their depositional environments and burial histories. The general formation properties are:

- **Matrix porosity:** The porosity of unconventional reservoirs ranges from 1 to 15 wt%. Hydrocarbons and/or water occupy the matrix porosity depending on reservoir conditions [39]. Pore size is classified into micropores (< 2 nm) and mesopores (2-50 nm) [32, 40]. Shale plays exhibit porosity within the kerogen and rock matrix. The porosity within the organic matter develops by shrinking the kerogen during the maturation process [41]. The average porosity in U.S. shale plays ranges from 5.6 to 7.4% [38].

- **Composition:** Shale reservoirs consist of particles with less than 0.062 mm grain size [32]. They comprise brittle minerals (e.g., quartz, calcite, feldspar), clay minerals, and organic matter. Most of the shale source rocks in the U.S. consist of less than 50% clay content. Marcellus, Barnett, and Eagle Ford have a dominant carbonate composition [38]. Haynesville and Barnett tend to be more siliceous. It is necessary to have more than 50% quartz or carbonate content for the shale to be potentially hydraulically fractured, and less than 40% clay content for a commercial hydrocarbon production [34].
- **Organic matter:** Kerogen content is the organic and insoluble matter which exists in the source rocks. It reveals higher porosity and permeability than the associated rock matrix [32]. The major shale oil plays in the U.S. comprise Type-II kerogen with more than 3% total organic content (TOC) [32]. In China, the kerogen is Type-I and Type-II [32].
- **Reservoir pore fluids:** The reservoir fluids are brine and hydrocarbons. The hydrocarbons are divided into three primary fluids: natural gas, condensates, and oil [39]. They vary from dry gas to oil, based on the degree of maturation and total organic matter quantity present in the rock matrix. The pressure and temperature control the occurrence of condensate in the reservoir.
- **Rock mechanical properties:** The parameters that play a fundamental role during the design of a fracturing job include Young's modulus and Poisson's ratio [34]. Young's modulus reflects the rock's rigidity, and Poisson's ratio represents the rock's elasticity [32]. Thus, a high Young's modulus and a low Poisson's ratio result in a target hydraulically fracturing region. Jiang et al. [32] proposed that a good shale reservoir should satisfy the following conditions:

Young's modulus higher than 20 GPa, Poisson's ratio value lower than 0.25, brittle mineral content of more than 40%, and less than 30% clay mineral content [32].

2.2 Horizontal Wells and Multi-stage Hydraulic Fracturing

Hydrocarbons in unconventional reservoirs are produced at economical rates using both horizontal well drilling and multi-stage hydraulic fracturing [42]. The horizontal well enhances the contact area between the well and target zone. It is a common practice to drill the wellbore in the direction of the minimum principal stress (S_{hmin}) [43]. The well is hydraulically fractured in multiple stages to create multiple fractures that transport the reservoir fluids (Figure 2.2). The hydrofractures propagate orthogonally to the least principal stress plane, and they may grow vertically out of the target zone. The expected hydraulic fracture geometry is a bi-wing vertical fracture. However, the hydrofractures may connect with pre-existing discontinuities that alter the fracture geometry.

The multi-stage hydraulic fracturing process is a stimulation method applied in horizontal wellbores to improve hydrocarbon production. During the process, operators inject fracturing fluid, proppant, and some chemicals into the rock matrix. These agents generate downhole pressures higher than the formation fracturing pressure. The fracturing fluid initiates and propagates the hydraulic fractures. The proppant supports compression stress and keeps the created flow conduits open during reservoir fluid production. This process occurs in stages along the horizontal section of the wellbore. Every stage is isolated using packers or plugs to enclose the fracturing fluid into one stage at a time. Each fracture stage contains multiple perforation clusters that supposedly initiate one fracture per cluster.

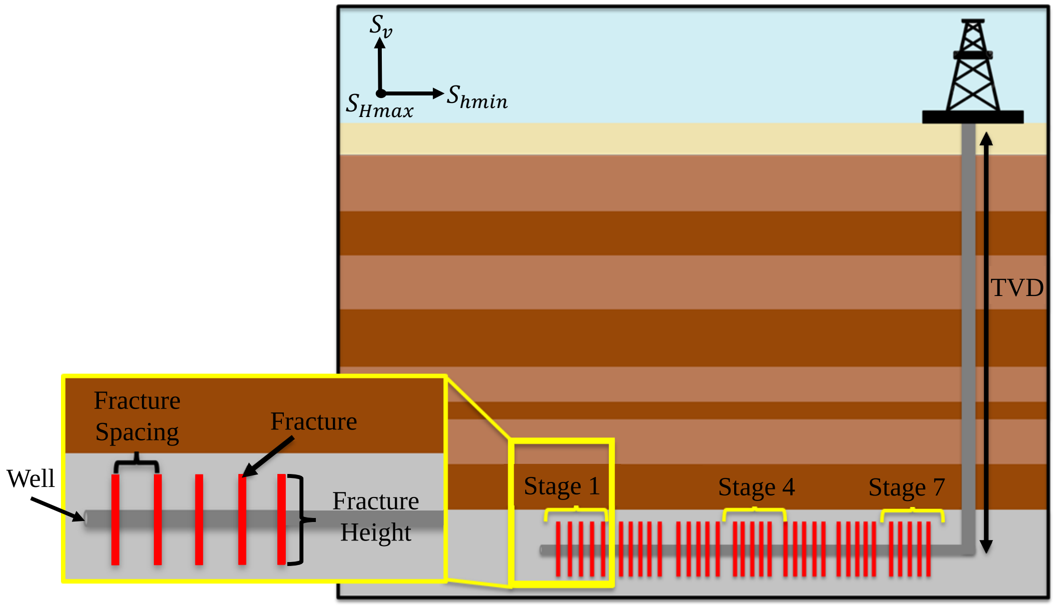

Figure 2.2: Idealized sketch of the horizontal wellbore along with multi-stage hydraulic fracturing (Cross-view along the wellbore). The vertical hydraulic fractures (red lines) are shown within the target zone, but they may grow out of the zone.

Barnett Shale was the first source rock completed using both horizontal drilling and multi-stage hydraulic fracturing [31]. Nowadays, wellbore completion includes much more hydraulic fractures spaced close to each other. Multiple hydraulic fractures, reactivated natural fractures and laminations, constitute the stimulated reservoir volume (SRV). Current treatments mostly use low-viscosity fracturing fluids (slickwater) that result in poor proppant transport.

2.2.1 Fracturing methods

The two most common types of fracturing techniques applied in the industry are:

- **Plug-and-perf:** This is the method most often used in unconventional reservoirs. The method uses perforation guns and plugs in a wireline tool [44]. The perforation guns and the plug set electrically, and create clusters at different points along the horizontal well before hydraulic fracturing [43]. The process is performed from the wellbore's toe to heel in cemented and cased wells [45].

Each stage of the process involves multiple fracture pressurization [43]. The objective is to propagate a hydraulic fracture from every perforation cluster [45]. However, the process does not initiate all the hydraulic fractures. Today's practice places each cluster 9 m (30 ft) apart to maximize the contact area [44]. After the completion of the last stage, the plugs are drilled out, and the well starts to flow back and recover the fracturing fluid.

- **Sliding sleeve:** This method consists of isolating several intervals and, subsequently, hydraulically fracturing them. The process starts from the wellbore's toe to heel. The sliding method creates one fracture per stage, which is not sufficient for the stimulation of an ultra-low permeability rock matrix [43]. However, the technique is more practical than the plug-and-perf method because it reduces stimulation cycle times [44]. This method can achieve a minimum cluster spacing of 12 m (40 ft) that is the length of the casing joint [44]. It is frequently used in shale oil reservoirs such as Bakken shale [44].

2.2.2 Fracturing fluids

Fracturing fluids generate the pressure to create and propagate the hydrofracture. They also act as a medium to transport the proppant within the fracture. There are several types of hydraulic fracture fluid systems that work according to the formation properties (Figure 2.3). This study reviews three of them.

- **Slickwater fluid:** Slickwater is a low-viscosity fluid composed of over 98% water and some chemical additives. The most common additives are surfactant polymers that reduce surface tension or friction [46]. This fluid has a limited capacity to transport proppant due to its low viscosity [31]. However, slickwater favors fracturing fluid leak-off from the hydrofractures to the reservoir discontinuities (Figure 2.4). Slickwater fluid is the most frequently used fluid in shale fracturing [47]. Operators currently apply this fluid in the United States shales, such as Marcellus and Barnett shale[46]. The key to success is to inject the fluid at high rates (70-100 bpm), connect as many pre-existing fractures as possible and reduce fluid leak-off [46]. The injection of this fluid aims to create complex fracture networks while changing to a high-viscosity fluid to create the dominant hydraulic fractures.

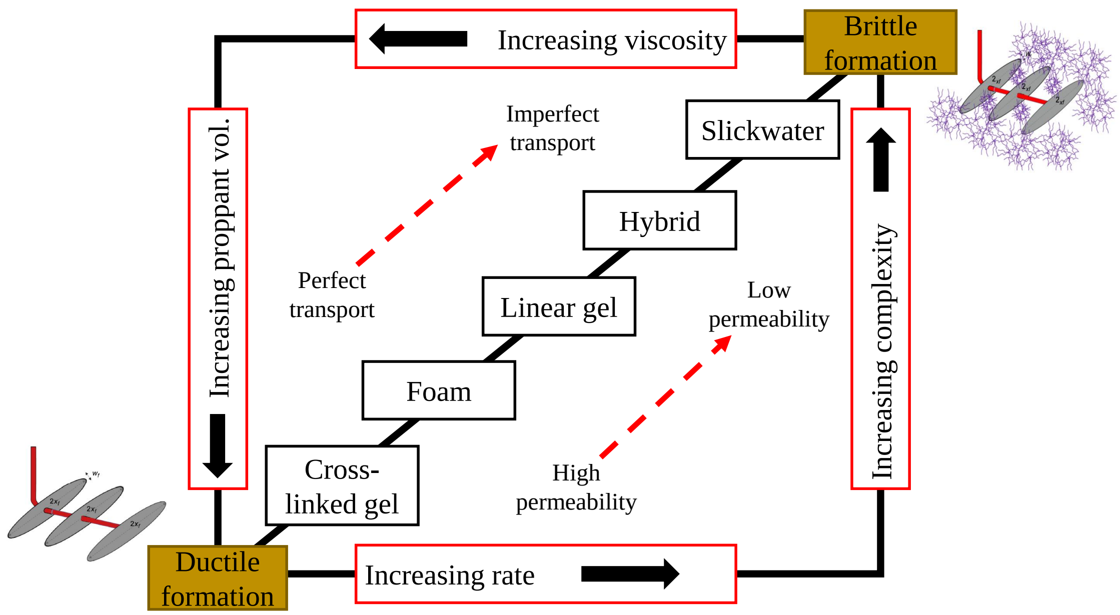

Figure 2.3: Fracturing fluid design. Modified from: [46, 48].

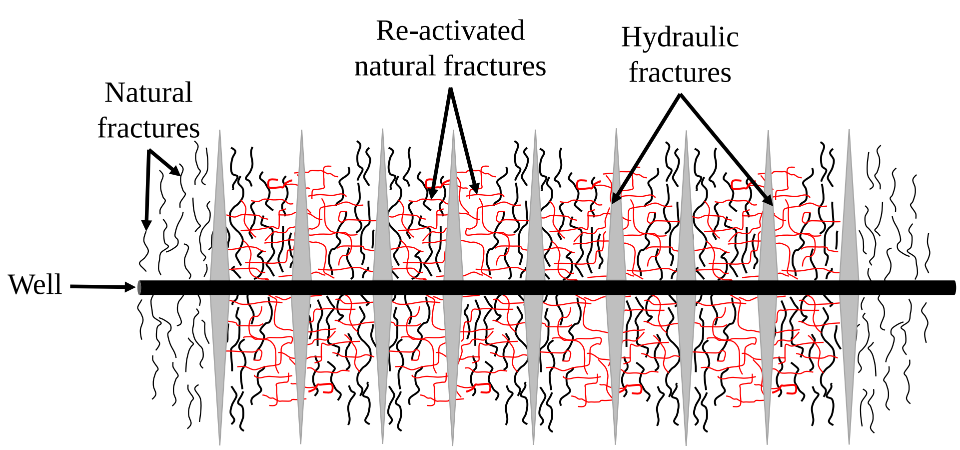

Figure 2.4: Schematic diagram of hydraulic fractures and natural fractures interaction when using slick water fracturing fluid (Map view). Modified from: [49].

- **Cross-linked gel fluid:** The injection of cross-linked gel generates dominant bi-wing hydraulic fractures (Figure 2.5) [46]. This fluid has a high capacity to transport proppant into the formation due to its high viscosity. The cross-linked gel fluid prevents fluid leak-off into the reservoir discontinuities. This fluid is applied in ductile formations with relatively high permeability, such as Bakken shale [46]. The usual pumping rate is between 25 and 70 bpm.

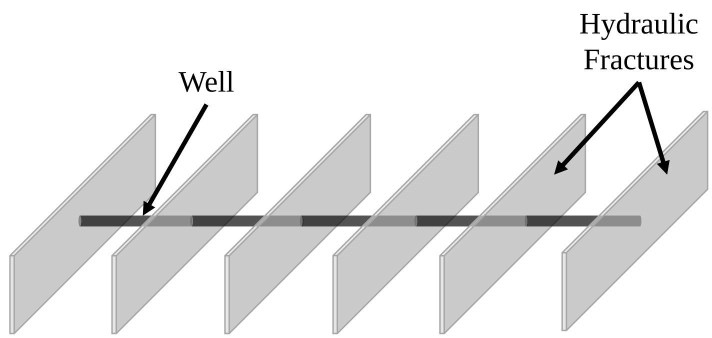

Figure 2.5: Schematic diagram of hydraulic fractures generated during the injection of cross-linked gel fluid. Modified from: [50].

- **Hybrid fluid:** The hybrid fluid system consists of slickwater injection at low proppant concentration, followed by the pumping of cross-linked gel fluid at higher proppant concentrations. This system increases the flow paths' conductivity [46].

2.2.3 Proppant

Proppant is a solid material pumped along with fracturing fluids into the rock during hydraulic fracturing jobs. The proppant prevents hydraulic fracture closure when the overburden stress increases [51]. Successful placement of proppant within the dominant hydraulic fractures may secure long-term production [52].

The proppant particle size is an important parameter during fracturing job design. Traditionally, proppant injection starts with small particle size. The operators then increase the proppant size to enhance near-wellbore conductivity [52]. The proppant particle sizes generally used in unconventional reservoirs are:

- **100 mesh:** This is the proppant with the smallest particle size. This proppant can travel within the reservoir discontinuities. The injection of the 100 mesh proppant reduces fracturing fluid leak-off through matrix cracks. This proppant creates high-resistant flow conduits because more particles fit in a fixed-volume and hold up the reservoir stresses. Operators recommend this proppant size for naturally fractured reservoirs [51].
- **40/70 mesh:** Operators pump this proppant after the injection of the 100 mesh proppant into shale plays [51]. This proppant particle size is larger than the 100 mesh proppant and creates the required fracture length [51].
- **30/50 mesh:** This mesh is larger than the 40/70 mesh. It has more conductivity than the previous size mesh. Some fracturing jobs use the100 mesh proppant followed by the 30/50 mesh proppant to enhance the conductivity near the wellbore, particularly in liquid-rich formations. This proppant does not travel a long distance into the formation because it has a high particle settling velocity [51].
- **20/30 mesh:** This is the largest proppant size. It maximizes the near-wellbore conductivity [51].

The different kinds of proppants (Figure 2.6) used during hydraulic fracturing processes are described below:

- **Sand:** This is the proppant with the lowest-strength. It is cheap and readily available in the market. Sand proppant can withstand up to 6,000 psi closure pressure [52], and it is the most typically used in the oil and gas industry [45]. There are two types of sand: Ottawa white sand, and brown sand [47].
- **Resin-coated sand:** This proppant has medium strength. It is costly compared to sand, but it has a higher conductivity [51]. This type of sand is suitable

in formations with closure pressure of between 6,000 and 8,000 psi [51]. Resin-coated sand is advantageous in that it prevents the migration of sand particles [51].

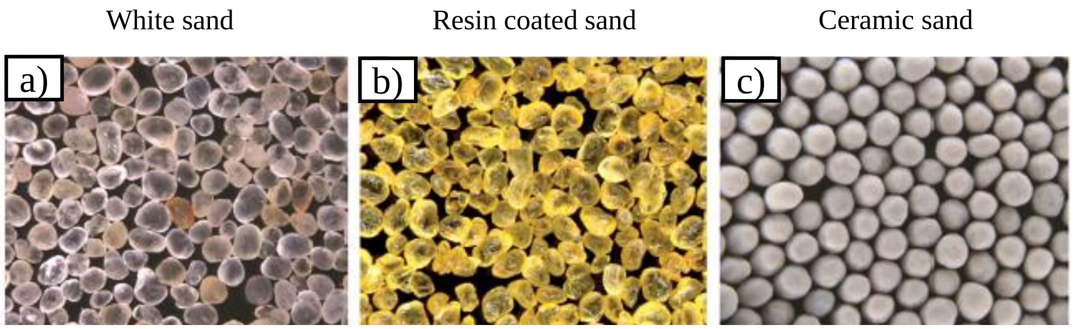

Figure 2.6: Different proppant types. (a) White sand, (b) Resin-coated sand, and (c) Ceramic proppant. Source: [45].

- **Ceramic proppant:** This is better quality than the resin-coated sand. It is thermally resistant, and it has a uniform particle size and shape [47]. There are three types of ceramic proppant: lightweight, intermediate-strength, high-strength. The lightweight ceramic proppant has a specific gravity of 2.72. It resists closure pressures between 6,000 and 10,000 psi [51]. The intermediate-strength proppant has a specific gravity of between 2.9 and 3.3. This proppant resists closure pressure ranging from 8,000 to 12,000 psi [51, 52]. Ceramic proppants form from sintered bauxite or magnesium silicate [52]. The high-strength proppant is the sintered bauxite. It can withstand closure pressures up to 20,000 psi. This proppant is applicable in deep and overpressured formations where the closure pressure is more than 10,000 psi [45, 47, 51].

2.3 Interactions between Hydraulic Fractures and Pre-existing Discontinuities

Discontinuities such as natural fractures and bedding planes play a critical role during hydraulic fracturing jobs and hydrocarbon production. The discontinuities act as planes of weakness that favor the interaction between created hydraulic fractures, pre-existing natural fractures, and laminations. The interaction causes fracturing fluid leak-off and complex fracture networks.

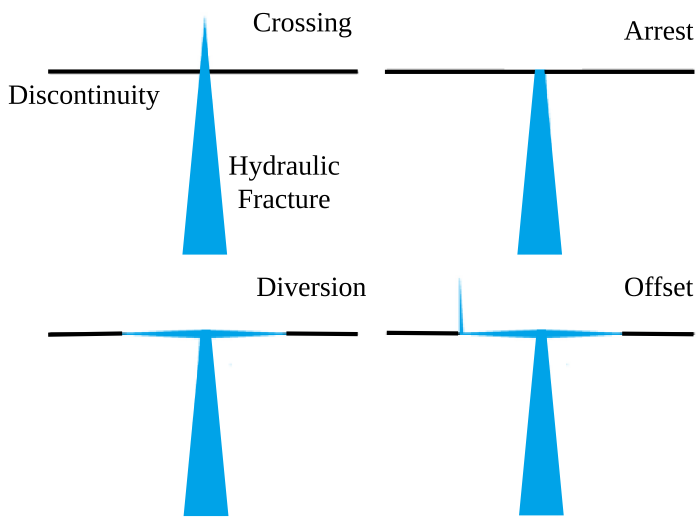

Figure 2.7: Sketch of the hydraulic fracture interaction with discontinuities such as natural fractures and bedding planes. Modified from: [53].

The intersection of the hydraulic fracture with the different discontinuities results into different interactions (Figure 2.7):

- **Crossing:** The hydraulic fracture crosses a discontinuity and propagates along its initial direction. Crossing interaction occurs when there is a high approach angle, and the stresses are lower than the compressive stress that is normal in relation to the discontinuity plane [5].
- **Diversion:** Fracturing fluid diversion occurs when the discontinuity has low-strength cement. The fracturing fluid diversion dilates the natural fracture or bedding plane by fluid pressure [54]. The fluid pressure needs to be higher than the compressive stress that is normal in relation to the discontinuity plane [53]. This study considers diversion as the interaction that generates horizontal bedding plane fractures.
- **Crossing with offset:** A hydraulic fracture diverts and crosses a discontinuity

to propagate along its original direction. These interactions occur during the reactivation of pre-existing natural fractures and generate orthogonal complex fracture networks.

- **Arrest/slippage:** Hydraulic fracture propagation stops when it approaches the pre-existing natural fracture or lamination.

Previous numerical and experimental studies analyzed the factors that affect hydraulic fracture interactions [5, 11, 55, 10, 56, 57]. These factors control whether the created primary hydraulic fracture crosses or diverges into a discontinuity, and include mechanical rock properties, discontinuity size and orientation, present-day in-situ stress anisotropy, and pore pressure [3, 2, 58, 59].

Hydraulic fracture interactions with the natural fractures or bedding planes may induce the well-known fracture growth containment effect. Some authors have proposed shear slippage as the principal mechanism that controls the vertical fracture height growth [4]. Teufel et al. [56] identified weak lamination strength, and an increase in the least horizontal stress, as geologic conditions that arrest vertical hydraulic fracture growth. According to Gudmundsson et al. [60], the factors that promote hydraulic fracture arrest are the opening of pre-existing discontinuities, changes in the stiffness of the layers, and abrupt changes in mechanical rock properties.

Chapter 3

Hydraulic Fracture Propagation Direction

3.1 Hydraulic Fracture Geometry

The most common hydraulic fracture shape is vertical, planar with symmetrical bi-wings. These fractures rarely occur in shale plays. Hydrofracture geometry is generally complex, but planarity develops in many reservoirs. The least principal stress direction controls fracture geometry. The hydraulic fracture opens against the minimum principal stress (least amount of energy).

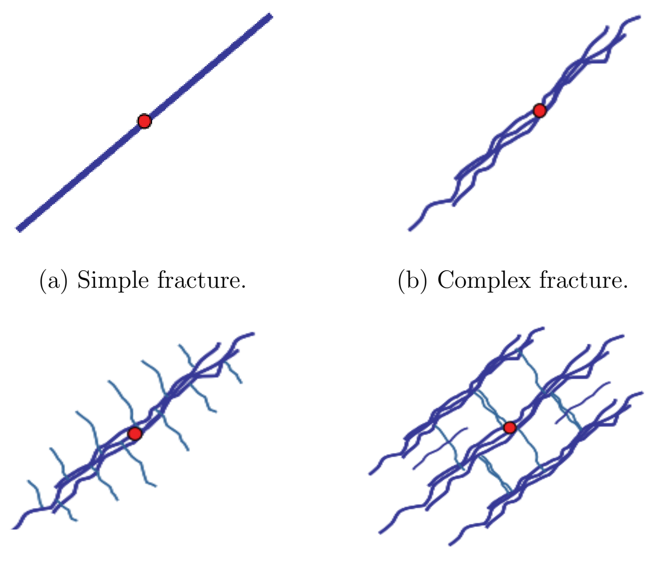

(a) Simple fracture.

(b) Complex fracture.

(c) Complex fracture with fissure opening.

(d) Complex fracture network.

Figure 3.1: Diagram illustrating the complex hydraulic fracture geometry. Source: [61].

Figure 3.1 is a diagram showing the complexity of the hydraulic fracture geometry [61]. The figure omits fracture geometries generated by the interaction between hydrofractures and discontinuities at oblique angles. The first geometry is a simple planar fracture that often occurs in homogeneous reservoirs. Figure 3.1b illustrates the fracture geometry generated when pre-existing natural fractures have the same orientation as hydraulic fractures. Fissure opening occurs due to the reactivation of pre-existing natural fractures oriented normally to the hydraulic fracture plane (Figure 3.1c). The last fracture geometry (Figure 3.1d) develops in reservoirs with orthogonal sets of natural fractures. Our study proposes different hydraulic fracture geometries that vary with the geological environment and the operational factors involved during hydraulic fracturing jobs.

- **Vertical, planar, bi-wing hydraulic fractures:** Hydraulic fractures initiate in a plane perpendicular to the wellbore and propagate symmetrically in the maximum horizontal stress direction. This geometry is likely to occur in reservoirs under normal stress faulting regime and normal pore pressure (below or equal to 10 MPa/km or 0.43 psi/ft) [39, 62]. Those reservoirs may have large vertical and horizontal stress anisotropies and discontinuities with high-strength cement. These conditions favor the crossing interaction between hydrofractures and discontinuities [62]. Our study considers this hydraulic fracture geometry as the reference scenario.
- **Vertical hydraulic fractures with reactivated natural fractures:** In this scenario, three types of interaction may occur: diversion, crossing, and arrest. Thus, the fracturing fluid diverges through pre-existing natural fractures. The primary hydraulic fractures can cross the natural fractures and propagate along their original direction. Natural fractures may act as a barrier for the hydraulic fracture height growth.

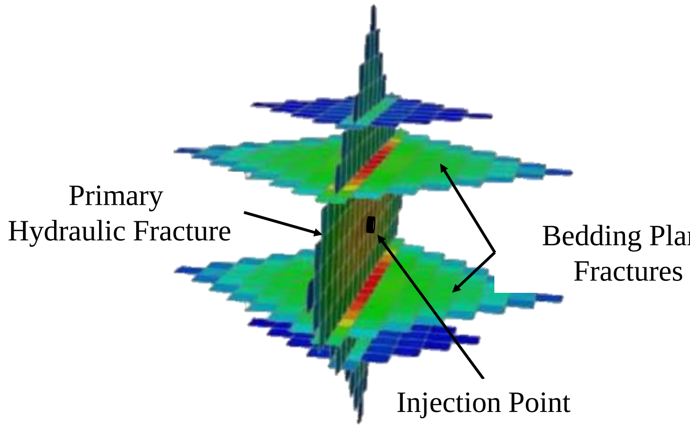

Figure 3.2: Diagram illustrating a primary hydraulic fracture with four bedding plane fractures. Source: [17].

- **Vertical hydraulic fractures with horizontal bedding planes fractures:** Hydrofractures propagate perpendicular to the wellbore. Additionally, low-strength cement favors the generation of a horizontal fracture component perpendicular to the vertical stress direction [62]. The shape of the bedding plane fractures and the vertical hydraulic fractures is an ellipse [62]. When multiple fractures generate (Figure 3.2), the horizontal fracture volume decreases as the injection point distance increases [17]. In this case, hydrofractures cross the weak bedding planes near the injection point. The last weak bedding planes arrest the hydraulic fracture height [53].
- **Vertical hydraulic fractures with bedding planes and reactivated natural fractures:** This is a more complicated scenario. The hydraulic fractures may interact with pre-existing natural fractures and weak bedding planes of the rock. The hydrofractures can cross the discontinuities with high-strength cement. Furthermore, they can also divert and propagate through the discontinuities with low-strength cement. In the case of low anisotropy and significant fracturing fluid leak-off, the hydraulic fracture growth may be stopped or slowed down [63, 64].

3.2 Evidence of Horizontal Hydraulic Fractures

Hydraulic fractures are created as the result of a stimulation pressure that exerts tensile stress higher than the tensile strength and fracture toughness of the stimulated formation. These fractures grow perpendicular to the minimum principal stress direction. Previous studied relied on vertical plane fracture propagation. They do not evaluate the possibility of horizontal fracture propagation in reservoirs with small differential stress conditions. However, recent studies have exhibited evidence of horizontal fracture generation in different shale plays around the world.

Celleri et al. [22] uncovered evidence of the creation of horizontal hydrofractures in Argentinan shales with a strike-slip stress environment. They observed that the well's performance is sensitive to the contrast between the overburden and the minimum horizontal stress. The wells drilled in zones with low-stress contrast (about 3%) had lower hydrocarbon recovery factors than wells drilled in regions with high-stress contrast (about 10%). In 2019, Nicholson et al. [23] presented evidence of horizontal fracture generation in the west Duvernay shale basin in Canada. They studied fluid leak-off and closure fracture behavior through Diagnostic Fracture Injection Test (DFIT) analysis.

Results from microseismic studies and field pilots of the Marcellus shale in southwest Virginia show that 14 out of 31 fracture stages revealed the generation of horizontal hydrofractures [21]. The analyzed area has a transitional strike-slip to reverse faulting stress environment. Horizontal fractures occurred in an organic-rich (TOC 6-8%) layer with similar vertical and minimum horizontal stress magnitudes [21].

Horizontal hydrofractures also occurred in the western Sichuan basin (China). The hydraulic fracture geometry was -T and -I shape [65]. Additionally, studies of signature in radioactive tracing, spectra gamma-ray logs, and fracturing pressure behavior revealed fracture height containment. The results uncovered the probability of creating near-horizontal or bedding-plane fractures in this basin [4].

Finally, microseismic events from a hydraulic fracture stimulation exhibited fracture reorientation in a thrust fault in Western Canada [66]. A horizontal fracture formed in the lower part of the fault. In contrast, a vertical hydrofracture grew at the top of the fault. The study associated fracture geometry variations with the rotation of the minimum principal stress direction.

3.3 Geological Parameters Affecting Hydraulic Fracture Propagation

Hydraulic fracture networks are important to maximize production in shale plays. The primary hydraulic fractures must connect with pre-existing natural fractures or bedding planes to create a hydraulic fracture system [2]. Several geological parameters influence the formation of hydraulic fracture networks and their associated geometry. Parameters include rock mineral composition, rock mechanical properties, natural fractures (orientation, size, and distribution), bedding plane cement strength, pore pressure, and stress anisotropy [3, 2, 58, 59]. This study analyzes the last four geological parameters that affect hydraulic fracture geometry.

1. **Formation discontinuities: Natural fractures and bedding planes**
   Discontinuities in shale plays contribute to the fracturing fluid leak-off and affect the hydraulic fracture geometry [67]. The main factors that affect the primary fracture geometry are the orientation of the discontinuities, cement strength, and the interaction angle between hydrofractures and discontinuities [5, 7, 68, 69, 2, 15].
   The interaction angle varies from 0 to 180 degrees. Interaction angles below 45 degrees and low-strength cement favor the diversion of the fracturing fluid through the natural fractures and bedding planes [5, 6, 7, 68, 8, 13]. However, under interaction angles higher than 45 degrees and high-strength cement,

hydrofractures may cross the pre-existing discontinuities [8, 16].

Hydrofractures often cross the pre-existing discontinuities when the interaction angle is near to 90 degrees [70]. However, low-strength cement (organic-rich laminations) favors the fracturing fluid's diversion and opening of the orthogonal natural fractures and horizontal bedding planes [53]. When discontinuities have high-strength cement, and the interaction angle is oblique, the hydraulic fractures may merge with the discontinuities. Fracturing fluid easily induces natural fractures because they commonly have a relatively low mechanical strength [71].

Hydraulic fracture height containment may occur when the fracturing fluid propagates through the discontinuities, or shear slip develops in the pre-existing discontinuities [72, 73, 7, 4, 65]. The hydraulic fracture growth limitation increases the fracture width, and the proppant concentration near-wellbore[70]. Shale plays have higher horizontal permeability than vertical permeability. Thus, fracturing fluid experience less resistance when propagation occurs through the horizontal bedding planes, rather than across them [65, 8, 53, 74, 75]. Simultaneous vertical and horizontal propagation can also occur during fracture growth. This mechanism is common in overpressured formations where the effective normal stress of the bedding plane (overburden effective stress) is low [73]. The simultaneous propagation reduces the propagation energy of the vertical fracture and decreases the fracture width and length.

2. **Present-day in-situ stress regime**

   Hydraulic fracture geometry varies according to the present-day in-situ stress regime [7, 10, 76]. However, the primary hydraulic fracture geometry also depends on the discontinuities distribution and the stress anisotropy. The standard fracture geometry reported based on the faulting stress conditions are the following:

- Normal faulting ($\sigma_{\mathrm{v}}>\sigma_{\mathrm{H}}>\sigma_{\mathrm{h}}$): Hydraulic fractures are vertical and planar with reactivated secondary fractures [7, 10, 76]. Hydrofractures propagate along the direction of the maximum horizontal stress. The fracture tip is subjected to the principal stresses (σ_{v}, σ_{H}, σ_{h}), and pore pressure [16].
- Strike-slip faulting ($\sigma_{\mathrm{H}}>\sigma_{\mathrm{v}}>\sigma_{\mathrm{h}}$): Hydraulic fracture geometry is non-planar due to the interaction between the primary hydraulic fracture and the rock matrix discontinuities [7, 10, 76].
- Reverse faulting ($\sigma_{\mathrm{H}}>\sigma_{\mathrm{h}}>\sigma_{\mathrm{v}}$): Hydraulic fracturing jobs create a complex fracture network. In this case, the dominant hydraulic fractures are horizontal [76]. The hydraulic fracture tip is subjected to principal stress σ_{H}, pore pressure, and tensile strength [16].

The hydraulic fractures a have higher width and shorter length under normal faulting stress conditions than the fractures generated in plays with reverse faulting stress conditions [76].

3. **In-situ differential stresses**

Low horizontal differential stress and low confining stress conditions (low-stress anisotropy) promote the generation of a complex fracture network [5, 7]. Thus, hydraulic fractures merge with natural fractures or bedding planes [13, 74, 15]. Numerical studies corroborate this finding for narrow and sealed natural fracture systems (natural fracture width less than 0.1 mm or 0.0003 ft) [13, 77, 59]. However, naturally fractured reservoirs with fracture widths of more than 0.1 mm (0.0003 ft) impede the generation of a complex fracture network under the same conditions[13].

High horizontal differential stress and high confining stress conditions favor the crossing interaction between hydrofractures and pre-existing discontinuities [74, 62, 78]. These conditions reduce the stimulated reservoir volume (SRV), increase the hydraulic fracture length, and create vertical and narrow hydrofractures [19, 59, 77]. It is essential to mention that treating pressures and fluid leak-off influence the vertical and horizontal stress magnitudes [16].

4. **Pore Pressure**

   High pore pressure is responsible for low differential stress in shale plays. The pore pressure acts in all directions. Therefore, it reduces all the effective stress magnitudes. The reduction in the effective stress magnitudes results in a reduction of the differential stress and convergence of the entire stress state towards the overburden.

   The overpressure develops delamination, shear failure, or overburden lift [4]. The opening and dilation of the bedding planes occur when the pore pressure exceeds the normal compressive stress applied to the lamination (overburden)[68].

3.4 Operational Parameters Affecting Hydraulic Fracture Propagation

Four main operational parameters may influence the hydraulic fracture geometry [3]:

1. **Treating pressure**

   The standard strategy to inject the fracturing fluid consists of initial low pumping rates followed by high pumping rates. This approach may not always be practical. Treating pressures lower than the overburden pressure favor fracturing fluid diversion through pre-existing discontinuities under low horizontal differential stress conditions[10]. Fracturing fluid leak-off can impede the generation of dominant hydraulic fractures at early times.

   High treating pressures increase hydraulic fracture width and prevent the reactivation of discontinuities under low differential stress [12, 17]. However, they may favor the creation of a complex fracture network under high differential stress. Treating pressures higher than the overburden pressure generate horizontal hydraulic fractures in shale formations [23, 4, 68].

2. **Fracturing fluid viscosity**

   Fracturing fluid viscosity impacts hydraulic fracture geometry in shale formations [19]. The higher the fluid's viscosity, the lower the complexity of the fracture network [3]. Experimental studies have shown that complex fracture networks generate close to the wellbore with the injection of low-viscosity fracturing fluid (viscosity of less than three mPa.s) [62, 19, 79, 74]. In contrast, high-viscosity fracturing fluid (viscosity of more than 50 mPa.s [13, 62]) favors the generation of vertical and planar hydrofractures [13, 74, 19, 62].

   Tan et al. [62] recommended high-viscosity fluid at the beginning of the fracturing treatment process to initiate dominant hydrofractures and prevent premature proppant screen-out. After that, slickwater (low-viscosity fluid) at high injection rates creates new fractures and connects the fracture network [12]. The injection of low-viscosity fluids at a low pumping rate may lead to total fluid leak-off into the discontinuities with no fracture initiation [12].

3. **Pumping rate**

   The pumping rate is a critical parameter for fracture system creation. High pumping rates (60-110 bpm [80]) promote the propagation of fracturing fluid through rock discontinuities under high differential stress conditions [3, 77, 81]. The higher the pumping rate, the bigger the stimulated reservoir volume (SRV), and the higher the fracture network complexity [77, 81].

   Under low differential stress, low pumping rates (less than 10 bpm [80]) enhance the activation of natural fractures and bedding planes [74, 12, 68, 15, 19]. In this case, high pumping rates reduce the fracturing fluid leak-off and generate the primary hydrofractures [62]. However, high pumping rates may generate high net pressure that opens pre-existing natural fractures or bedding planes.

4. **Fracturing treatment stimulation design**

   Barnett shale was one of the first shales to apply horizontal well drilling and hydraulic fracturing stimulation. The operator companies tried a massive treatment with high volumes of fracturing fluids injected at high pumping rates. The stimulation successfully created a complex fracture system [82]. Consequently, operators concluded that the bigger the fracturing fluid volume, the bigger the stimulated reservoir volume (SRV) [3]. However, the massive fracturing treatments may not always produce the expected hydrocarbon recovery factor. These massive treatments may only be favorable for shale plays with high differential stress conditions [71, 77].

   An increase of the fracturing fluid volume combined with an increase in the number of perforation clusters along the horizontal well reduces the hydraulic fracture spacing. Therefore, under low differential stress conditions, the short fracture spacing favors the joining of nearby fractures [71]. Thus, the fracture network in far-wellbore regions is non-uniform and weak, producing undesirable wellbore performance.

3.5 Proppant Transport in a Complex Fracture Network

Proppant injection into the rock aims to keep hydrofractures open during hydrocarbon production. Therefore, stimulation jobs require effective transport and settling of the proppant particles within the created permeable flow conduits. However, proppant transport within complex hydraulic fracture systems is not fully understood.

Several experimental and numerical studies have sought to understand proppant transport in hydraulic fracture networks [82, 79, 83, 84, 85]. The fracturing fluid flow through pre-existing discontinuities increases the fracture network complexity and reduces the fracture width. The reduction of hydrofracture width is one of the aspects that makes proppant transportation and settling difficult [86]. This difficulty may promote proppant bridging and premature screen-out [87]. Adequate proppant transportation into the hydrofractures may occur when their width is three to four times wider than the proppant particle diameter [18].

Low-viscosity fracturing fluid (Slickwater) produces poor proppant transport into the hydrofractures [88]. Based on numerical studies, this fluid settles the proppant in about 30% of the volume hydraulically opened [18]. The proppant rarely settle into pre-existing natural fractures and bedding planes [89]. In contrast, viscous fracturing fluid increases the propped area to 65% [18]. The effective proppant transport through the pre-existing discontinuities depends on several factors such as proppant concentration, proppant particle size, and pumping rate [84]. The higher the pumping rates and the proppant concentration, the better the proppant transportation within the natural fractures or bedding planes.

A 100 mesh proppant might propagate successfully through the bedding planes[79]. Based on Stoke's law, this proppant has a low settling velocity. Therefore, the proppant particles can propagate over a long distance into the laminations. Proppant transportation into the bedding planes produces proppant accumulation in the intersection between the hydrofracture and the bedding plane. The high proppant concentration in the intersection may reduce the fracture connectivity and act as a barrier to the flow [70].

Proppant embedment may occur when there is a rapid decline in hydrocarbon production. This phenomenon is harmful when a small proppant particle size is pumped into the reservoir [1]. It might reduce the hydraulic fracture width by 60% in weakly consolidated reservoirs [1]. This phenomenon does not affect the fracturing fluid flowback production, but it decreases the ultimate hydrocarbon recovery.

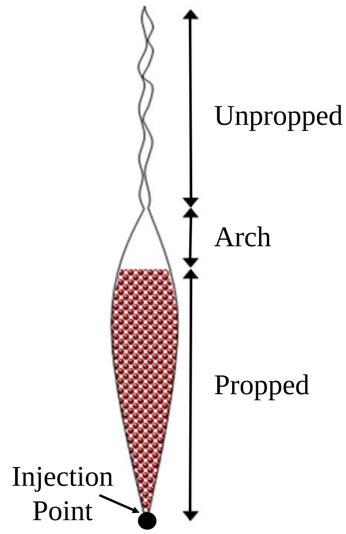

Figure 3.3: Sketch of proppant distribution in a vertical hydraulic fracture (Map view). Modified from: [86].

Experimental studies have shown that low pumping rates facilitate the entry of proppant into the bedding planes when lamination intersects the hydrofracture in the upward wing [79]. In contrast, high pumping rates favor the propagation of proppant in the lamination when the bedding plane is located in the downward wing of the hydrofracture.

Cipolla et al. [86] proposed a fracture height divided into three separate zones: propped zone, arch zone, and unpropped zone. Figure 3.3 shows that the hydraulic fracture region closer to the injection point is propped, and the fracture tip is unpropped. The propped zone remains open after pressure release, while the unpropped zone closes when the well starts to produce. The unpropped region may have a residual permeability after closure, but the low conductivity harms the hydrocarbon production.

Chapter 4

Shale Oil Reservoir Modeling

Reservoir simulation helps engineers to understand reservoir physical mechanisms and make decisions for optimal hydrocarbon recovery. The proper modeling and simulation of naturally fractured reservoirs are challenging due to the scale of heterogeneity. These reservoirs comprise a rock matrix that serves as the primary storage for hydrocarbons. They also have a set of natural fractures that acts as the main flow paths to carry reservoir fluids to hydrofractures [90]. Therefore, they are classified as double-porosity systems [91].

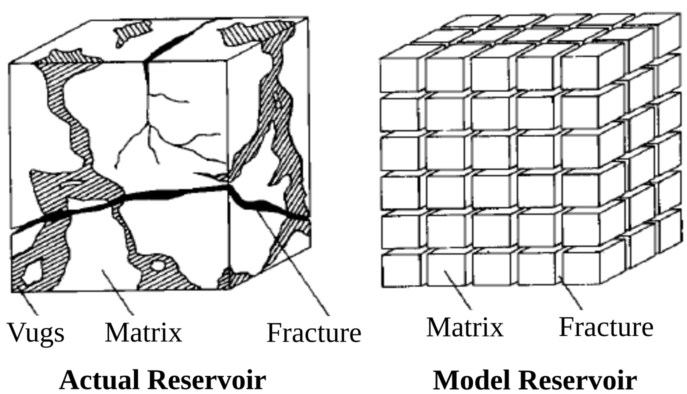

Figure 4.1: Idealized naturally fractured system. Source:[92].

The optimal way to represent the matrix-fracture system at the simulation scale is a topic of research. Despite this, some existing models can mimic the storage and flow characteristics of naturally fractured reservoirs. One of those models is the dual-permeability model, a standard and widely used approach for modeling these reservoirs [93]. We applied the dual-permeability method to model the shale oil play. We also implemented the "logarithmically spaced-locally refined-dual permeability (LS-LR-DK)" model to simulate the stimulated reservoir volume (SRV). This model is numerically efficient, and better captures the mass transfer between matrix-hydraulic fractures blocks. The following sections present detailed information about the different models.

4.1 Naturally Fractured Reservoir Modelling

1. **Dual-porosity and dual-permeability model**

   Warren et al. [92] proposed a dual-porosity and single permeability model. This model is an idealized representation of a complex and heterogeneous reservoir. The model consists of an isotropic rock matrix with primary (intergranular) and secondary porosity (Figure 4.1). The primary porosity represents the matrix's pore space that grants pore volume. The secondary porosity refers to the pre-existing fractures that contribute to flow capacity. The authors introduced the natural fractures as an orthogonal fracture system with uniform spacing [92]. The set of natural fractures can have different fracture width and spacing to increase the reservoir's anisotropy. Fluid flow occurs from the matrix to fracture blocks and between fracture blocks. The model ignores mass exchange between matrix blocks (Figure 4.2) [94]. This model does not capture transient flux between matrix-fracture blocks.

   The dual-porosity model is a scheme for many applications and further investigations. Kazemi et al. [91] were the first to incorporate this concept into a numerical model. Their research extended the concept to multiphase flow with transient communication between matrix and fractures. According to Blaskovich et al. [95], this model works successfully only in highly fractured reservoirs with ultra-low permeability.

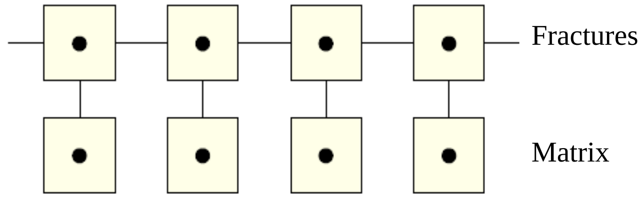

Figure 4.2: Schematic figure of the connectivity between fractures and matrix blocks for the dual-porosity model. Source:[96].

Blaskovich et al. [95] and Hill et al. [97] introduced the dual-permeability model (DK). This model added the matrix to matrix mass transfer to the dual-porosity concept (Figure 4.3) [93, 96]. The simulation model assigns the properties of the matrix in the center of the simulation block [98].

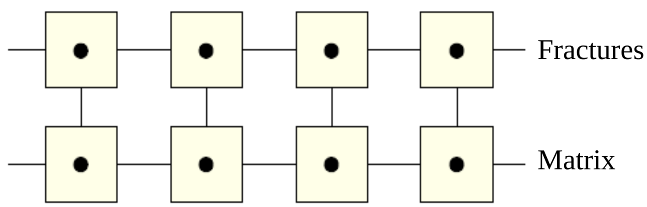

Figure 4.3: Schematic figure of the connectivity between fractures and matrix blocks for the dual-permeability model. Source:[96].

The dual-permeability approach is numerically efficient. This model captures the effect of natural fractures on fluid flow [99]. The dual-permeability model became the framework for the discrete fracture models (DFM) [98]. One of the model's limitations is that it assumes a dense interconnected natural fracture network. Furthermore, the model needs to determine transfer functions between natural fractures and the matrix for accuracy [100]. The model also fails to capture the transient flow between the matrix and the fracture blocks in low-permeability fractured shales [96].

2. **Multiple interacting continua**

The multiple interacting continua (MINC) model adopts the dual-porosity concept. This model divides the matrix blocks into nested grid blocks as visualized in Figure 4.4 [96]. The matrix blocks partitions can apply logarithmical refinement to better capture the pressure drop in those blocks [93].

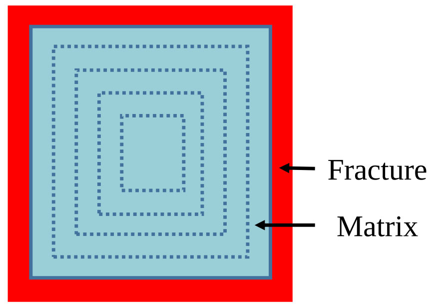

Figure 4.4: Multiple-interacting continua (MINC) nested rings division. Based on [96].

This model captures the transient flow between the fracture and the matrix blocks. The mass (heat) transfer occurs from the matrix to the fracture, fracture to fracture, and between the matrix-nested grid blocks as displayed in Figure 4.5.

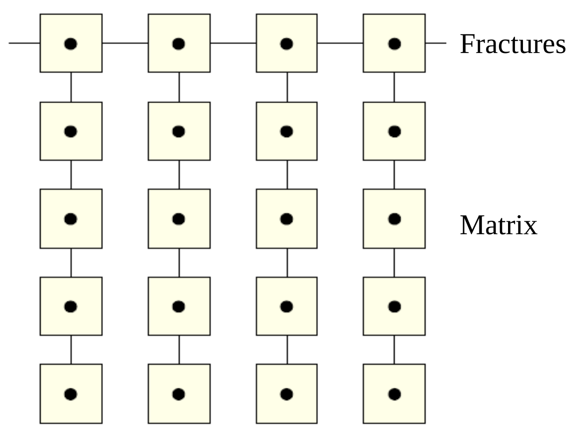

Figure 4.5: Schematic figure of the connectivity between fractures and matrix blocks for the MINC model. Source:[96].

The MINC model is computationally time-consuming due to the division of the matrix blocks. This approach also replicates the lack of mass transfer between the matrix blocks, and fails to capture the pressure drop within the fractures

[96]. This approach may be suitable for a naturally fractured reservoir with low matrix permeability and high-conductivity fractures [96].

3. **Discrete fracture model**

   The discrete fracture method (DFM) is an expensive but convenient model that simulates fluid flow in naturally fractured reservoirs [98]. The discrete fracture model upscales the geological formation discontinuities to add the natural fracture complexity into the fluid-flow modeling [101]. The model represents the three-dimensional spatial distribution of interconnected natural fractures within the rock matrix. The method explicitly models the fluid flow in each natural fracture embedded within the rock matrix blocks. The detailed modeling is an advantage. However, the combination of fluid flow equations and fracture-matrix volume elements results in CPU limitations for running the model [100]. These make this approach computationally challenging and impractical to implement in some numerical studies.

4.2 Hydraulic Fracture Modeling

Hydraulic fractures have variable dimensions and conductivities according to the distance to the wellbore. A simple approach to model the hydrofractures requires the assumption of symmetrical fracture geometry with constant fracture properties. The following three methods can be used to model hydraulic fractures in naturally fractured plays [102]:

1. **Explicit hydraulic fracture**

   The explicit hydraulic fracture (EHF) approach integrates three different software applications. The first application models each hydraulic fracture stage using different simulation software [102]. The hydrofractures modeling process develops a geological model. The process also incorporates hydraulic fracture features into the geological model. It then upscales the geological model into a reservoir simulation model [102]. Finally, the simulation model is run to perform the history match of wellbore production. This process is robust and time-consuming, which makes it expensive and computationally difficult.

2. **Stimulated reservoir volume**

   The stimulated reservoir volume (SRV) approach constrains the size of the volume around the wellbore that contains the hydraulic fractures. This method considers uniformly distributed hydrofractures. The model applies the local grid refinement (LGR) concept to refine the near-wellbore zone [102]. The LGR method allows the assignment of specific properties such as permeability, porosity, and compressibility to the hydraulic fracture blocks [102]. The stimulated reservoir volume approach is simpler than the explicit hydraulic fracture method. Therefore, we applied this method in our study with a logarithmic grid refinement to model the hydrofractures.

3. **Logarithmically spaced-locally refined-dual permeability (LS-LR-DK) model**

   Rubin (2010) [93] proposed this new model that simulates hydraulic fractures in naturally fractured reservoirs. This approach combines the dual-permeability model, the blocks partitioning concept of the MINC model, and the SRV theory. The method applies the dual-permeability concept to model fluid flow in the matrix blocks, and also explicitly models the hydraulic fractures using logarithmic grid spacing. The logarithmic refinement enhances mass transfer modeling and the pressure drawdown calculation between matrix-fracture blocks, matrix-matrix blocks, and fracture-fracture blocks [96]. Figure 4.6 shows the differences in the gridding of the MINC model and the LS-R-DK model. Figure 4.7 illustrates the explicit planar hydraulic fracture.

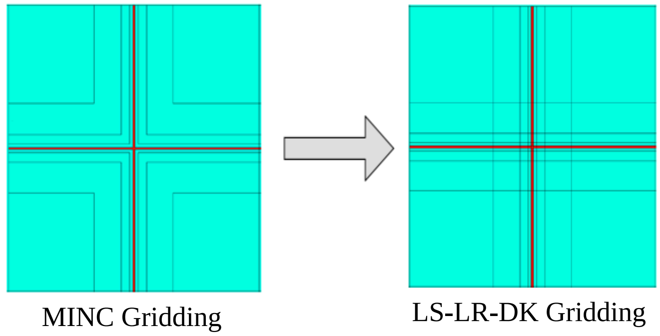

Figure 4.6: Comparison between the gridding used in the MINC model and the LS-LR-DK model (map view). Source:[96].

This model scales the width of the hydraulic fracture blocks up to 0.6 m (2 ft) to reduce the computational time [96]. However, the fracture conductivity of the modeled hydraulic fracture must be the same as the "real" fracture. Thus, we modified the permeability of the fracture block using the following equation[93, 96]:

$$\mathrm{k_{eff}} = \frac{\mathrm{k_f} \times \mathrm{w_f}}{\mathrm{w_{block}}} \tag{4.1}$$

Where $\mathrm{w_{block}}$ is the width of the block containing the hydraulic fracture in m (ft.), $\mathrm{k_f}$ is the hydraulic fracture permeability in $\mathrm{m^2}$ (mD), $\mathrm{w_f}$ is the hydraulic fracture width in m (ft.), and $\mathrm{k_{eff}}$ is the equivalent permeability of the hydraulic fracture when applying the change in hydraulic fracture width in $\mathrm{m^2}$ (mD).

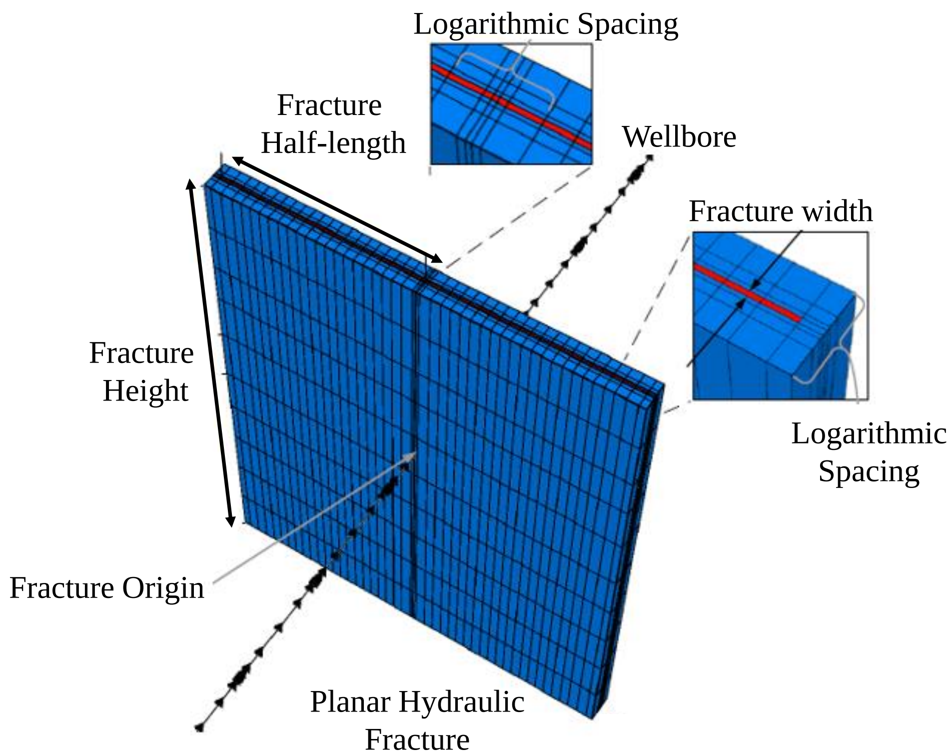

Figure 4.7: Diagram of a planar hydraulic fracture in the simulation model. Modified from [96].

Chapter 5

Application: Simulation of Shale Oil Reservoirs by Varying the Hydraulic Fracture Geometry

5.1 Numerical Simulation Model Description

We used a commercial black oil simulator (CMG, IMEX) to build and run several conceptual numerical models. The reservoir model applies the dual-permeability method to represent the natural fracture system and the shale play matrix. The model dimension is 350 m (1,150 ft) in the I-direction, 762 m (2,500 ft) in the J-direction, and 41 m (135 ft) in the K-direction as displayed in Figure 5.1. The modeled formation comprises three horizons where the target zone is the middle horizon. Table 5.1 presents the reservoir layers' attributes.

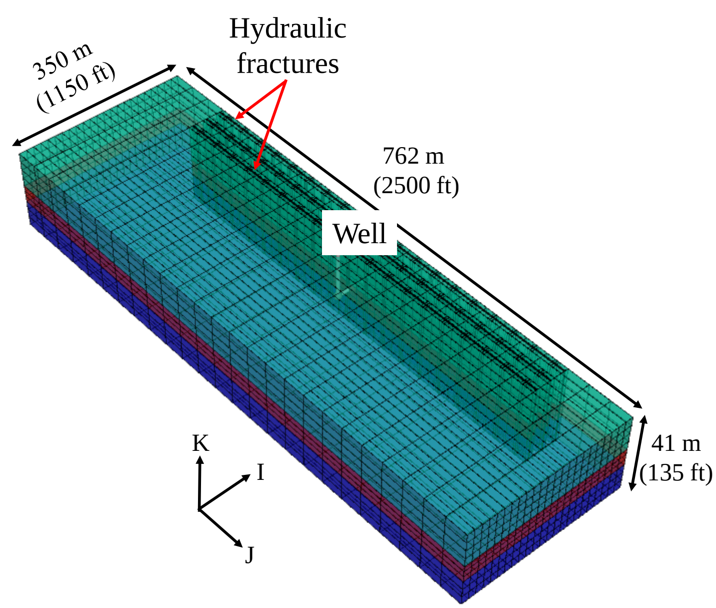

Figure 5.1: Reservoir model (CMG-IMEX).

The reservoir model simulates a single stage of the fracturing process with a horizontal fractured wellbore of 90 m (300 ft) in length. In contrast, our analysis considers a multi-stage hydraulic fracturing process with 22 stages. Thus, the total wellbore length is 2,000 m (6,600 ft) and is located in the center of the target horizon. We calculated the total production of the multi-stage fractured model by multiplying the results of the single-stage simulation model by the 22 stages [42, 103]. The single-stage model reduces the time of the simulation runs (Figure 5.2).

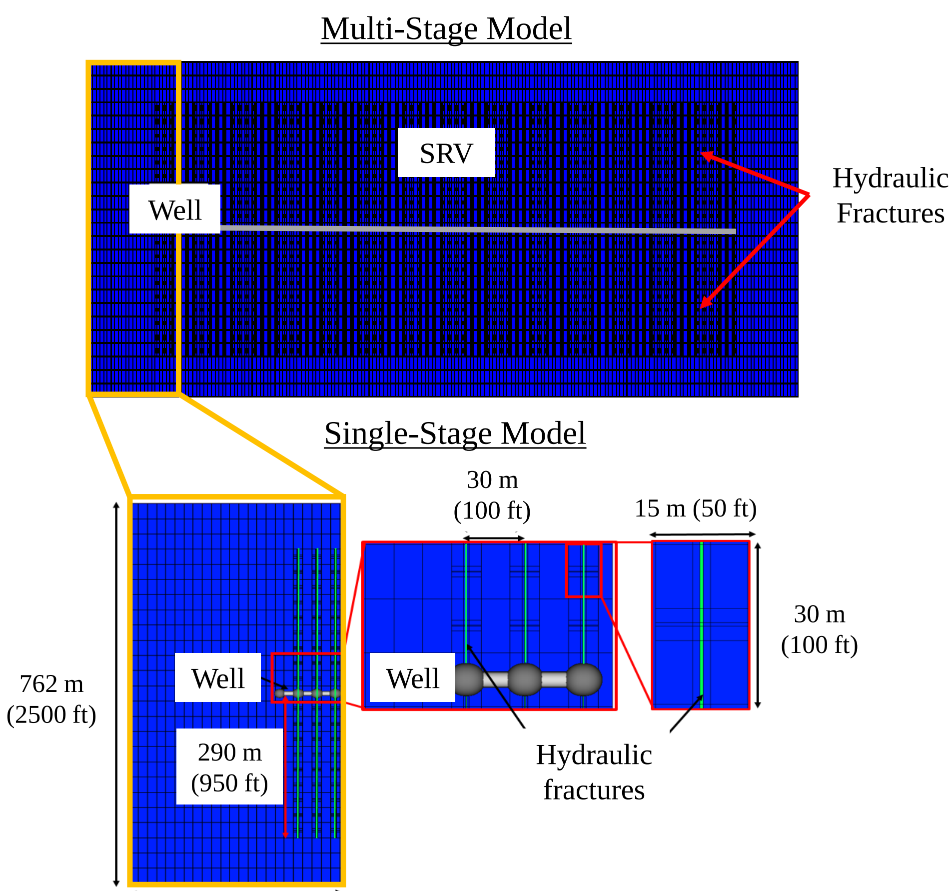

Figure 5.2: Comparison between the multi-stage model (including 22 stages) and the single-stage model.

Our reference scenario comprises three vertical and planar hydrofractures per stage. We predetermined the hydraulic fracture geometry for each scenario. The total fracturing fluid volume injected into the rock is 12,700 m^3 (80,000 bbls). We considered the same fracturing fluid volume for all proposed scenarios. The next section shows the reservoir model properties in more detail.

1. **Reservoir properties and fluid properties**

   The modeled formation is undersaturated during the studied production time. Thus, the bubble point pressure is below the reservoir pressure. We assumed a matrix compressibility value of $1{\times}10^{-9}$ Pa^{-1} ($9{\times}10^{-6}$ psi^{-1}) [50, 104, 105]. Table 5.1 presents the list of properties of the shale oil formation considered in this study. Additionally, Table 5.2 shows the reservoir fluid properties.

Table 5.1: Properties of the horizons of the reservoir simulation model.

Layer	Thickness [m]	Thickness [ft]	Initial Water Saturation [fraction]	Porosity [fraction]	Permeability [mD]
Upper zone	18	60	0.58	0.05	3.1E-05
Target zone	9	30	0.20	0.07	1.4E-04
Lower zone	14	45	0.60	0.04	2.0E-05

General Reservoir Properties

Parameter	SI unit	Field unit
Reservoir temperature	138 °C	280 °F
Reservoir compressibility	1E-09 Pa^{-1}	9E-06 psi^{-1}
Reservoir thickness	41 m	135 ft
Reservoir depth	3,000 m	10,000 ft

Table 5.2: PVT reservoir fluid properties.

Parameter	SI Unit	Field Unit
Oil bubble point pressure	23.44 MPa	3,400 psi
Oil API density	45.6	45.6
Oil density at stock tank conditions	798.2 kg/m^3	49.8 lbm/ft^3
Under-saturated oil compressibility	2.0E-09 Pa^{-1} [(a)]	1.4 E-05 psi^{-1} [(a)]
Gas specific gravity	0.8651	0.8651
Gas density at standard conditions	1.06 kg/m^3	0.07 lbm/ft^3
Water compressibility	1.3E-10 Pa^{-1} [(a)]	9.0E-06 psi^{-1} [(a)]
Water phase viscosity at reference pressure (14.7 psi)	0.3 mPa.s	0.3 cp
Water density at stock tank conditions	996.9 kg/m^3	62.2 lbm/ft^3
Water formation volume factor	1.04 m^3/m^3	1.04 Bbl/STB

Sources: [a][104, 106].

2. **Relative permeability curves**

   We considered the two-phase flow (oil-water) relative permeability curves in this study. Figure 5.3a and Figure 5.3b display the relative permeability curves for the rock matrix and the fracture system, respectively.

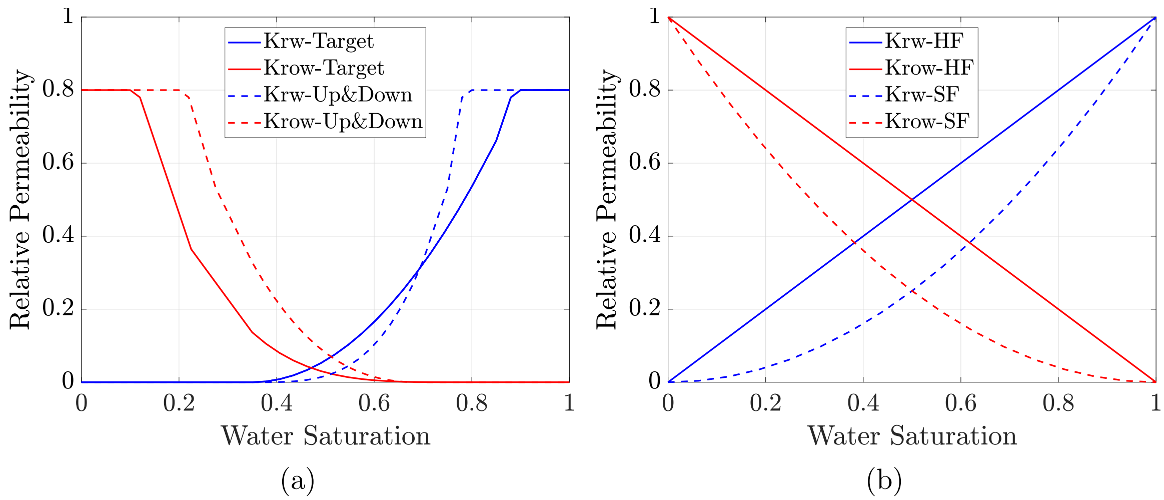

Figure 5.3: Water-Oil relative permeability curves. (a) Rock matrix relative permeability curves: solid curves represent the target zone and dashed curves the upper and lower zone (Up&*D*own). (b) Fractures relative permeability curves: solid curves represent the hydraulic fractures (HF), and dashed curves represent secondary fractures (SF).

This study assumes an organic-rich target zone that has mixed to oil wettability [107]. Experimental studies have shown that kerogen maturation increases meso and micropores in the rock matrix [108]. These pores increase the residual hydrocarbon saturation and irreducible water saturation [108]. Figure 5.3a shows that relative permeability values vary in a narrow window of water saturation values (0.4-0.6). It leads to sharp hydrocarbon decline rates and an extended period with low water rates.

Figure 5.3a also displays a cross-point between the oil and water relative permeability curve higher than 0.5 for the upper and underlying layers (dashed line) that is characteristic of a water-wet system. Although the cross-point of the relative permeability curves belonging to the target zone (solid line) is below 0.5, which is common in oil-wet systems. Figure 5.3b shows an X-shaped relative permeability curve characteristic of the hydraulic fractures. This shape indicates high conductivity with no influence of capillarity.

3. **Initial reservoir conditions**

   This study considers an overpressured reservoir. The initial reservoir pressure is 59 MPa (8,500 psi) at a depth of 3,000 m (10,000 ft). The reservoir fluid pressure gradient is 0.019 MPa/m (0.85 psi/ft). This model lacks an initial gas cap and aquifer. Therefore, the gas-oil contact and water-oil contact were established outside the reservoir boundaries. Table 5.1 shows the initial reservoir fluid saturation considered in this study. Additionally, Table 5.3 summarizes the initial reservoir conditions.

Table 5.3: Initial reservoir conditions.

Parameter	SI Unit	Field Unit
Initial reservoir pressure	59 MPa	8,500 psi
Well bottom-hole pressure	24 MPa	3,500 psi
Vertical-horizontal permeability ratio (k_v/k_h)	0.1	
Initial water saturation in the natural fracture network	0.2	

4. **Natural fracture network**

   The characterization of natural fracture network distribution is difficult due to the shale matrix complexity. To simplify, we applied the dual-permeability method to model the shale play. It is an idealized but efficient approach that captures the physics behind the shale system fluid flow. This method considers an orthogonal and uniform natural fracture system, as shown in Figure 5.4.

   Natural fracture systems can be classified into narrow fracture systems (aperture of less than 0.05 mm or 0.00016 ft) and wide and open systems (aperture greater than 0.1 mm or 0.003 ft) [13, 1, 90]. Thick formations revealed longer and more widely spaced natural fractures than thin rock beds [99]. Our reference simulation case considers narrow natural fractures with a height equal to the reservoir height (41 m or 135 ft). For simplicity, the natural fractures are equally spaced at 9 m (30 ft) in both I-direction and J-direction. Table 5.4 summarizes the natural fracture properties.

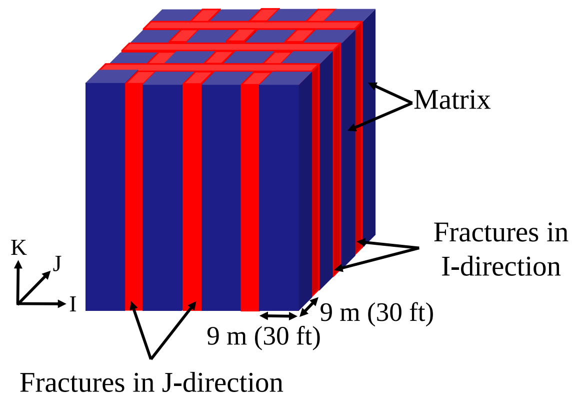

Figure 5.4: Schematic figure of an orthogonal natural fracture system. Based on [92].

Table 5.4: Natural Fracture Network Properties.

Parameter	SI Unit	Field Unit
Fracture permeability	1.97E-14 m^2	200 mD
Fracture aperture	0.03 mm	0.0001 ft
Fracture porosity	0.0000067	
Distance in I-direction	9 m	30 ft
Distance in J-direction	9 m	30 ft

5. **Hydraulic fractures**

We modeled the hydraulic fractures using the locally spaced-logarithmically refined-dual permeability approach (LS-LR-DK). The approach considers the stimulated reservoir volume (SRV) concept that assumes a uniform hydraulic fracture distribution along the horizontal wellbore and similar fracture properties. The SRV concept generates a symmetrical reservoir with hydrofracture stages behaving identically. These conditions make the single-stage method applicable to model the shale play [109]. The reference case has three hydraulic fractures, spaced 30 m (100 ft) from each other (Figure 5.6). Table 5.5 summarizes the hydraulic fracture properties.

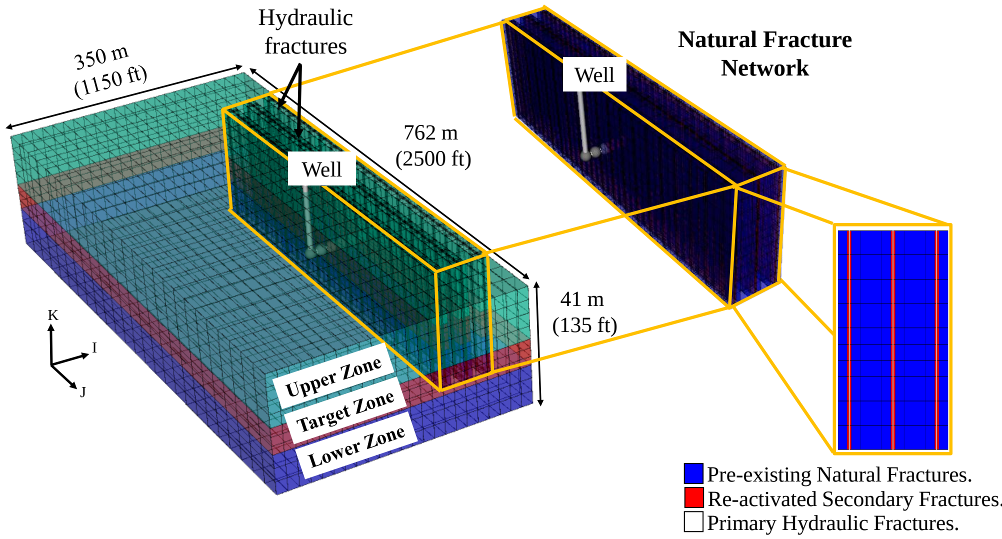

Figure 5.5: Natural fracture network in the reservoir simulation model.

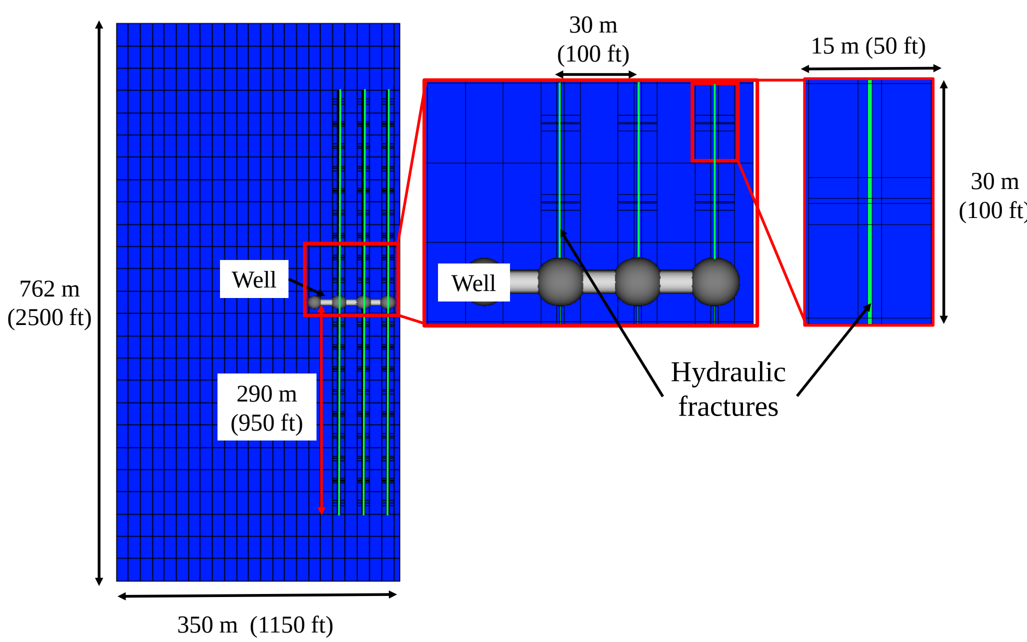

Figure 5.6: Hydraulic fracture system (map view).

Table 5.5: Hydraulic fracture properties of the reference simulation case.

Parameter	SI Unit	Field Unit
Number of stages	22	
Number of clusters per stage	3	
Fluid injected/cluster	190.8 m^3	1,200 bbls
Fracture spacing	30.5 m	100 ft
Fracture permeability	1.97E-12 m^2	2000 mD
Fracture propped half-length	137 m	450 ft
Fracture unpropped half-length	152 m	500 ft
Fracture block width	0.6 m	2 ft
Fracture aperture	9 mm	0.031 ft

6. **Compaction curves**

We implemented compaction curves in the reservoir simulation scenarios to model fracture closure. These curves consist of pressure-dependent permeability and porosity multipliers assigned to the hydraulic fracture grid blocks (Figure 5.7). The fracture-closure mechanism results from the increase in effective stress during reservoir fluid production.

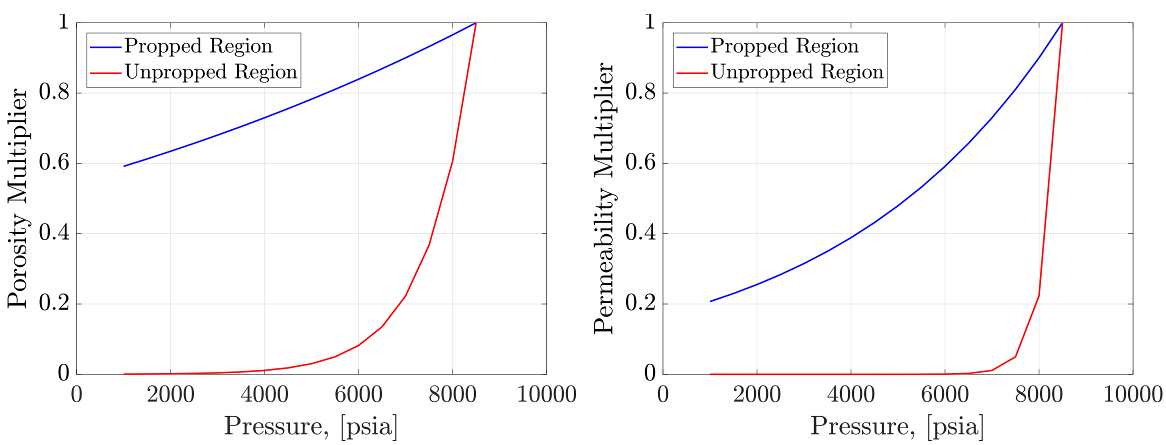

(a) (b)

Figure 5.7: Compaction curves for the propped (blue line) and the unpropped (red line) zone of the hydraulic fractures, (a) Porosity multipliers and (b) Permeability multipliers.

The effective stress is the stress acting on the matrix in a saturated porous medium [37]. Terzaghi's equation (Equation 5.1) describes it as the difference between the total stress, also known as confining stress or overburden rock pressure, and the fluid pore pressure [110].

$$\sigma_{\mathrm{eff}} = \sigma - \mathrm{P_p} \tag{5.1}$$

- σ_{eff}: Effective stress, psi.
- σ: Total stress or confining stress, psi.
- $\mathrm{P_p}$: Fluid pore pressure, psi.

Nur&Byerlee (1971) corrected this equation by Biot coefficient that describes the relative effect of pore pressure on effective stress [37]:

$$\sigma_{\mathrm{eff}} = \sigma - \alpha \mathrm{P_p} \tag{5.2}$$

- α: Biot coefficient (Biot, 1941).

Numerous studies have examined the relationship between effective stress, permeability, and porosity. The studies described the relationships using empirical models (e.g., power model, exponential model, and logarithmic model) that consider the confining pressure constant [111, 112, 113]. These studies revealed that permeability has a higher stress sensitivity than porosity [114]. We applied the following equations to calculate the permeability and porosity multipliers [115, 1]:

$$\frac{\phi}{\phi_{\mathrm{i}}} = \mathrm{e}^{\,\mathrm{C_{frac}} \times\, \mathrm{P_{net}}} \tag{5.3}$$

$$\frac{\mathrm{k}}{\mathrm{k_i}} = \frac{\phi}{\phi_{\mathrm{i}}} = \mathrm{e}^{\,3\times\, \mathrm{C_{frac}} \times\, \mathrm{P_{net}}} \tag{5.4}$$

Where,

- ϕ_{i}: Initial porosity, fraction.
- $\mathrm{k_i}$: Initial permeability, m^2 (mD).

– P_{net}: Net pressure, MPa (psi). It is the difference between the initial pressure and the current pressure [1].
– C_{frac}: coefficient of stress sensitivity, MPa^{-1} (psi^{-1}).

Figure 5.7 shows two compaction curves (red and blue lines). The red line represents the unpropped region of the hydraulic fracture. In contrast, the blue line describes the propped zone of the hydraulic fracture. Proppant support makes closure rate lower in the propped zone than in the unpropped zone [1].

5.2 Basic Numerical Simulation Case: Vertical, Planar, Symmetrical Hydraulic Fractures with Reactivated Secondary Fractures.

The reference simulation model is an idealized case that discretizes the media into a matrix and an orthogonal natural fracture network. We considered natural fractures equally spaced at 9 m (30 ft) with a fracture aperture of 0.03 mm (0.0001 ft). We also assumed that the model comprises a set of hydraulic fractures equally spaced along the horizontal wellbore (30 m or 100 ft). The hydrofractures have an aperture of 9 mm (0.031 ft) and a permeability of 2000 mD. As previously mentioned, for simplicity, the model has a single stage of three hydraulic fractures, as displayed in Figure 5.8.

We assumed vertical, bi-wing, and symmetric hydraulic fractures with small vertical secondary fractures (Figure 5.9). The hydrofractures propagate in the direction of the maximum horizontal stress, and they open in the direction of the least horizontal stress [76, 116]. In this scenario, a net pressure higher than the horizontal stress difference and the rock's tensile strength, combined with a high pumping rate, favor the fracturing fluid leak-off into pre-existing natural fractures [81]. Consequently, secondary fractures hydraulically open, but the primary hydrofracture geometry is preserved [12, 69]. The reactivation of secondary fractures does not limit the vertical fracture growth. The hydrofractures height is 41 m (135 ft).

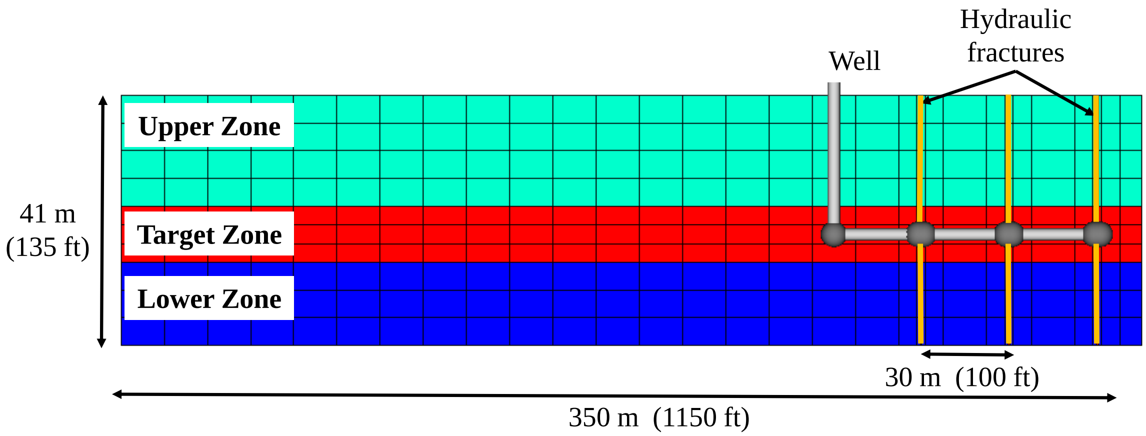

Figure 5.8: Basic numerical simulation case model (Cross-view along the wellbore).

The secondary fractures are narrower than the primary hydraulic fractures. Their aperture is 3 mm (0.01 ft). We considered the secondary fractures self-propped and filled with fracturing fluid. In contrast, the hydraulic fractures have a propped and unpropped region simulated with two different compaction curves (Figure 5.9).

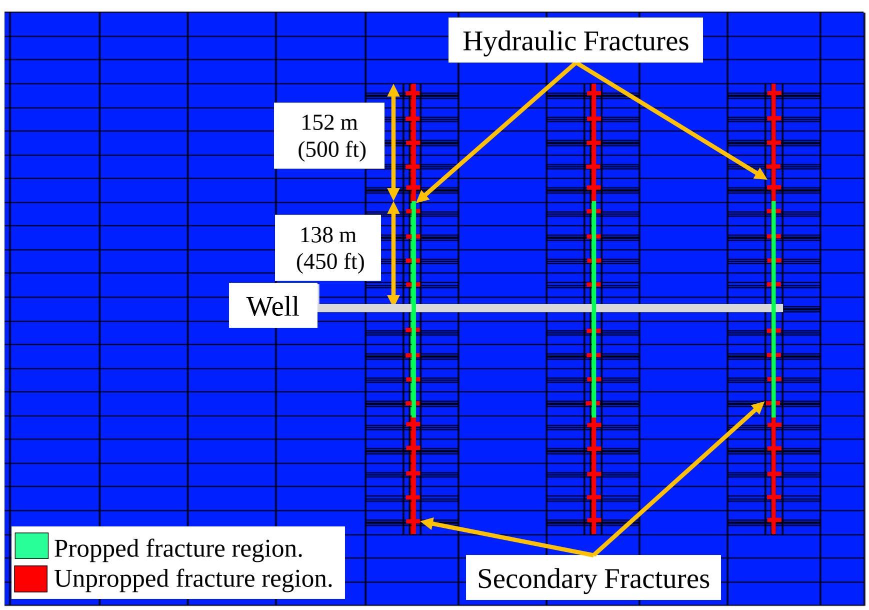

Figure 5.9: Basic numerical simulation case model (map view).

In this study, the total fracturing fluid injected into the rock is 12,700 m^3 (80,000 bbls), and it is distributed in 22 stages. Therefore, the fracturing fluid volume per fracture is 190 m^3 (1,200 bbls). We considered this treatment size based on data reported for U.S. and Middle East shales [43].

5.2.1 Comparison between the multi-stage model and the single-stage model

This section compares reservoir fluid production data obtained using the multi-stage simulation model (22 stages) and the single-stage simulation model multiplied by 22 stages. The comparison aims to validate the assumption of the single-stage model applied in this study (Figure 5.2).

Figure 5.10 shows that the results obtained from the single-stage model multiplied by 22 stages yield a good match with the results obtained using the multiple-stage model (22 stages). The difference in cumulative reservoir fluid production at 15 years obtained with both models is less than 5%. Furthermore, the water cut performance shows a difference of about 10% at 15 years. The water cut differs due to the distinct reservoir volumes of the simulation models, which lead to less water cut when using the small model. Reservoir pressures within the stimulated reservoir volume (SRV) show a difference of about 5% at 15 years. In contrast, the small model depletes a smaller reservoir volume than the multi-stage model resulting in a higher field reservoir pressure at 15 years.

In conclusion, the single-stage model is a valid simplification to model hydraulically fractured reservoirs when the analysis includes the stimulated reservoir volume (SRV) concept. This simplification reduces the computational time from an hour to a few minutes.

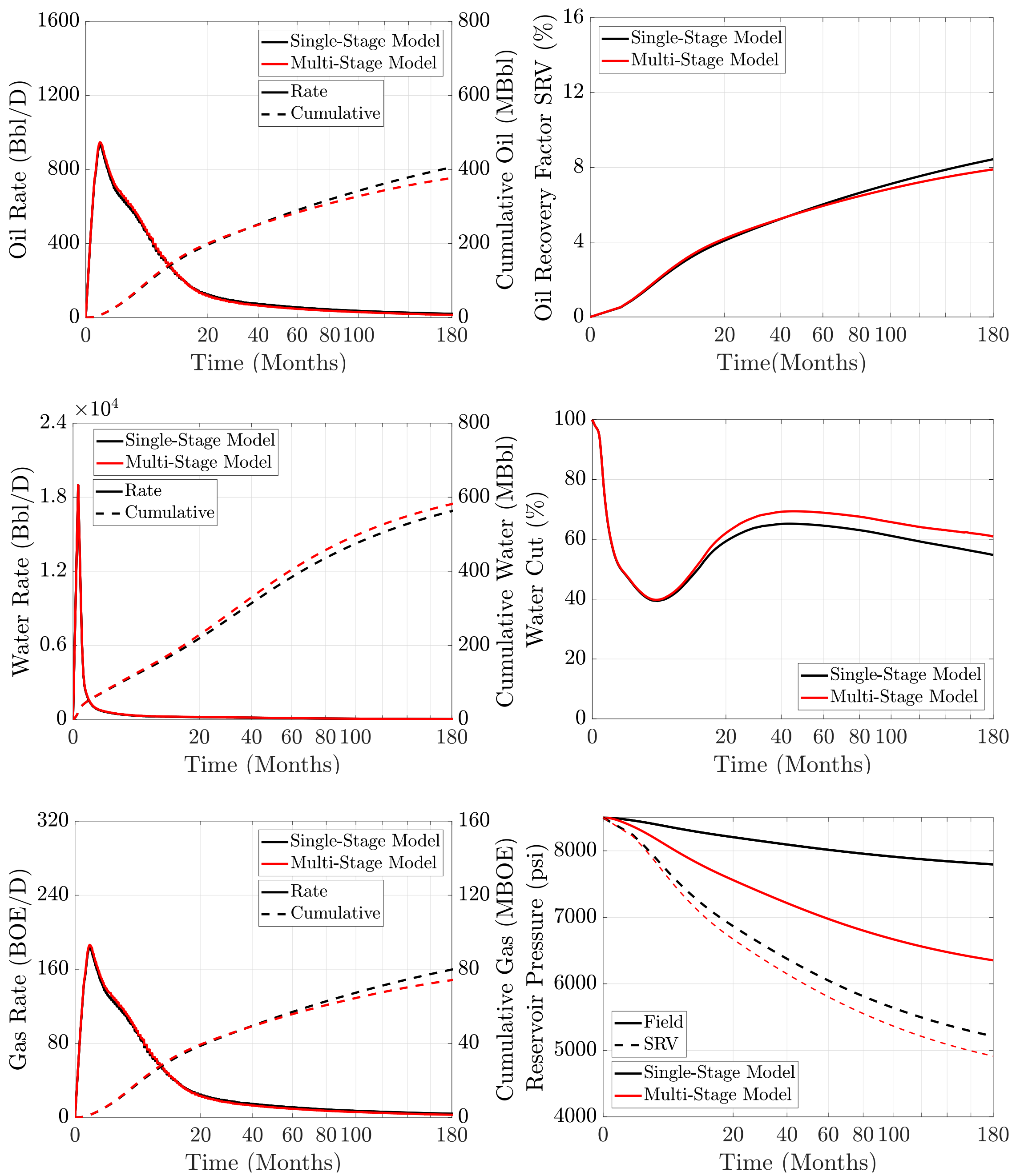

Figure 5.10: 15 years of reservoir fluid production for the single-stage simulation model and the multi-stage simulation model (22 stages).

5.2.2 The effect of natural fracture network density

This study aims to analyze the effect of natural fracture network (NFN) density on hydrocarbon production. The fracture spacing determines the network density. We proposed three scenarios (Figure 5.11) with fracture spacing of 6 m (20 ft), 9 m (30 ft), and 12 m (40 ft). The scenario with the highest natural fracture network density has the smallest fracture spacing (6 m or 20 ft). The simulation models have the same fracture spacing in both directions, parallel and perpendicular to the well. They also have the same natural fracture aperture (0.03 mm or 0.0001 ft).

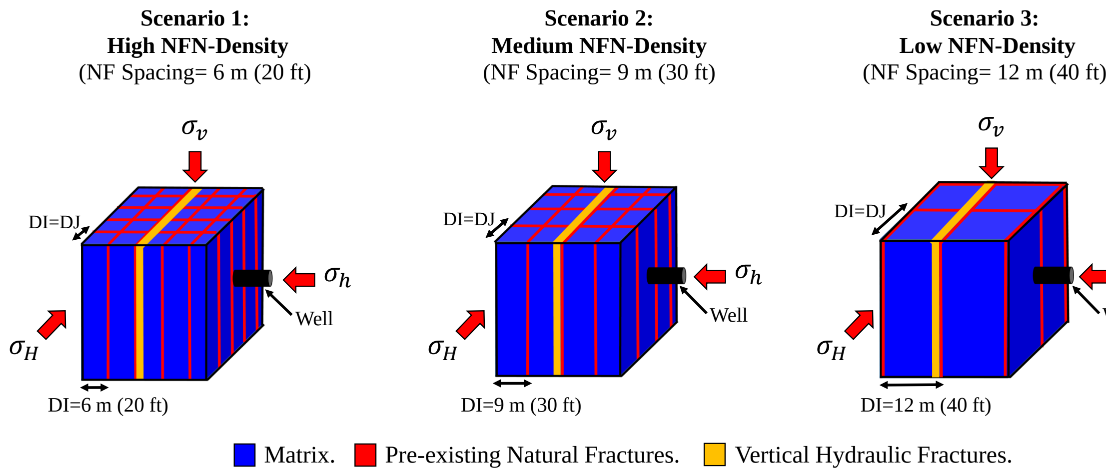

Figure 5.11: Three different scenarios varying the natural fracture (NF) spacing

We compared the proposed scenarios with a simulation case without natural fractures. Figure 5.12 exhibits the importance of the natural fracture system for reservoir fluid production. Naturally fractured reservoirs produce about 30% more hydrocarbon than reservoirs with no natural fractures. The results also show that reservoir fluid production increases with the reduction of fracture spacing. Less spacing between fractures results in more flow conduits per reservoir volume, which enhances reservoir permeability. Furthermore, the water rate experiences a sharp decline, followed by an increase in hydrocarbon production. The sharp decline indicates a fast fracturing fluid flowback (less than five months). Hydrocarbon rates decrease rapidly in the first year.

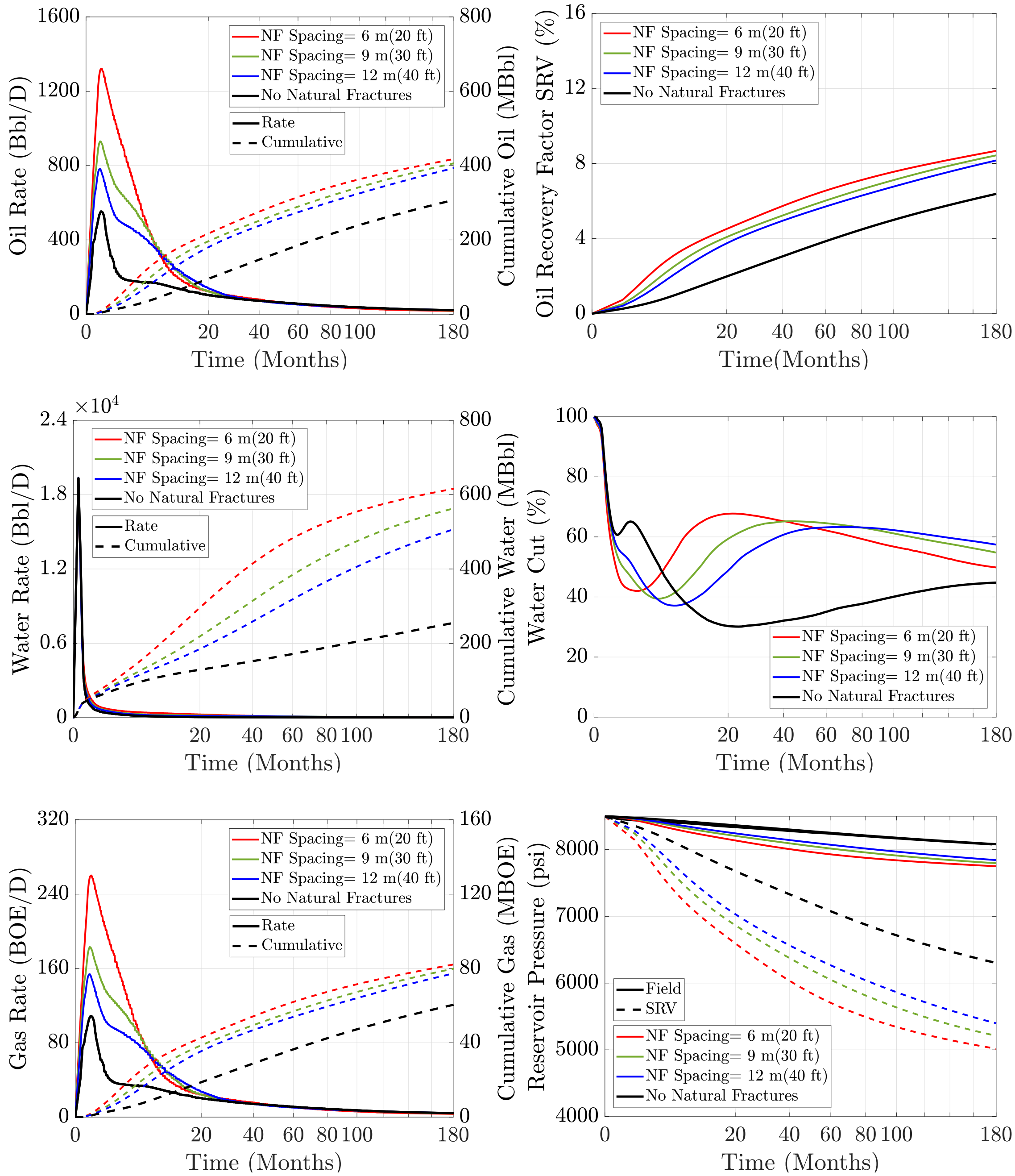

Figure 5.12: 15 years of reservoir fluid production obtained by varying the natural fracture spacing from 6m (20 ft) to 12 m (40 ft). The black curves show the production of a reservoir with no natural fractures.

The scenario with medium natural fracture density (9 m spacing) has an oil recovery factor of 8.5% at 15 years. The recovery factor obtained from the scenario with the highest natural fracture network density (6 m or 20 ft spacing) increases by

4%, and it decreases by the same magnitude in the scenario with the lowest fracture network density (12 m or 40 ft spacing). The similarity is because the fracture spacing varies by 3 m (10 ft) in each case.

Table 5.6: Comparison between the scenarios with high, medium and low natural fracture network (NFN) density and the scenario with no natural fractures

Parameter	High NFN Density NF Spacing = 6 m (20 ft)	Medium NFN Density NF Spacing = 9 m (30 ft)	Low NFN Density NF Spacing = 12 m (40 ft)
Water Rate Peak [%]	**-2**	**-2**	0
Oil Rate Peak [%]	139	68	41
Gas Rate Peak [%]	139	68	41
Ultimate Water Production [%]	141	121	99
Ultimate Oil Production [%]	36	32	28
Ultimate Gas Production [%]	36	32	28

Table 5.6 presents a comparison of different parameters between the proposed scenarios and the case without natural fractures. The results show that the fracture network density does not affect the initial water production, and neither does it impact the fracturing fluid flowback. In contrast, the hydrocarbon rate peak increases significantly as the fracture spacing decreases. The cumulative water production at 15 years increases by up to 140% in naturally fractured reservoirs, and it varies by about 20% between the proposed scenarios with natural fractures. The cumulative hydrocarbon production at 15 years differs by about 4% as the fracture spacing decreases by 3 m (10 ft).

Natural fracture network density affects reservoir fluid production, especially during the initial stages. Fracture closure reduces the reservoir conductivity as production time increases. Thus, the presence of flow conduits loses its effect on long-term hydrocarbon production. The ultimate hydrocarbon production at 15 years is similar between all the proposed scenarios.

5.2.3 The effect of natural fracture orientation

This sensitivity analysis studies the effect of natural fracture orientation on hydrocarbon production. We introduce three scenarios with different fracture orientations (Figure 5.13). The first scenario comprises an orthogonal set of natural fractures. Thus, natural fractures are parallel and perpendicular to the well. The second scenario only has natural fractures parallel to the well. The last scenario has a set of natural fractures oriented perpendicular to the well. The three cases have the same natural fracture properties, including aperture and spacing (9 m or 30 ft).

Figure 5.14 shows that natural fractures oriented perpendicular to the well, slightly contribute to reservoir fluid production. Therefore, the scenario with a set of orthogonal natural fractures (red line) has a similar wellbore performance as the case that comprises only fractures parallel to the wellbore (green line). The ultimate water production for the second scenario (green line) is about 81,000 m^3 (510,000 bbls) at 15 years. It decreases by 33% when the reservoir has only natural fractures perpendicular to the well (blue line). In contrast, the cumulative hydrocarbon production differs by less than 10% between the proposed cases. The average oil recovery factor at 15 years is 8%.

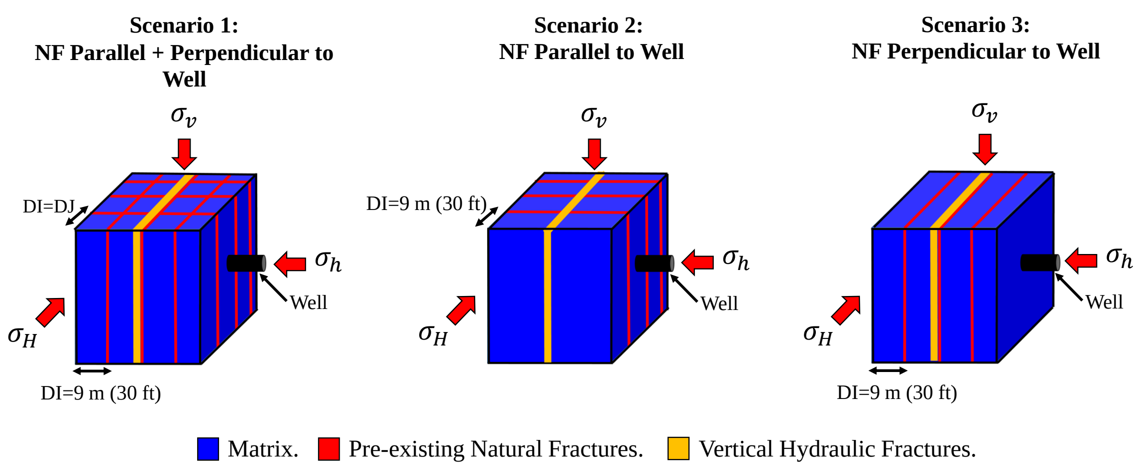

Figure 5.13: Three different scenarios with varying natural fracture orientation.

Table 5.7: Comparison between the proposed scenarios and the case with no natural fractures. The scenarios are: the first scenario has natural fractures (NF) oriented parallel and perpendicular to the well, the second scenario has natural fractures parallel to the well, and the last scenario has natural fractures perpendicular to the wellbore.

Parameter	NF Parallel + Perpendicular to Well	NF Parallel to Well	NF Perpendicular to Well
Water Rate Peak [%]	**-2**	3	**-1**
Oil Rate Peak [%]	68	43	2
Gas Rate Peak [%]	68	43	2
Ultimate Water Production [%]	121	99	32
Ultimate Oil Production [%]	32	28	20
Ultimate Gas Production [%]	32	28	20

Table 5.7 compares different parameters between the three scenarios and the scenario with no natural fractures. The two scenarios that contain natural fractures parallel to the well increase the ultimate water production by about 80% compared to the case with only natural fractures perpendicular to the wellbore. The natural fracture orientation impacts hydrocarbon production, especially in the early stages. On average, the oil rate peak increases by 50% when the reservoir has natural fractures oriented parallel to the well. In this case, the ultimate hydrocarbon production increases by about 10% compared to the case which only has fractures perpendicular to the well.

In conclusion, the natural fracture orientation has a significant effect on wellbore flow performance. The fractures parallel to the wellbore enhance the connectivity between the reservoir matrix and the hydrofractures, favoring hydrocarbon production. The natural fractures impact mainly the initial production. After that, the closure mechanism harms the reservoir permeability and long-term production. The ultimate hydrocarbon production at 15 years is similar between the proposed cases.

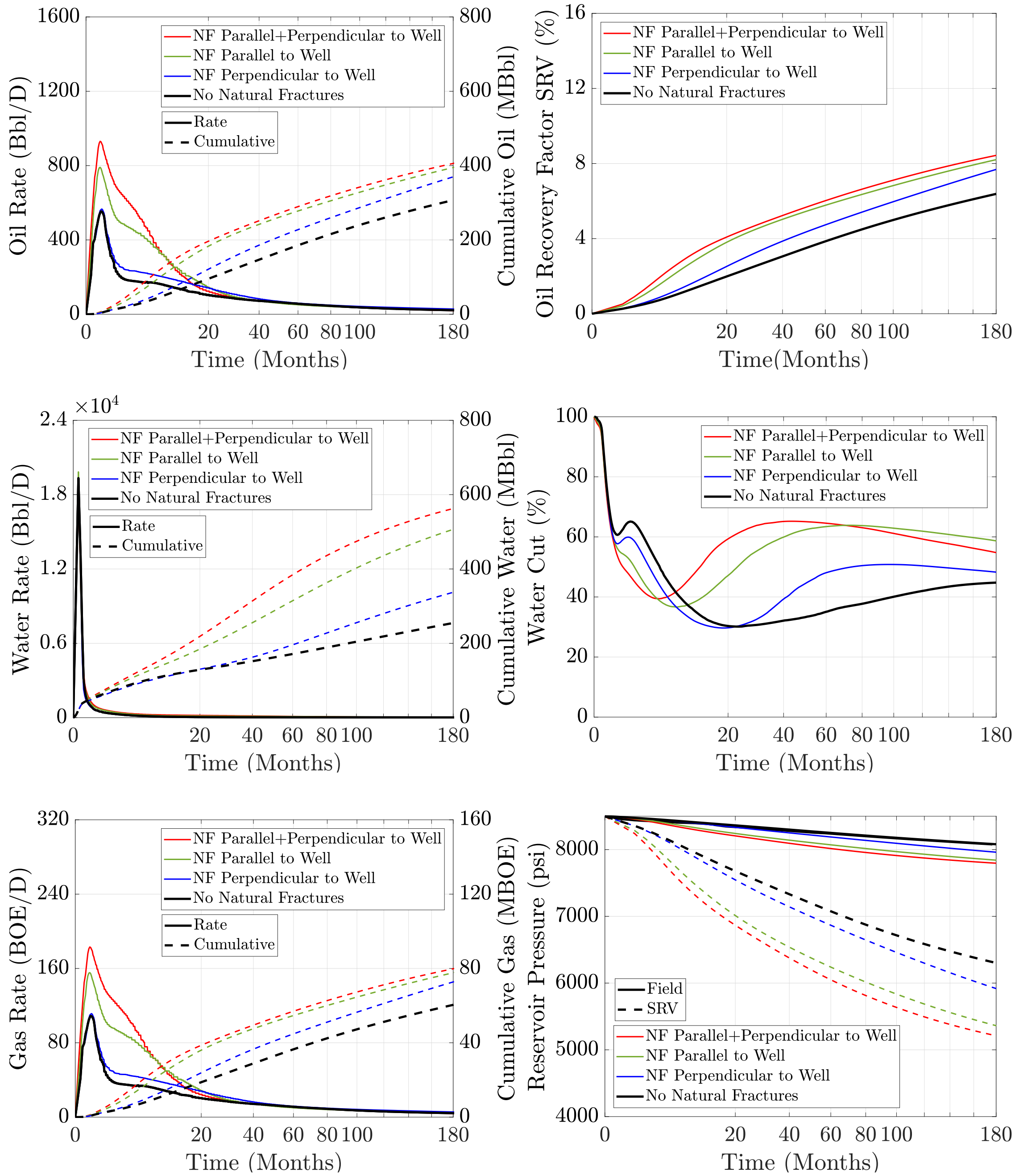

Figure 5.14: 15 years of reservoir fluid production obtained by varying the natural fracture orientation. The black curves show the production of a reservoir with no natural fractures.

5.2.4 Geomechanics effect in natural fractures

Pre-existing natural fractures are often sealed by precipitated minerals such as calcite in shale reservoirs [35, 36]. Several natural fractures are opened as a result of the stimulation jobs. Those fractures create a secondary fracture network and increase the reservoir flow capacity [117]. The secondary fracture network is unpropped or poorly propped, making it responsive to effective stress variation. The increase in effective stress causes fracture closure and alters fracture permeability.

This section examines the effect of natural fracture closure on the wellbore flow performance. We calculated the pressure-dependent porosity and permeability curves using Equation (5.3) and Equation (5.4). These equations require the estimation of the coefficient of stress sensitivity (C_{frac}), known as fracture compressibility. Several studies analyzed the effect of pressure-dependent natural fracture permeability on shale reservoir performance [118, 117, 119]. They estimated fracture compressibility by fitting laboratory measurements with empirical correlations. The reported values vary by a maximum of two orders of magnitude compared to the rock matrix compressibility. Based on the literature reviewed, we proposed four natural fracture compressibility values (Table 5.8) to build the compaction curves shown in Figure 5.15. The least compressible natural fracture set has a stress sensitivity coefficient of 1×10^{-9} Pa^{-1} (9×10^{-6} psi^{-1}), and the most compressible set has a stress sensitivity coefficient of 3×10^{-8} Pa^{-1} (2×10^{-4} psi^{-1}).

Table 5.8: Stress sensitivity coefficient values assigned to the natural fracture system.

Scenarios	Stress sensitivity coefficient, C_{frac} (Pa^{-1})	Stress sensitivity coefficient, C_{frac} (psi^{-1})
Least compressible	1×10^{-9}	9×10^{-6}
–	7×10^{-9}	5×10^{-5}
–	1×10^{-8}	9×10^{-5}
Most compressible	3×10^{-8}	2×10^{-4}

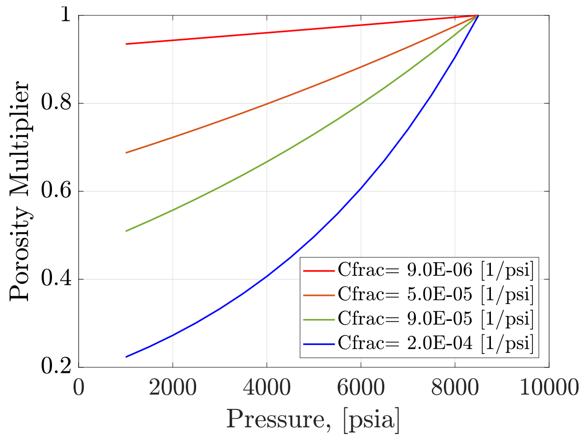

(a)

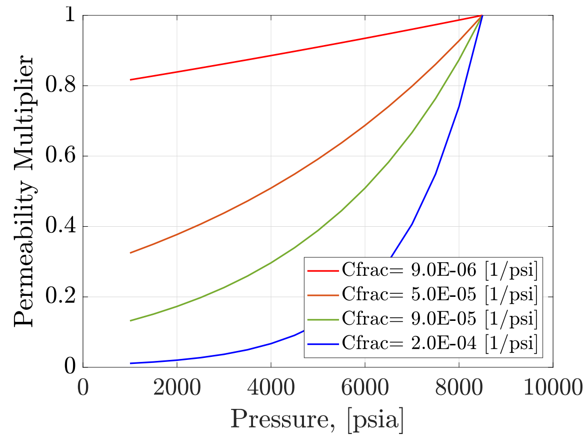

(b)

Figure 5.15: Compaction curves applied to the natural fractures to simulate the natural fracture closure mechanism. The curves have different stress sensitivity coefficient (C_{frac}). (a) Porosity multipliers and (b) Permeability multipliers.

In this study, the initial natural fracture permeability is 1.97×10^{-14} m^2 (200 mD) and the natural fracture spacing is 9 m (30 ft). The least compressible set of natural fractures has the same rock matrix compressibility (1×10^{-9}Pa^{-1} or 9×10^{-6}psi^{-1}). This scenario gives an insight into the wellbore flow production when the analysis excludes the fracture closure effect. We simulated fracture closure using porosity and permeability multipliers. These fracture properties decrease with reservoir pressure. The simulator applies the following equations to vary the initial fracture porosity and permeability [96]:

$$\phi_{\mathrm{f}}(\mathrm{P}) = \phi_{\mathrm{mult}} \times \phi_{\mathrm{fi}} \tag{5.5}$$

$$\mathrm{k_f}(\mathrm{P}) = \mathrm{k_{mult}} \times \mathrm{k_{fi}} \tag{5.6}$$

Where, $\phi_{\mathrm{f}}(\mathrm{P})$ is the fracture porosity, ϕ_{fi} is the initial fracture porosity, $\mathrm{k_f}(\mathrm{P})$ is the fracture permeability in m^2 (mD), $\mathrm{k_{fi}}$ is the initial fracture permeability in m^2 (mD), and ϕ_{mult} and $\mathrm{k_{mult}}$ are the multipliers for the porosity and the permeability respectively.

Figure 5.16 shows that natural fracture closure impacts reservoir fluid production. The scenario with the least compressible set of fractures has the highest production. Table 5.9 presents a comparison of different parameters of the proposed scenarios with one that lacks natural fractures. The water rate peak variation shows that the increase in fracture compressibility accelerates the fracturing fluid flowback. The hydrocarbon rate peak increases by about 20% with the decrease of fracture compressibility. The scenario with the most compressible fracture set has an 8% oil recovery factor at 15 years. It increases by about 15% for the scenario with stiffer natural fractures. The cumulative water production at 15 years increases by about 100% when the reservoir has conductive natural fractures.

Table 5.9: Comparison between the four scenarios in which the stress sensitivity coefficient (C_{frac}) varies and the scenario with no natural fractures.

Parameter	$C_{frac}= 9\times10^{-6}$ [psi^{-1}]	$C_{frac}= 5\times10^{-5}$ [psi^{-1}]	$C_{frac}= 9\times10^{-5}$ [psi^{-1}]	$C_{frac}= 2\times10^{-4}$ [psi^{-1}]
Water Rate Peak [%]	**-13**	**-4**	**-2**	3
Oil Rate Peak [%]	80	73	68	55
Gas Rate Peak [%]	80	73	68	55
Ultimate Water Production [%]	134	128	121	101
Ultimate Oil Production [%]	42	36	32	24
Ultimate Gas Production [%]	42	36	32	24

This sensitivity analysis exhibits the importance of the natural fracture network within the stimulated reservoir volume. It also shows that the high-conductivity of the hydrofractures minimizes the natural fracture closure effect on hydrocarbon production. Thus, the variation of the compaction curves slightly impacts the wellbore flow performance. The scenario with stiffer natural fractures generates the highest reservoir fluid production.

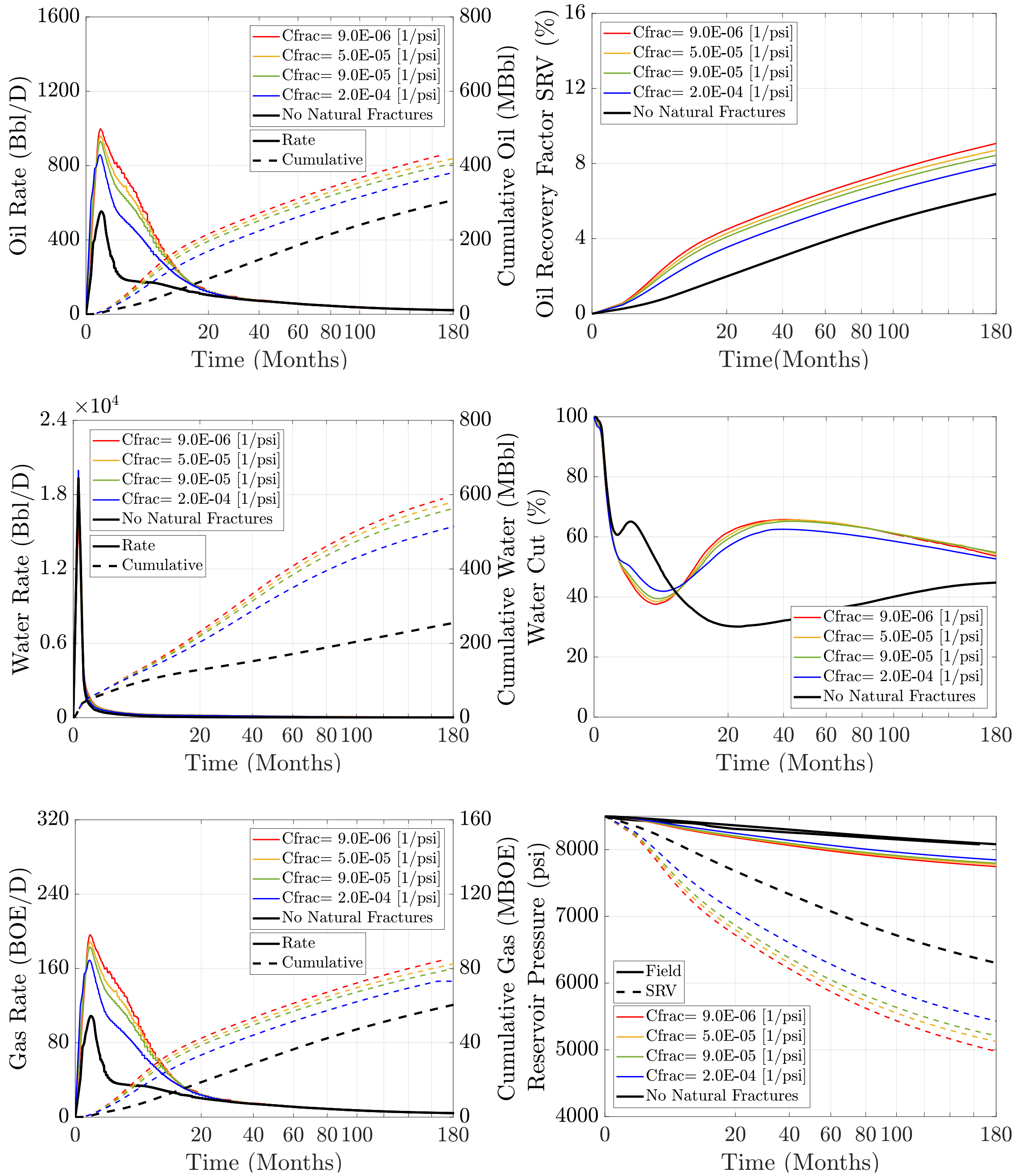

Figure 5.16: 15 years of reservoir fluid production obtained by varying the compaction curves applied to the natural fractures to simulate the closure mechanism. The black curves represent the wellbore flow performance of a reservoir that lacks natural fractures.

5.2.5 Geomechanics effect in hydraulic fractures

This analysis intends to understand the hydraulic fracture closure effect on wellbore flow performance. We proposed three scenarios that apply different compaction curves to the hydrofractures. Compaction curves model the hydrofracture closure mechanism as the pore pressure decreases. The first scenario lacks the compaction curves. Thus, the hydraulic fractures remain open during the production time. The second scenario assigns two compaction curves to the hydrofractures, one to the propped region and the other to the unpropped zone (Figure 5.17). The closure rate of the unpropped zone is much higher than the closure rate of the propped zone. The last scenario assigns the same closure rate to the propped and unpropped regions (green line in Figure 5.17). This case increases the hydrofracture length open to flow.

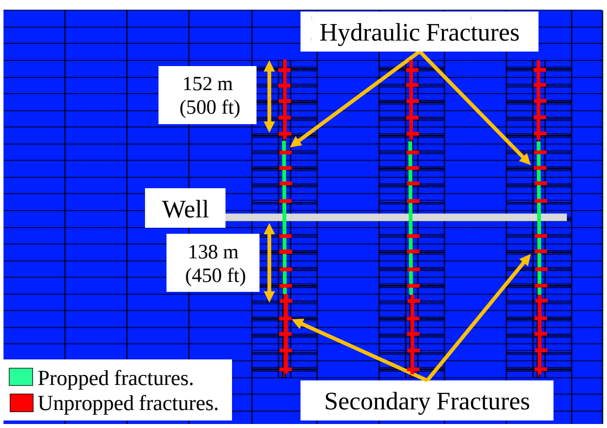

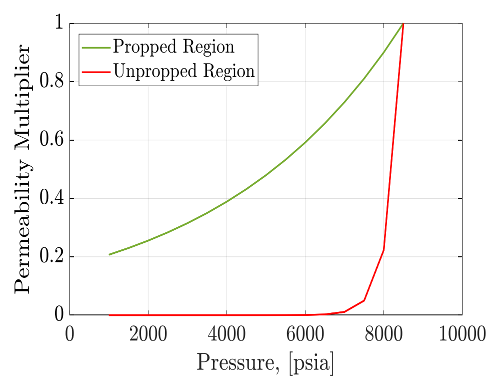

Figure 5.17: On the left, a map view of three vertical hydraulic fractures with the propped region (green area) and unpropped region (red area). On the right, the compaction curves assigned to the propped region (green line) and unpropped region (red line).

Figure 5.18 shows that fracture closure impacts reservoir fluid production. We found that the oil recovery factor at 15 years is about 12% when hydrofractures remain open to flow during production (No compaction curves in Figure 5.18). It decreases to 8.5% when fracture tips experience rapid closure due to a lack of proppant support. Also, there is a slight variation in initial production when the fracture tip has the same closure rate as the propped zone compared to the case that lacks compaction curves. It indicates that despite the reduction of 90% of the initial fracture permeability, the hydrofractures have excessive conductivity compared to the rock matrix.

Table 5.10: Comparison between the scenario with two compaction curves, the scenario with the same fracture closure rate and the scenario that lacks compaction curves.

Parameter	Propped & Unpropped Compaction Curves	Only Propped Compaction Curves
Water Rate Peak [%]	33	12
Oil Rate Peak [%]	**-32**	**-12**
Gas Rate Peak [%]	**-32**	**-12**
Ultimate Water Production [%]	**-20**	0
Ultimate Oil Production [%]	**-28**	0
Ultimate Gas Production [%]	**-28**	0

The fracture closure exhibits a higher impact on initial production due to an exponential decrease of fracture aperture. Table 5.10 presents the comparison between the scenarios with compaction curves and the scenario that lacks compaction curves. It shows that the hydrocarbon rate peak decreases by 12% when the fracture tip has the same closure rate as the propped region. The hydrocarbon rate peak decreases by 32% when fracture tips have a rapid closure. The initial water rate production increases with the fracture closure rate. Although the third scenario comprises a low hydrofracture closure rate, the cumulative reservoir fluid production is the same as the scenario that lacks a fracture closure mechanism. Fracture closure significantly impacts the production of the scenario with two compaction curves. The fracture tip's rapid closure reduces the effective fracture length (propped length) and harms reservoir permeability.

In conclusion, the hydrofracture closure significantly impacts the reservoir fluid production when the fracture is partially propped. The fracture tips are often unpropped or poorly propped, which leads to rapid closure. In contrast, an effective proppant placement into the hydrofractures enhances wellbore flow performance.

Propped fractures still experience porosity and permeability reduction, but they keep a high conductivity when no proppant embedment occurs.

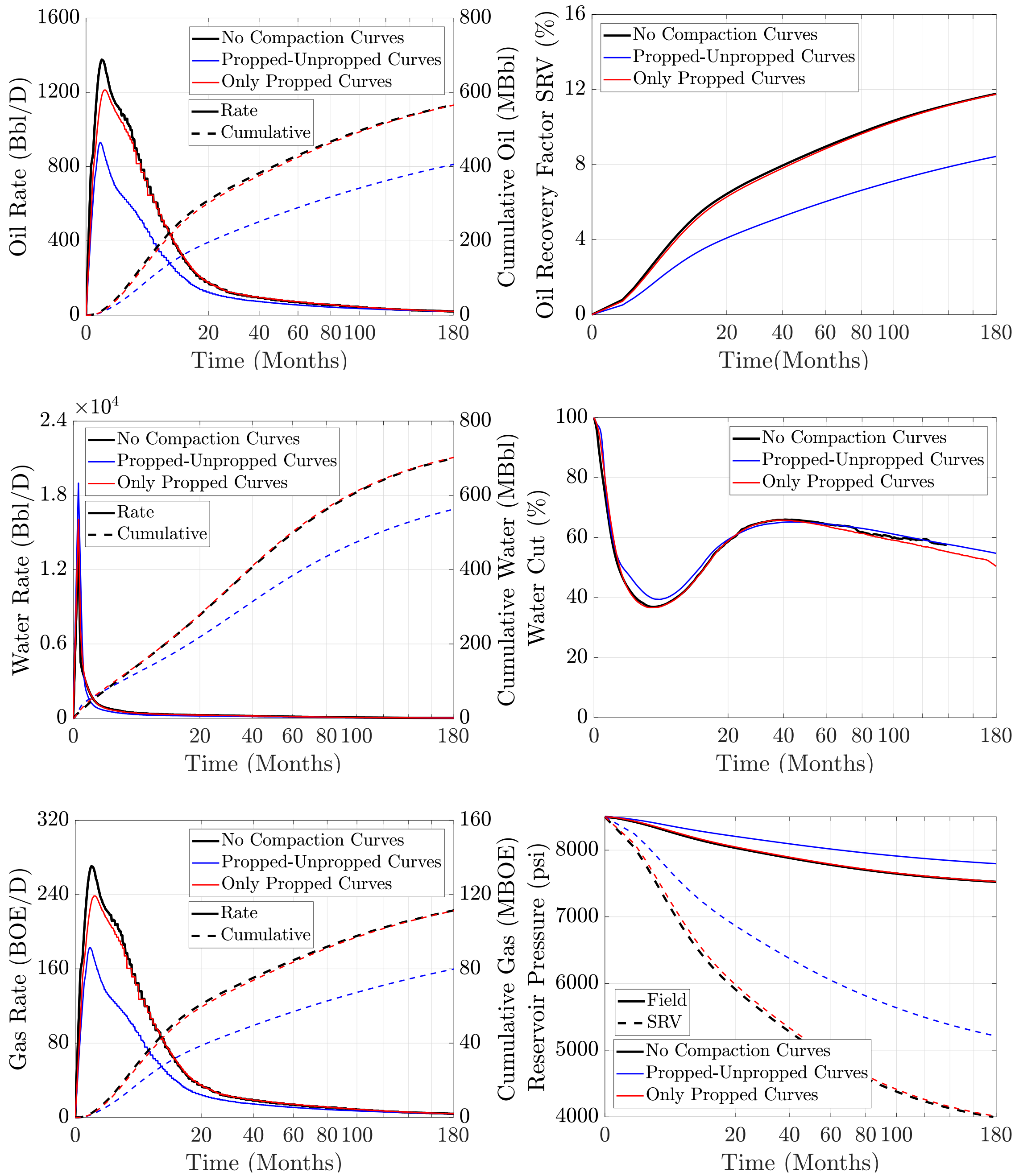

Figure 5.18: 15 years of reservoir fluid production obtained by varying the compaction tables applied to the principal hydraulic fractures. The compaction curves model the fracture closure mechanism. The black line represents the scenario that lacks compaction curves. The red line is the scenario where the unpropped and propped zone has the same closure rate. The blue line represents the scenario that assigns two compaction curves to the hydrofractures.

5.2.6 The effect of number of clusters per stage

This analysis evaluates the effect of the number of clusters per stage on hydrocarbon production. We proposed three scenarios in which the number of clusters per stage varies from two clusters to five clusters, as shown in Figure 5.19. The increase in the number of clusters per stage implies less fracture space. All three scenarios have a fracturing fluid volume per fracture of 190 m^3 (1200 bbls) and a wellbore length of about 2,000 m (6,600 ft).

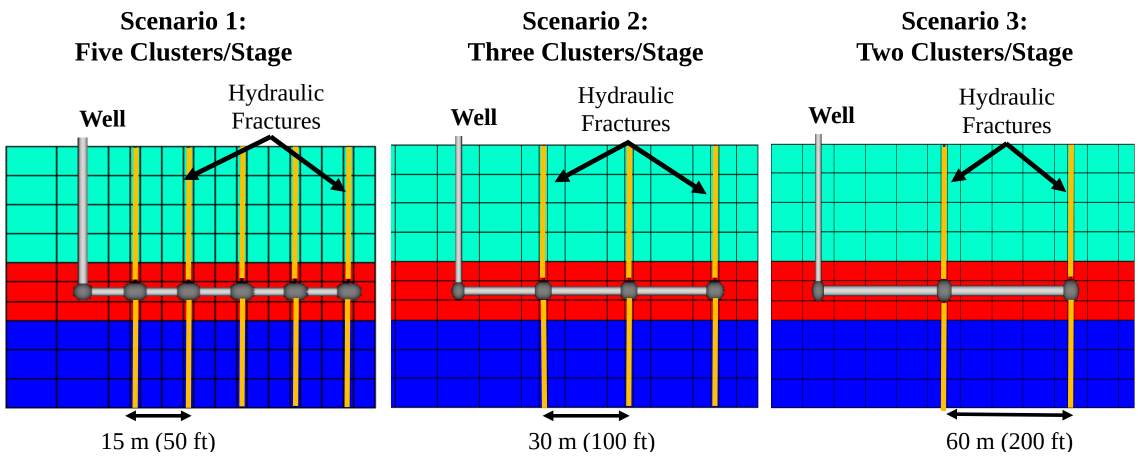

Figure 5.19: The three scenarios with a varying number of clusters per stage (Cross-view along the wellbore).

Table 5.11: Hydraulic fracturing treatment data.

Parameter	Five Clusters/Stage	Three Clusters/Stage	Two Clusters/Stage
Fractures per stage	5	3	2
Number of stages	26	22	16
Fracture width	9 mm (0.031 ft)	9 mm (0.031 ft)	9 mm (0.031 ft)
Fracture spacing	15 m (50 ft)	30 m (100 ft)	60 m (200 ft)
Total water injected	24,800 m^3 (156,000 bbls)	12,700 m^3 (80,000 bbls)	6,400 m^3 (40,000 bbls)

Figure 5.20 compares the wellbore flow performance between the different scenarios. It shows that the initial reservoir fluid production increases significantly with the

number of clusters per stage. In contrast, the cumulative hydrocarbon production at 15 years converges for the scenarios with three and five clusters per stage. Table 5.10 presents a comparison between the scenarios with five and two clusters per stage with the scenario that comprises three clusters per stage. The results show that the ultimate water production at 15 years increases by 18% for the scenario with five clusters per stage, and it decreases by the same magnitude for the scenario with two clusters per stage. The similarity in magnitude is because the total fracturing fluid volume increases twice for each case (Table 5.11). The ultimate oil recovery factor increases by 20% when the number of clusters per stage varies from two to three. However, it remains almost the same when the number of clusters per stage increases from three to five. Thus, there is an optimum number of clusters per stage to make the well profitable for a more extended period.

Table 5.12: Comparison between the scenario with five and two clusters against the scenario with three clusters.

Parameter	5 Clusters/Stage	2 Clusters/Stage
Water Rate Peak [%]	96	**-51**
Oil Rate Peak [%]	67	**-45**
Gas Rate Peak [%]	67	**-45**
Ultimate Water Production [%]	18	**-17**
Ultimate Oil Production [%]	**-1**	**-19**
Ultimate Gas Production [%]	**-1**	**-19**

In summary, the increase in the fracturing fluid volume and the number of clusters per stage enhance the initial reservoir fluid production, but it may harm the long-term production. Operators can opt for massive stimulation jobs to recover the initial investment in the first few years of hydrocarbon production. They also can optimize the hydraulic fracturing design to make the well profitable for a longer time. However, the latter option results in lower hydrocarbon production rates and a longer time to obtain wellbore profits.

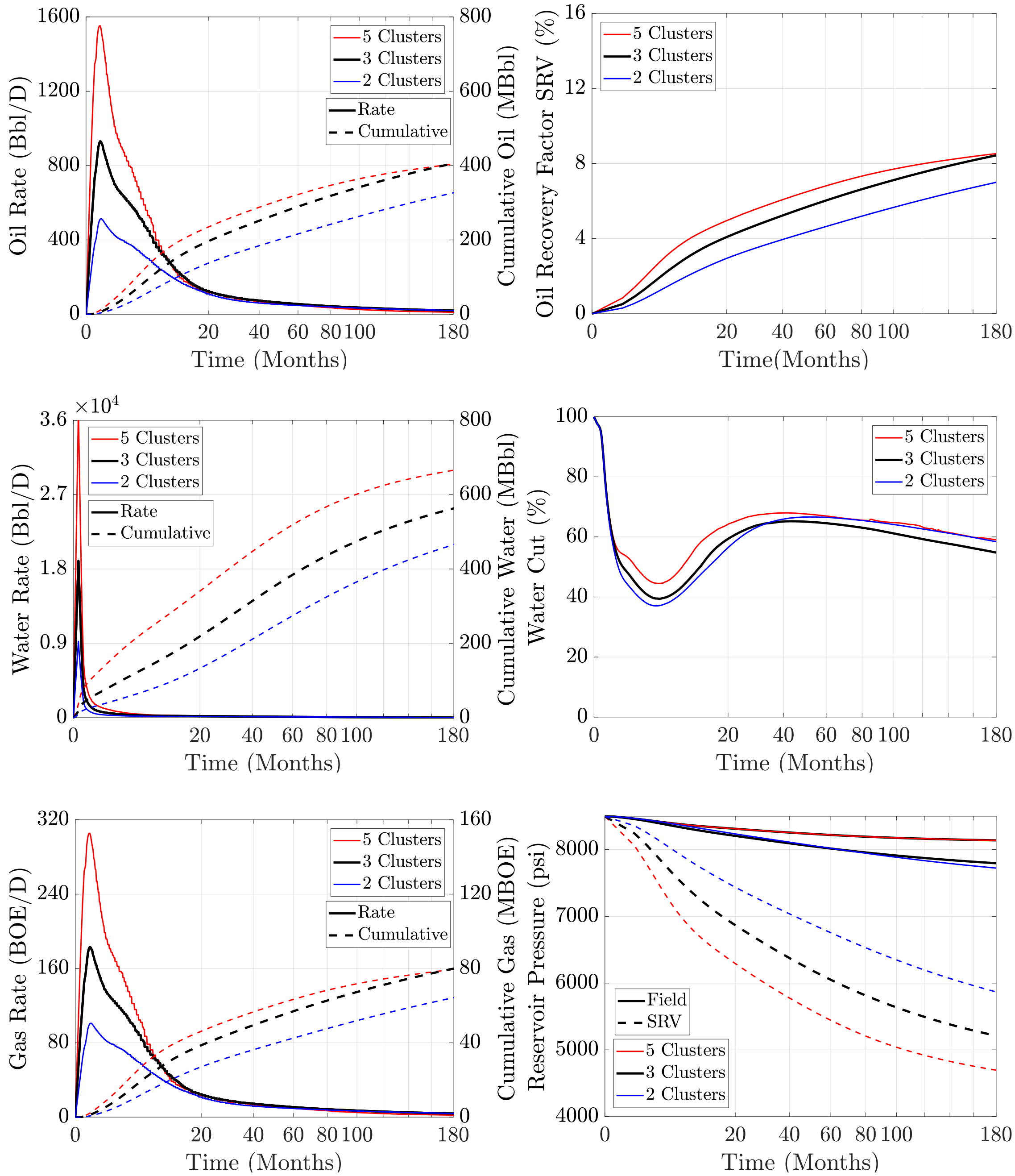

Figure 5.20: 15 years of reservoir fluid production obtained by varying the number of clusters per stage. Each of the clusters has a fracturing fluid volume of 190 m^3 (1200 bbls).

We performed a fundamental economic analysis by calculating the net present value (NPV) at different oil prices for each proposed scenario. This analysis evaluates the utility of the project [120]. Table 5.13 presents the parameters required to calculate the net present value (NPV), and Appendix A shows the equations applied for the economic evaluation. The project may be accepted if the NPV value is positive and rejected if the NPV value is negative. The break-even point is when the total investment has been paid, and the operators start to receive project profits. It occurs when the NPV value is zero.

Table 5.13: Parameters to calculate the net present value.

Parameter	Abbreviation	Unit	Value
Oil price	PRICE	$/bbl	5-100
Drilling cost	DRILL	$ million	3[a]
Completion cost	COMP	$ million	3-5[a]
Land cost	LAND	$ million	1[a]
Operating cost	OPECOST	$/Mbbl	30[a]
Royalty rate	R	Fraction/year	0.2[b,d]
Intangible to tangible cost	INTAN	Fraction/year	0.6[b]
Declining balance	DB	%	150[b]
Time period in which equipment is amortized	t	years	5[b]
Severance tax rate	SEVTAX	Fraction/year	0.046[c,e]
Corporate tax rate	CORPTAX	Fraction/year	0.35[b,c]
Discount rate	DR	%	5-10[b]

Sources: [a][121],[b][120],[c][122],[d][123],[e][124].

We assumed the drilling cost, completion cost, and land cost to calculate the capital expenditures. According to the EIA report [121], the drilling cost in U.S. shales ranges from $2 million to $3 million, and the completion cost varies from $3 million to $6 million. We assumed the drilling cost to be $3 million for all the cases because the wellbore length is the same, but we considered different completion costs. This is $3 million, $4 million, and $5 million for the scenarios with two, three and five clusters per stage, respectively. EIA also reported that the land cost might add $1 to $2 million per well [121]. In this study, the land cost is $1 million. According to Kaiser et al. [120], the royalty rate in Haynesville ranged from 20% to 28%. Based on that, we assumed a 20% royalty rate. We adopted a 150% declining balance for tangible assets (e.g. equipment) [120].

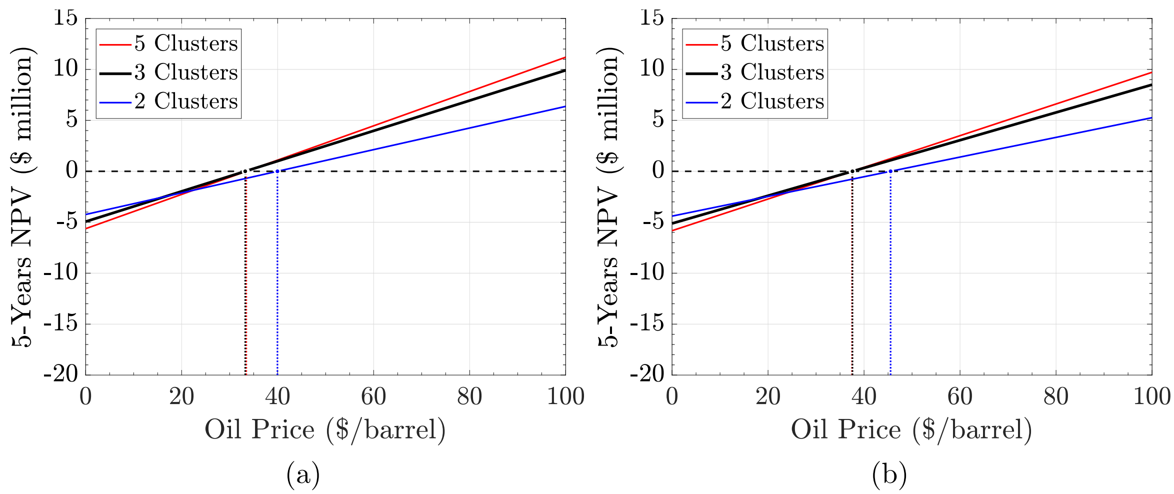

Figure 5.21: Net present value (NPV) at different oil prices for three different scenarios where the number of clusters per stage varies from two to five. The net present values were calculated at: (a) 5% discount rate and (b) 10% discount rate.

The resulting 5-year NPV plot (Figure 5.21) illustrates that the break-even points are about 33 $/bbl for scenarios with five and three clusters per stage and 40 $/bbl for the case with two clusters per stage at a 5% discount rate. The points increase to 38 $/bbl and 46 $/bbl at a 10% discount rate. In 2019, the average West Texas Intermediate (WTI) crude oil price was 57 $/bbl. By June 2020, the average price was 38 $/bbl. At these WTI crude oil prices, the stimulation jobs with five and three clusters per stage are profitable for both discount rates scenarios. The scenario with two clusters per stage is profitable at more expensive oil prices, still in the range of oil prices during the current year. The massive stimulation jobs generate sufficient initial hydrocarbon production. Operators have opted for completions with a higher number of clusters per stage to recover the initial investment faster, even though it harms long-term production.

5.3 Second Case: Vertical Hydraulic Fractures with Perpendicular Secondary Fractures

This scenario comprises three vertical, bi-wing, and symmetric hydrofractures with eight perpendicular secondary fractures (Figure 5.23). These fractures create an interconnected orthogonal hydrofracture network (Figure 5.22). It also has the orthogonal natural fracture network described in the reference numerical simulation case. The hydraulic fracture half-length is 230 m (750 ft), which is smaller than the fracture half-length of the reference case. The reduction in length occurs due to the initiation of secondary fractures and their interaction with primary hydrofractures. We assumed equal primary and secondary fracture aperture (7 mm or 0.024 ft). The fracturing fluid volume within the stimulated fractures is 12,700 m^3 (80,000 bbls) distributed in 22 stages.

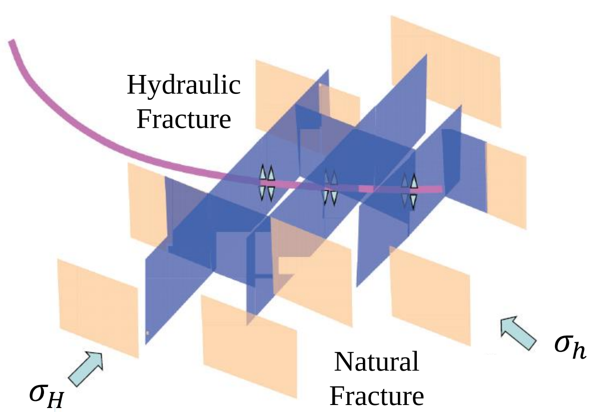

Figure 5.22: Orthogonal fracture network. Source:[58].

In this case, stimulation jobs reactivate pre-existing natural fractures and add complexity to hydrofracture geometry (Figure 5.22). Conditions such as the low horizontal differential stress and high organic content favor the interaction between primary hydrofractures and natural fractures. This scenario lacks hydraulically opened bedding planes, considering the large difference between the vertical and the minimum horizontal stress magnitudes.

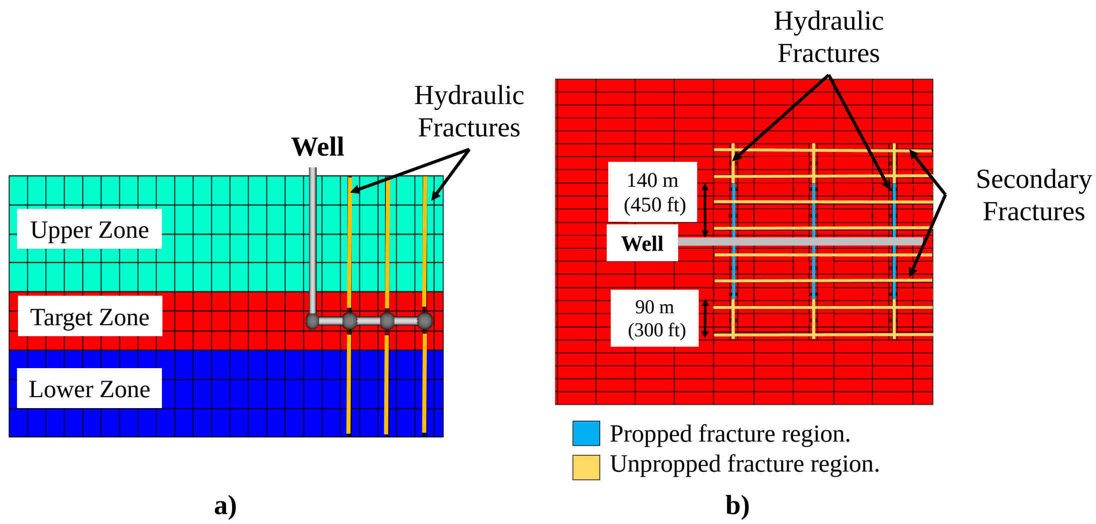

Figure 5.23: Vertical hydraulic fractures with perpendicular secondary fractures. a) Cross-view of the model along the wellbore and b) map view of the model.

5.3.1 The geomechanics effect of secondary fractures

Primary hydrofractures may interact with pre-existing natural fractures during stimulation jobs. This initiates and hydraulically opens secondary fractures. These fractures are sensitive to the increase in effective stress during hydrocarbon production due to a lack of proppant support. This study aims to assess the effect of secondary fracture closure on wellbore flow performance. We proposed different scenarios that apply the compaction curves shown in Figure 5.15 on the secondary hydrofractures.

Figure 5.24 shows a slight variation in water and hydrocarbon production with the change of secondary fracture closure rate. The results reveal a higher impact on initial production than on long-term production. The initial production increases with the fracture compressibility. In contrast, the fracture closure mechanism, combined with the high primary fracture conductivity, minimizes the secondary fracture compressibility's effect on long-term production. The ultimate oil recovery factor at 15 years is 7.8% and 8.5% for this scenario and the reference case. They differ because the primary fracture length decreases with the generation of secondary fractures.

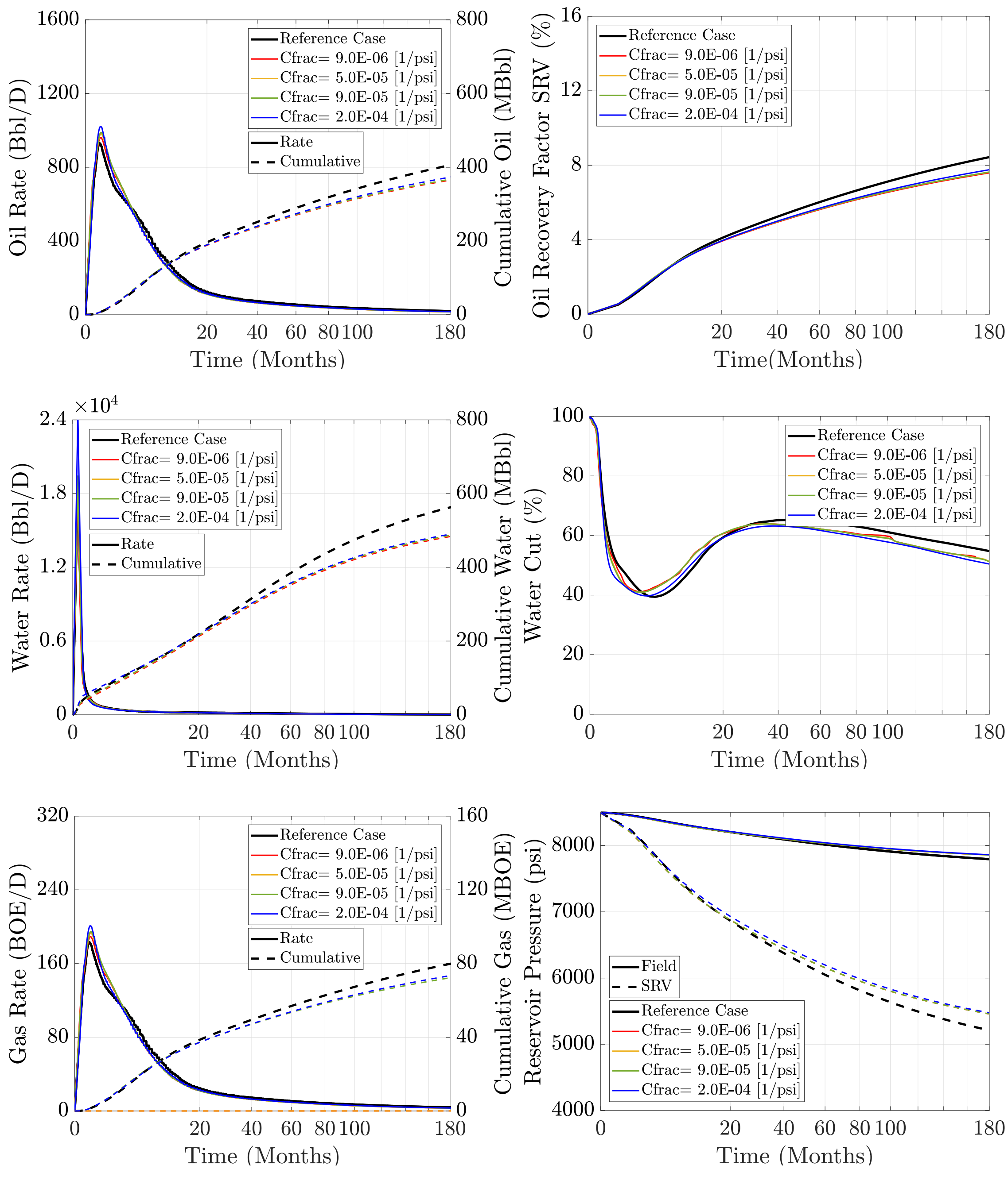

Figure 5.24: 15 years of reservoir fluid production obtained by varying the compaction curves applied to the secondary fractures. The reference case only has vertical, symmetrical and planar fractures (ideal case).

This study also shows that the generation of perpendicular secondary fractures enhances reservoir permeability and initial hydrocarbon production when they reach similar primary hydrofracture conductivity. Additionally, they reduce the propagation energy of primary hydrofractures, which reduces fracture aperture and length. Thus, they may negatively impact long-term hydrocarbon production. Furthermore, we can infer that proppant placement within secondary fractures may not improve hydrocarbon production.

5.3.2 The effect of the number of perpendicular secondary fractures

This sensitivity analysis evaluates the effect of the number of perpendicular secondary fractures on hydrocarbon production. We proposed three scenarios with 14, 8, and 6 secondary fractures, as shown in Figure 5.25. The three scenarios have a total hydraulic fracturing volume of 12,700 m^3 (80,000 bbls). We assumed equal primary and secondary fracture aperture. The apertures are 5 mm (0.018 ft), 7 mm (0.024 ft), and 8 mm (0.027 ft) for the scenarios with 14, 8, and 6 secondary fractures, respectively.

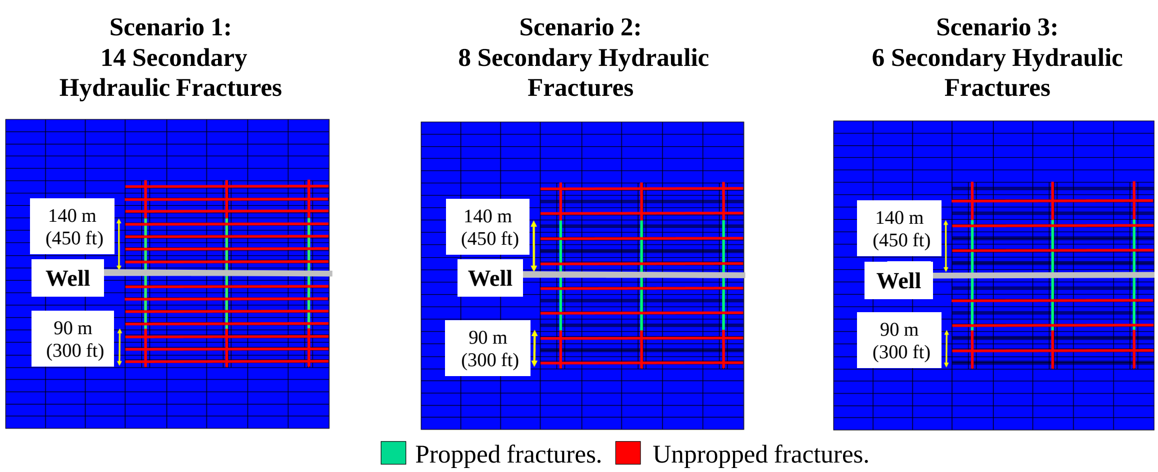

Figure 5.25: The three scenarios with varying numbers of secondary hydraulic fractures (map view).The red lines are the unpropped fractures and the green lines are the propped fractures.

The generation of perpendicular secondary fractures creates a complex hydraulic fracture system. Figure 5.26 illustrates that the number of secondary fractures enhances initial reservoir fluid production. However, they do not significantly impact the cumulative reservoir fluid production at 15 years. Table 5.14 compares the different parameters between the proposed scenarios and the reference case. It shows that the hydrocarbon rate peak increases between 7% and 22% with the generation of perpendicular secondary fractures during stimulation jobs. The water rate peak increases between 20% and 33%, depending on the number of secondary fractures. The generation of those fractures decreases the ultimate hydrocarbon and water production at 15 years by about 8% and 13%, respectively. The table shows that the ultimate reservoir fluid production at 15 years varies by less than 2% between the proposed scenarios.

Table 5.14: Comparison between the scenarios with 14, 8 and 6 secondary fractures and the scenario with only vertical hydraulic fractures (reference case).

Parameter	14 Perpendicular Secondary Fractures	8 Perpendicular Secondary Fractures	6 Perpendicular Secondary Fractures
Water Rate Peak [%]	33	29	20
Oil Rate Peak [%]	22	10	7
Gas Rate Peak [%]	22	10	7
Ultimate Water Production [%]	**-14**	**-13**	**-13**
Ultimate Oil Production [%]	**-6**	**-8**	**-9**
Ultimate Gas Production [%]	**-6**	**-8**	**-9**

This study shows that the generation of high-permeable flow conduits enhances reservoir permeability and mass transfer between the rock matrix and fractures. Thus, the initial reservoir fluid production increases with the number of secondary fractures. The lack of proppant within the conduits generates rapid fracture closure, but they remain permeable. The secondary fracture closure and the high primary fracture conductivity reduce the effect of the number of secondary fractures on the cumulative fluid production at 15 years.

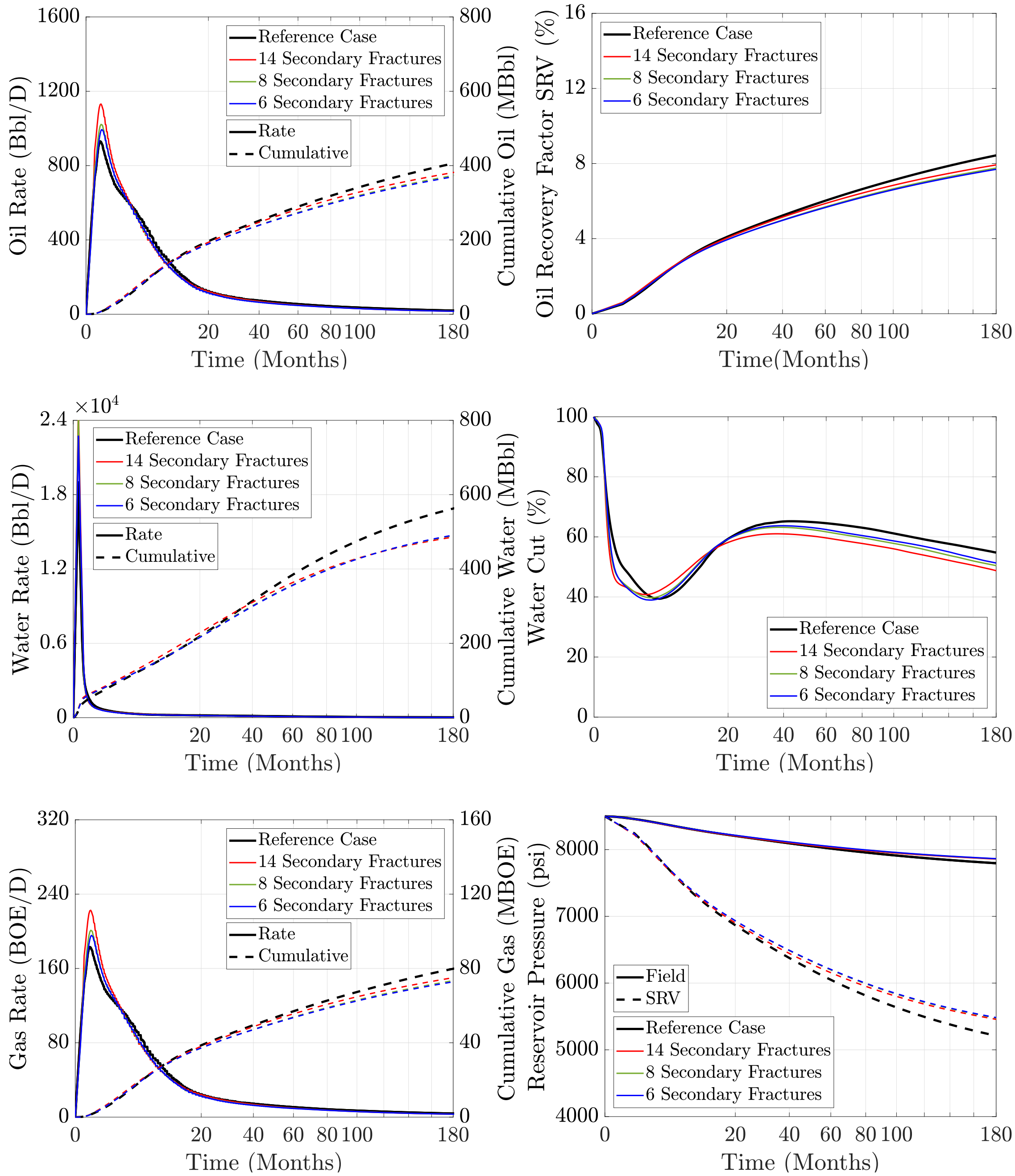

Figure 5.26: 15 years of reservoir fluid production obtained by varying the number of perpendicular secondary fractures. The reference case only has vertical, symmetrical and planar fractures (ideal case).

5.4 Third Case: Vertical Hydraulic Fractures with Horizontal Bedding Plane Fractures.

The third simulation model comprises three vertical and planar hydrofractures with two horizontal bedding plane fractures (Figure 5.28). It also has the orthogonal natural fracture network described in the reference numerical simulation model. The primary fracture half-length is 230 m (750 ft), and they are equally spaced at 30 m (100 ft) along the horizontal wellbore. Furthermore, we considered equal primary and bedding plane fracture aperture (4 mm or 0.013 ft). The total fracturing fluid volume is 12,700 m^3 (80,000 bbls) distributed in 22 stages. The size of the stimulation job is the same as the other two simulation scenarios presented before.

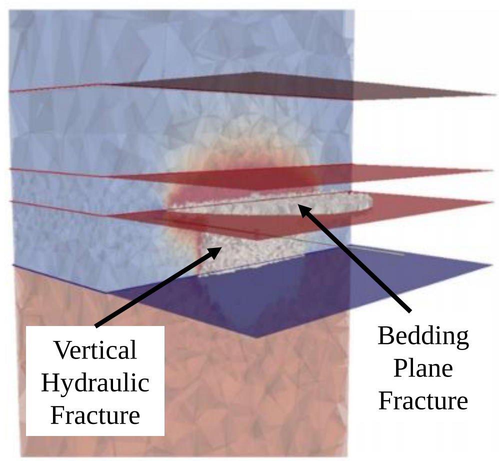

Figure 5.27: Horizontal bedding plane fractures. Source:[22]

In this case, the generation of horizontal bedding plane fractures increases the complexity of the hydrofracture geometry (Figure 5.27). Horizontal fractures propagate parallel to the minimum horizontal stress direction. This fracture geometry may occur in shale plays with transitional strike-slip to reverse stress regime conditions when the vertical and minimum horizontal stress magnitudes are similar to the least principal stress magnitude [21]. Such conditions have been reported in some unconventional source rock plays (e.g., Marcellus shale in southern West Virginia and

Tuwaiq Mountain formation in Jafurah basin, Saudi Arabia [21, 29, 30]).

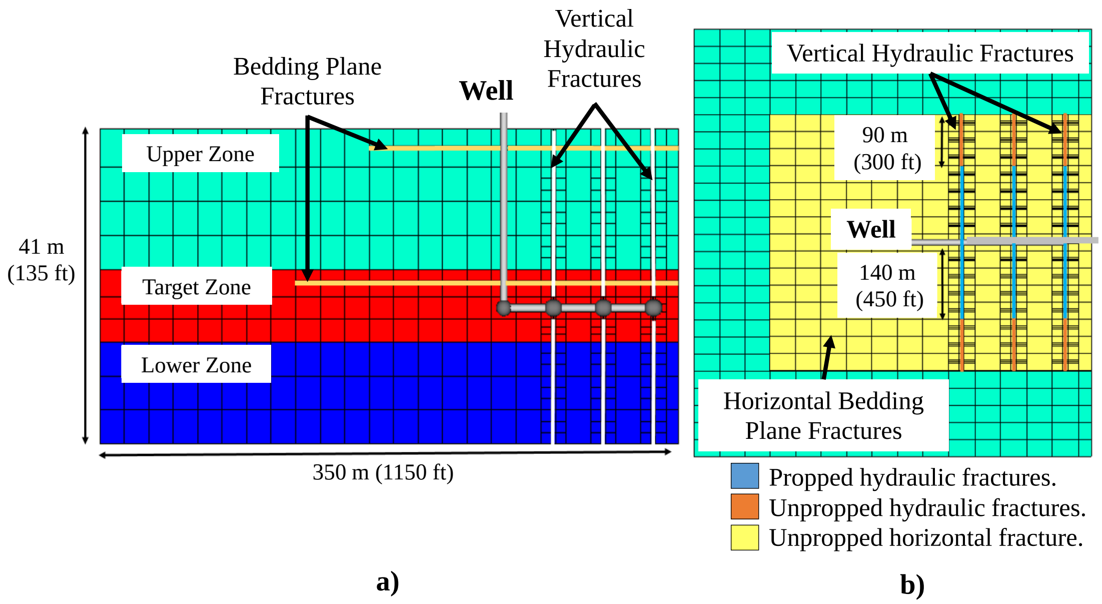

Figure 5.28: Vertical hydraulic fractures with bedding plane fractures. a) Cross-view of the model along the wellbore and b) map view of the model.

The high pore pressure in shale plays reduces the effective stress magnitudes [20]. High pore pressure and high organic content generate low differential stress conditions. This scenario considers high horizontal differential stress conditions that hinder the reactivation of pre-existing natural fractures. In contrast, a low horizontal and vertical differential stress, low-strength cement of the laminations, and high pumping rate promote the interaction between primary hydrofractures and horizontal bedding planes [13, 62]. The bedding planes fail by debonding, and hydraulically open during fluid injection [72]. We assumed unpropped horizontal bedding plane fractures. Thus, they rapidly close during the first months of reservoir fluid production.

This hydraulic fracture system requires simultaneous fracture growth in the vertical and horizontal directions. The fracturing fluid propagates more easily along laminations than across them due to high horizontal permeability in shale plays [53]. Despite this, hydrofractures can cross laminations and continue their vertical propagation when the fracture's pressure is sufficiently high [75].

5.4.1 The effect of bedding plane fracture closure

Horizontal bedding plane fractures are sensitive to the increase in effective stress during reservoir fluid production. This study evaluates the effect of bedding plane fracture closure on wellbore flow performance. We carried out this study by assigning different compaction curves to the bedding plane fractures, as shown in Figure 5.29. The blue curves assign a rapid closure rate to the fractures that are characteristic of unpropped fractures. The other two compaction curves assign a lower fracture closure rate, which simulates partially propped fractures. The fracture closure rate increases with fracture compressibility.

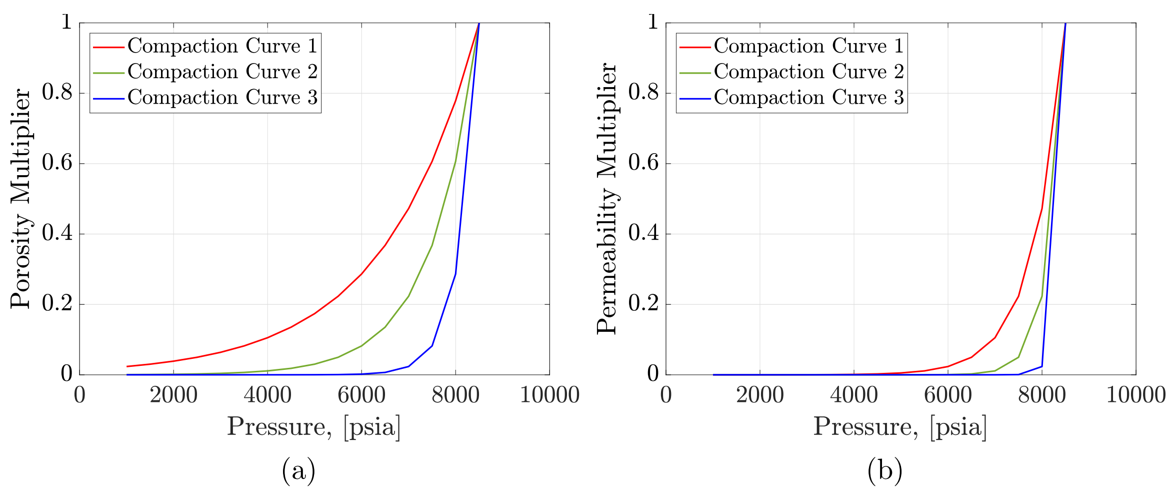

Figure 5.29: Different compaction curves applied to the bedding plane fractures to simulate fracture closure. (a) Porosity multipliers and (b) permeability multipliers.

Figure 5.30 shows that horizontal bedding plane fracture compressibility slightly influences water production, while it significantly impacts hydrocarbon production. The results illustrate that hydrocarbon production increases with fracture stiffness. An efficient proppant placement is unlikely to occur in horizontal fractures, which makes them highly compressible. Thus, the compaction curves that better simulate them are the blue curves in Figure 5.29. The oil recovery factor varies between 7.6% and 9.6% with the reduction of horizontal fracture compressibility.

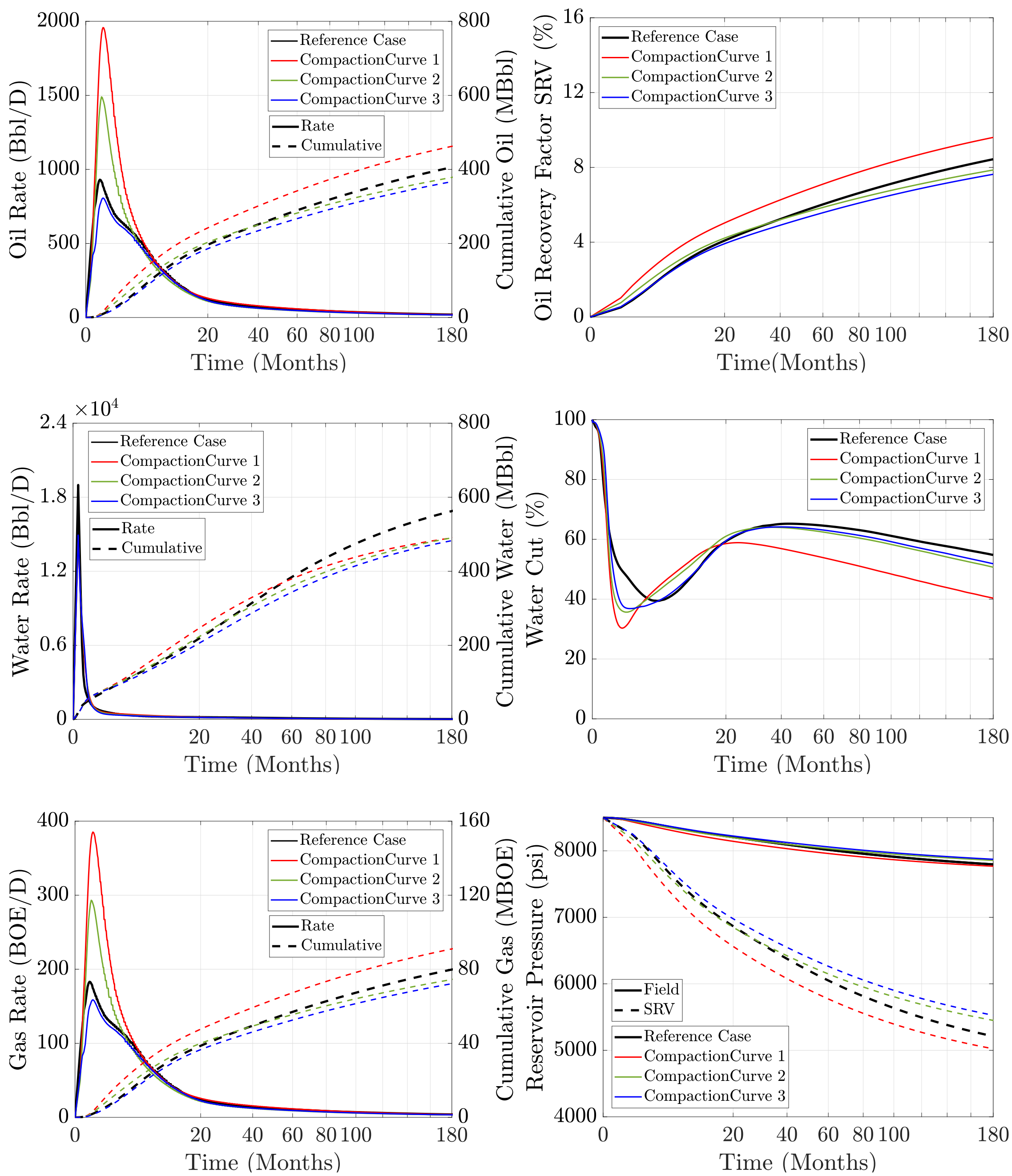

Figure 5.30: 15 years of reservoir fluid production obtained by varying the compaction curves assigned to the horizontal bedding plane fractures. The reference case only comprises vertical and planar hydraulic fractures. The blue curves illustrate a case with highly compressible horizontal fractures while the red lines describe a case with less compressible horizontal fractures.

Table 5.15 presents a comparison between the proposed scenarios and the reference case. The results revealed that the generation of horizontal fractures reduces water rate peak by about 22% and the cumulative water production at 15 years by 13%. Despite this, the horizontal fracture compressibility impacts water production by less than 2%. Furthermore, the creation of horizontal fractures significantly affects hydrocarbon production. Unpropped horizontal fractures decrease initial hydrocarbon production by 13% while it increases by up to 110% with partially propped fractures. The cumulative hydrocarbon production increases with a reduction in fracture compressibility. Unpropped horizontal fractures reduce cumulative hydrocarbon production at 15 years by 10%.

Table 5.15: Comparison between the scenarios with different compaction curves and the scenario with only vertical and planar fractures (Reference case).

Parameter	Compaction Curves 1	Compaction Curves 2	Compaction Curves 3
Water Rate Peak [%]	**-23**	**-22**	**-21**
Oil Rate Peak [%]	110	60	**-13**
Gas Rate Peak [%]	110	60	**-13**
Ultimate Water Production [%]	**-13**	**-13**	**-14**
Ultimate Oil Production [%]	14	**-7**	**-10**
Ultimate Gas Production [%]	14	**-7**	**-10**

Proppant placement into horizontal fractures is difficult due to their narrow aperture and the fracturing fluid's low-viscosity. The lack of proppant within those fractures generates rapid fracture closure. This fact disconnects a large fracture volume and harms the hydrocarbon production.

5.4.2 The effect of horizontal bedding plane fracture position

This sensitivity analysis assesses the effect of the horizontal bedding plane fracture (BPF) position on wellbore flow performance. We proposed three scenarios where we varied the position of those fractures (Figure 5.31). All the scenarios have two bedding plane fractures in the upward wing of the primary hydrofracture. The first scenario has a horizontal fracture near the wellbore and the other on the primary hydraulic fracture height. The second scenario has both horizontal fractures near the wellbore, and the last case has them on the primary hydraulic fracture height (far from wellbore).

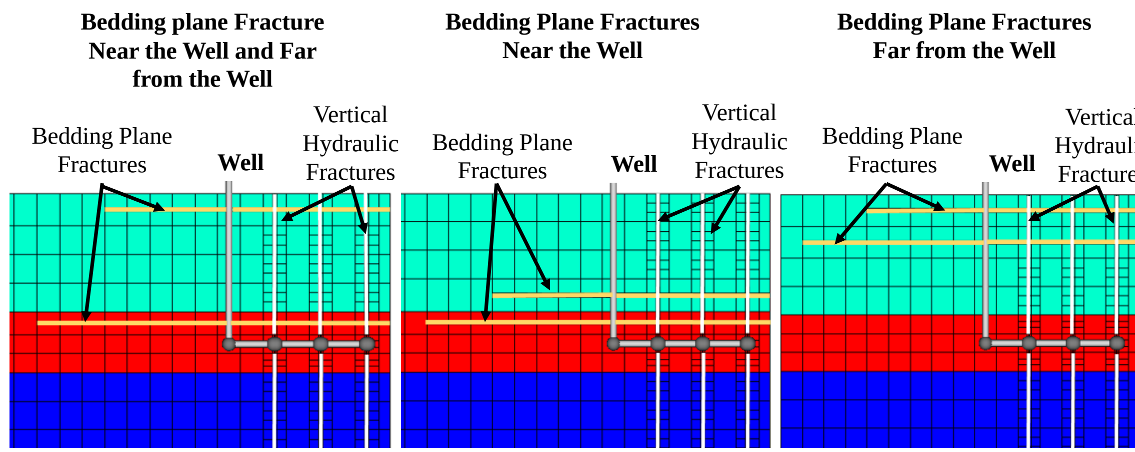

Figure 5.31: Three different scenarios with varied bedding plane fracture positions (Cross-view along the wellbore).

Figure 5.32 presents the results of 15 years of reservoir fluid production for all the proposed scenarios. The results show that the horizontal fracture position slightly impacts the wellbore flow performance. Thus, it is not a critical parameter on reservoir fluid simulation. The effect is higher at early-times before the fracture closure. Furthermore, the results also show the negative impact on reservoir fluid production generated by horizontal fractures. The initial water production decreases by 40%, and the cumulative water production at 15 years differs by 15% compared to the reference case (only vertical fractures). The oil recovery factor at 15 years is 7.6% for the scenarios with horizontal fractures while it is 8.5% for the reference case. Based on the literature reviewed, the intersection of a second bedding plane often stops vertical fracture propagation [53]. Also, the horizontal fracture volume decreases with an increase of the distance to the injection point [17]. Thus, the first scenario presents a more realistic fracture geometry.

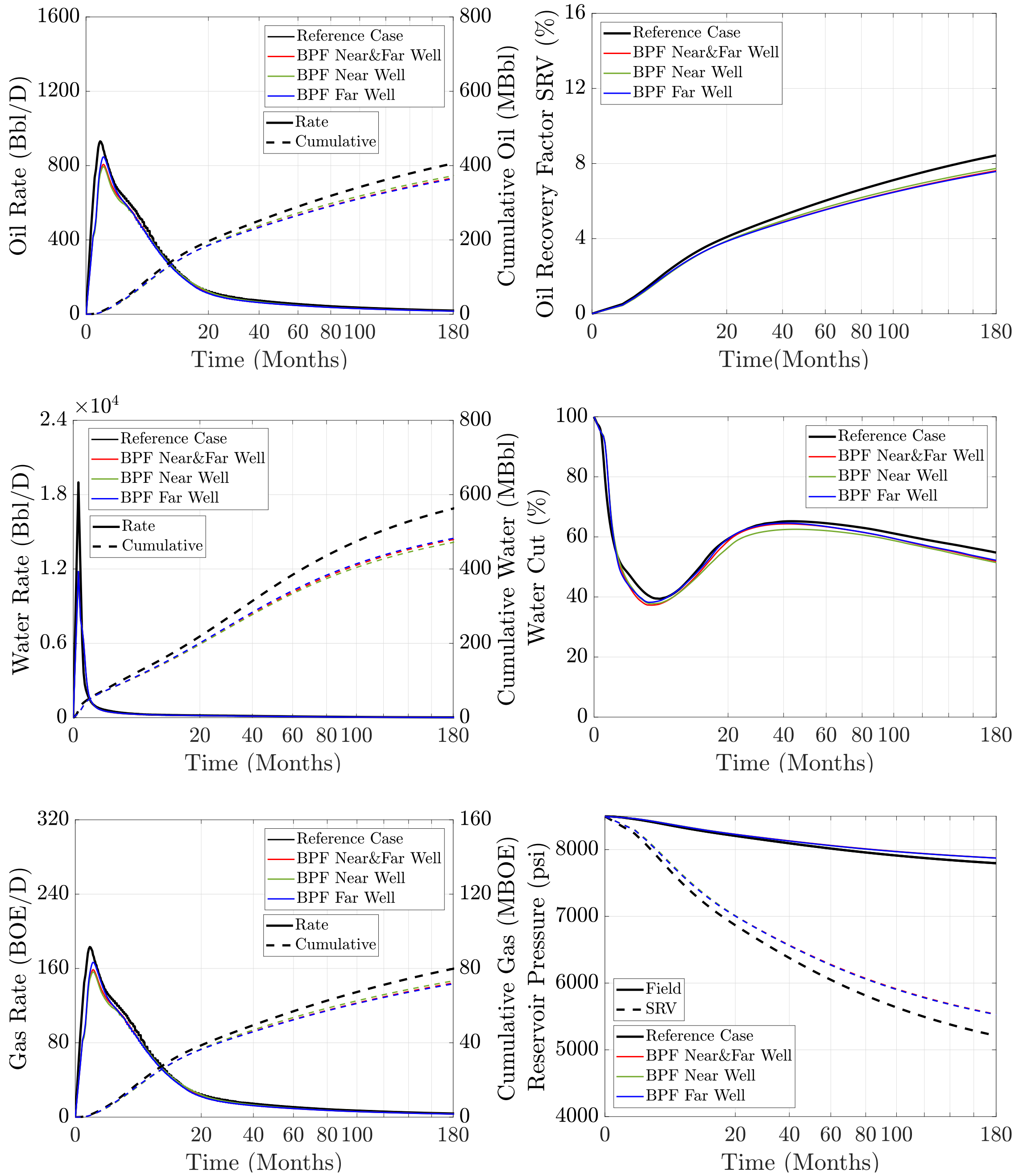

Figure 5.32: 15 years of reservoir fluid production obtained by varying the horizontal bedding plane fracture (BPF) position. All the scenarios have the horizontal fractures in the upward wing of the hydraulic fractures. The first scenario has a bedding plane fracture near the wellbore and the other one far from the wellbore (red line). The second scenario has horizontal fractures near the wellbore (green line). The last scenario has the horizontal fractures (BPF) far from the wellbore (blue line). The reference case only has vertical and planar hydraulic fractures.

5.4.3 The effect of number of horizontal bedding plane fractures

This study evaluates the effect of the number of horizontal bedding plane fractures on wellbore flow performance. We proposed three scenarios with a varied number of horizontal fractures, as shown in Figure 5.33. All three scenarios have a total fracturing fluid volume of 12,700 m^3 (80,000 bbls). The fracture apertures are 3 mm (0.009 ft), 4 mm (0.013 ft) and 6 mm (0.019 ft) for the scenarios with three, two and one horizontal fractures, respectively.

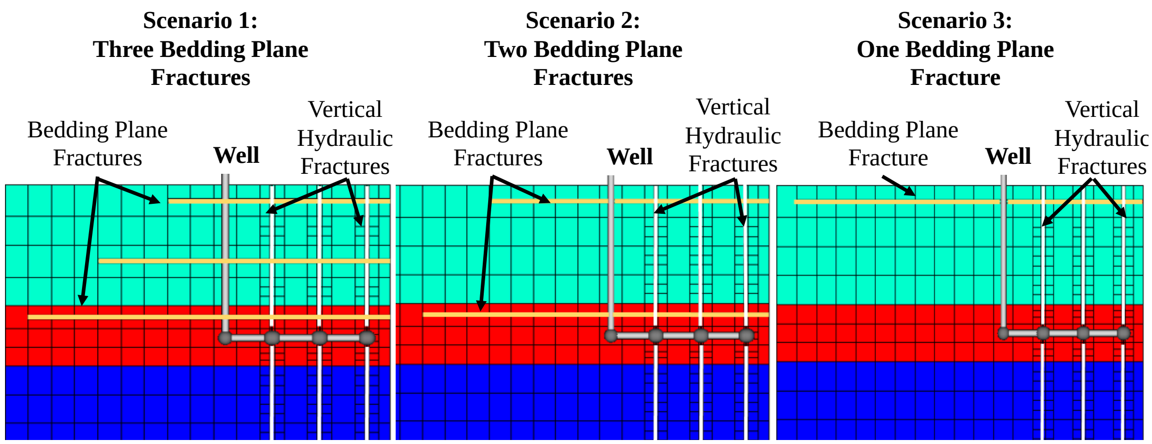

Figure 5.33: Three different scenarios, each consisting of a varied number of bedding plane fractures (Cross-view along the wellbore).

Figure 5.34 shows that the number of horizontal fractures significantly impacts the initial reservoir fluid production while it does not affect cumulative production at 15 years. The initial reservoir fluid production increases with the number of horizontal fractures. These fractures enhance reservoir permeability and mass transfer between matrix and fractures. The horizontal fracture closure disconnects an enormous stimulated volume that harms cumulative reservoir fluid production. The generation of horizontal fractures reduces the oil recovery factor at 15 years by about 10%.

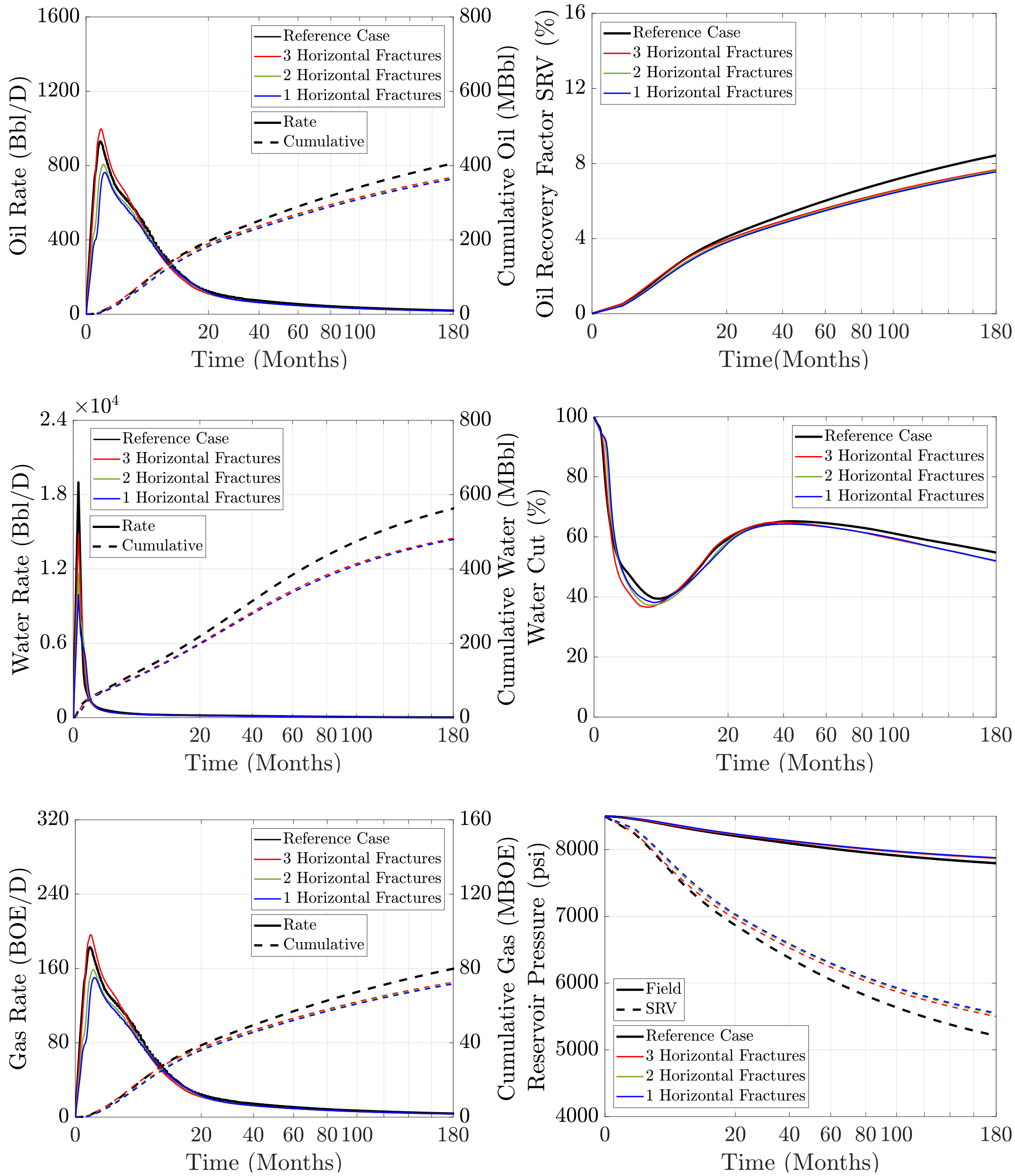

Figure 5.34: 15 years of reservoir fluid production obtained by varying the number of horizontal bedding plane fractures. The reference case only has three vertical and planar hydraulic fractures.

Table 5.16 compares the scenarios with horizontal bedding plane fractures and the reference case, which only has vertical hydraulic fractures. The table shows that the generation of horizontal fractures reduces reservoir fluid production. The initial reservoir fluid production increases with the number of horizontal fractures. The generation of a single horizontal fracture decreases the water rate peak by 48%, while it reduces by 22% with the presence of three horizontal fractures. Furthermore, the initial hydrocarbon production decreases by between 13% and 18% with the generation of two and one horizontal fractures, respectively. It can increase by up to 7% when three horizontal fractures are hydraulically opened. The opening of horizontal fractures decreases the cumulative water production at 15 years by 15% and the cumulative hydrocarbon production by 10%. The difference in cumulative reservoir fluid production at 15 years is less than 2% for the proposed scenarios with horizontal fractures.

Table 5.16: Comparison between the scenarios with three, two and one horizontal fractures and the scenario with only vertical hydraulic fractures.

Parameter	3 Bedding plane fractures	2 Bedding plane fractures	1 Bedding plane fracture
Water Rate Peak [%]	**-22**	**-39**	**-48**
Oil Rate Peak [%]	7	**-13**	**-18**
Gas Rate Peak [%]	7	**-13**	**-18**
Ultimate Water Production [%]	**-14**	**-15**	**-15**
Ultimate Oil Production [%]	**-9**	**-10**	**-10**
Ultimate Gas Production [%]	**-9**	**-10**	**-10**

In conclusion, the initial reservoir fluid production increases with the number of horizontal fractures when the primary hydrofractures are well propped and highly conductive. The horizontal fracture closure harms cumulative fluid production. The stresses near the intersection between bedding planes and primary hydrofractures and a narrow horizontal fracture aperture complicate the proppant placement into those fractures. Thus, horizontal fractures are responsive to the reduction of pore pressure that leads to rapid closure and low wellbore flow performance.

5.4.4 The effect of loss in vertical hydraulic fracture conductivity

Primary hydraulic fractures may interact with bedding planes during stimulation jobs in shales with high pore pressure and small differential stress. This interaction significantly enhances fracturing fluid leak-off into the discontinuities and reduces the propagation energy of the primary hydrofractures. This fact reduces the fracture aperture, which may generate premature screen-out of proppant and poor proppant placement. This study aims to analyze the effect of loss in primary hydrofracture conductivity on wellbore flow performance. We proposed three scenarios with different primary fracture permeability. The permeabilities considered are 100 mD, 500 mD, 1000 mD, and 2000 mD. All the scenarios have the same horizontal fracture properties, and total fracturing fluid volume (12,700 m^3 or 80,000 bbls).

Figure 5.35 illustrates that primary hydrofracture permeability is a critical parameter during shale reservoir simulation. The reservoir fluid production significantly increases with hydrofracture permeability. The impact is higher on initial production than on cumulative production. Hydrofracture permeability over 500 mD slightly influences the cumulative reservoir fluid production at 15 years. The oil recovery factor varies between 7.2% and 7.6% for the scenarios with fracture permeability higher than 500 mD. The scenario with a permeability of 100 mD has an oil recovery factor of 5.9%.

Table 5.17 presents the comparison of different parameters between the proposed scenarios with horizontal fractures, and the reference case, which only has vertical hydraulic fractures. The generation of horizontal fractures significantly decreases the initial reservoir fluid production. It varies by about 20% between the proposed scenarios with horizontal fractures. In this study, the presence of horizontal fractures reduces the ultimate reservoir fluid production at 15 years by about 15% when the vertical fracture permeability ranges between 500 mD and 2000 mD. It reduces by up to 30% when the fracture permeability is 100 mD.

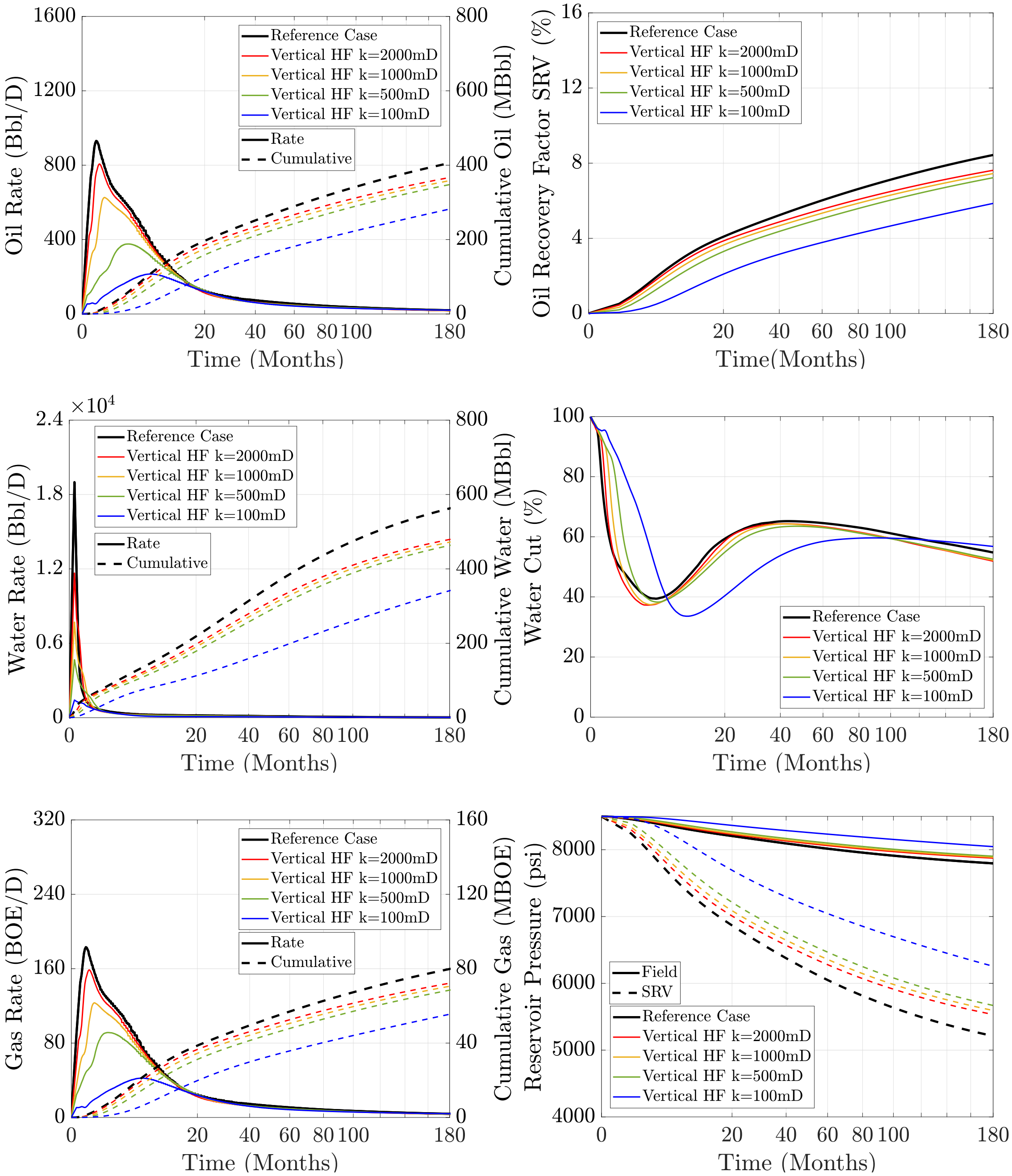

Figure 5.35: 15 years of reservoir fluid production obtained by varying the vertical hydraulic fracture (HF) permeability. The reference case only has three vertical and planar hydraulic fractures.

In conclusion, the interaction between hydrofractures and bedding planes reduces the primary fracture aperture and generates poor proppant placement. Thus, it reduces primary fracture permeability that significantly harms hydrocarbon production. This study illustrates more realistic scenarios that consider the loss in primary fracture conductivity produced by horizontal fracture generation.

Table 5.17: Comparison between the scenarios with varied vertical hydrofracture (HF) permeability and the scenario with only vertical hydraulic fractures.

Parameter	Vertical HF k=2000 mD	Vertical HF k=1000 mD	Vertical HF k=500 mD	Vertical HF k=100 mD
Water Rate Peak [%]	**-39**	**-59**	**-75**	**-93**
Oil Rate Peak [%]	**-13**	**-33**	**-60**	**-77**
Gas Rate Peak [%]	**-13**	**-33**	**-60**	**-77**
Ultimate Water Production [%]	**-15**	**-16**	**-18**	**-39**
Ultimate Oil Production [%]	**-10**	**-12**	**-14**	**-30**
Ultimate Gas Production [%]	**-10**	**-12**	**-14**	**-30**

Chapter 6

Discussion

Operators have applied massive stimulation jobs in shale plays to produce at economical rates. The mean fracturing fluid volume normalized by the horizontal wellbore length is about 24 m^3/m in U.S. shales [24]. Similarly, based on the literature reviewed, we estimate that 12 m^3 of fracturing fluid was injected per wellbore meter in the Jafurah basin in Saudi Arabia [25, 26, 27]. The large fluid volume enhances the interaction between hydrofractures and discontinuities and generates complex hydrofracture geometries. Thus, 90% of this fluid is retained in the rock discontinuities, which can result in undesirable hydrocarbon production [125]. The formation of complex fracture geometries is expected to occur in shale reservoirs with high pore pressure and small differential stress. Several shale plays have reported high pore pressure conditions (more than 0.45 psi/ft) such as Eagle Ford (U.S.), Haynesville (U.S.), Marcellus (U.S.), Duvernay (Canada), Silurian (China) and Tuwaiq Mountain Formation (Saudi Arabia) [126, 25, 30].

This thesis aims to study the effect of three hydraulic fracture geometries on wellbore flow performance in overpressured shale oil plays using a commercial reservoir simulator. It also examines the effect of different natural fracture and discontinuity properties on reservoir fluid production. It is a parametric investigation which assumes an idealized natural fracture network and hydraulic fracture system. Despite this, the reservoir simulation results obtained from this study enable us to understand the impact of complex fracture geometries on hydrocarbon production.

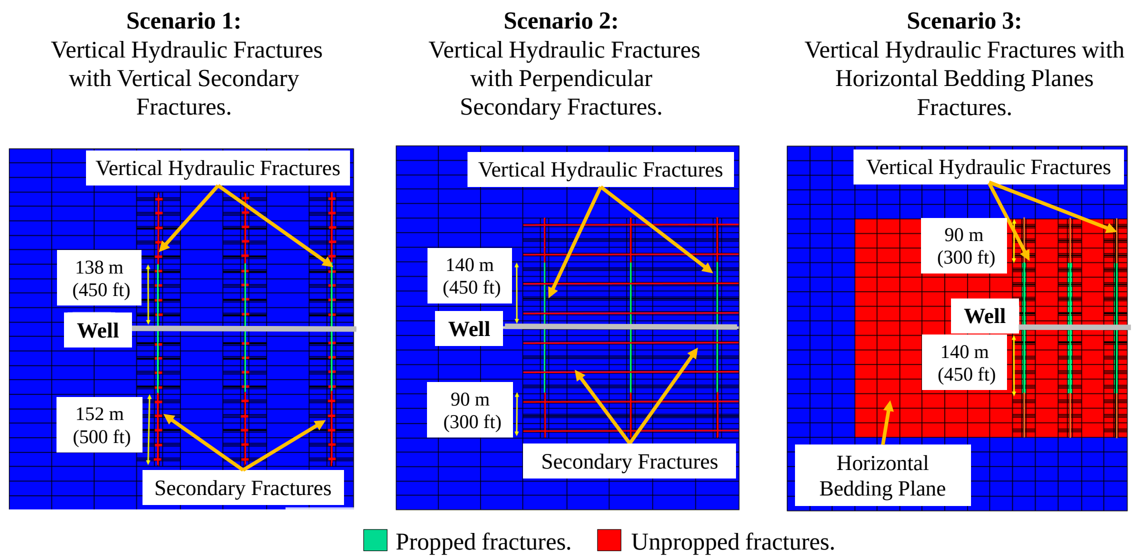

Figure 6.1: Map view of three hydrofracture geometries (scenarios). The first scenario is the reference case, which only has three vertical hydraulic fractures. The second scenario comprises three vertical hydraulic fractures and eight perpendicular secondary fractures. The last scenario has 3 vertical hydraulic fractures and 2 horizontal bedding plane fractures.

The first fracture geometry (reference scenario) comprises three vertical, bi-wing, and symmetric hydraulic fractures with small vertical secondary fractures. This scenario represents an ideal and the most common fracture shape studied during fracture treatment designs. In this case, a high horizontal and vertical differential stress impedes the interaction between hydrofractures and discontinuities. Despite this, a net pressure higher than the horizontal stress difference and the tensile strength of the rock, combined with a high pumping rate, reactivate and open small secondary fractures [81].

The second fracture geometry consists of three vertical, bi-wing hydraulic fractures with eight perpendicular secondary fractures. In this scenario, the stimulation jobs reactivate pre-existing natural fractures and add complexity to the hydrofracture system. Low horizontal differential stress and high organic content favor the interaction between primary hydrofractures and natural fractures. Thus, they create an interconnected orthogonal hydrofracture network. The case lacks horizontal fractures due to a markedly high vertical stress magnitude. The last fracture geometry comprises three vertical and planar hydrofractures with two horizontal bedding plane fractures. This is a particular case that may be generated in shale reservoirs with high pore pressure and small differential stress. The three scenarios have a total fracturing fluid volume of 12,700 m^3 (80,000 bbls). We considered a hydraulic fracture aperture of 9 mm (0.031 ft), 7 mm (0.024 ft), 4 mm (0.013 ft) for the scenarios with only vertical fractures, vertical fractures with perpendicular secondary fractures, and vertical fractures with horizontal fractures, respectively (Figure 6.1).

Figure 6.2 and Figure 6.3 show the wellbore flow performance of the proposed scenarios. Compared to the reference scenario, the results show that the reactivation of pre-existing natural fractures enhances the initial reservoir fluid production, while the generation of horizontal fractures harms the initial production. The results also illustrate that the interaction between hydrofractures and discontinuities reduces the cumulative reservoir fluid production at 15 years. Fracture interactions favor fracturing fluid leak-off into the discontinuities and reduce primary fracture length and aperture. After fracture closure, the stimulated discontinuities close due to lack of proppant. This reduces the stimulated reservoir volume and harms long-term fluid production.

The simulation scenarios in Figure 6.2 assume an efficient proppant placement and high conductivity in primary hydrofractures. The primary fracture permeability is 2000 mD in all scenarios. Therefore, cumulative fluid production slightly differs between the scenario with secondary fractures and the scenario with horizontal fractures. Table 6.1 compares the different parameters between the three proposed scenarios. It shows that the generation of perpendicular secondary fractures increases the initial water production by 29% and the initial hydrocarbon production by 10%. These fractures are highly conductive pathways that enhance reservoir permeability. Despite this, the poorly propped secondary fractures close after few months of production, but they retain some conductivity. Thus, it reduces the cumulative reservoir fluid production at 15 years by about 10% compared to the reference case.

On the other hand, the presence of horizontal bedding plane fractures reduces the initial water production by 40% and the initial hydrocarbon production by 13%. In this case, the unpropped horizontal fractures experience a rapid closure when production starts. Thus, it disconnects a huge stimulated reservoir volume that harms the wellbore flow performance. The ultimate oil recovery factor at 15 years is about 7.6%. The scenario with stimulated perpendicular natural fractures has the same recovery factor because we considered the same primary fracture length and conductivity in both scenarios. The reference case has an ultimate oil recovery factor of 8.5%.

Table 6.1: Comparison between the scenarios with secondary fractures, horizontal bedding plane fractures, and the reference case (only vertical hydraulic fractures) when all the scenarios have the same vertical hydraulic fracture permeability (2000 mD).

Parameter	3 Vertical HF + 8 Secondary Fractures	3 Vertical HF + 2 Horizontal Fractures
Water Rate Peak [%]	29	**-40**
Oil Rate Peak [%]	10	**-13**
Gas Rate Peak [%]	10	**-13**
Ultimate Water Production [%]	**-13**	**-15**
Ultimate Oil Production [%]	**-8**	**-10**
Ultimate Gas Production [%]	**-8**	**-10**

The interaction between hydrofractures and bedding planes reduces the primary fracture aperture and generates poor proppant placement. Therefore, we considered the loss in primary fracture conductivity caused by horizontal fracture generation to simulate the third scenario shown in Figure 6.3. In this scenario, the vertical hydraulic fracture permeability is reduced by 90% (200 mD). It illustrates more realistic results of wellbore flow performance obtained from shale plays with high pore pressure and small differential stress. The results show that horizontal fracture generation significantly reduces reservoir fluid production. In this case, the ultimate oil recovery factor at 15 years is 6.7%.

Table 6.2 compares the different parameters between the three proposed scenarios. The scenario with horizontal fractures has a primary fracture permeability of 200 mD, and the other two scenarios have a primary fracture permeability of 2000 mD. The results show that the presence of horizontal fractures reduces the initial water production by about 80% and the initial hydrocarbon production by 55% compared to the reference case. The cumulative hydrocarbon production at 15 years is reduced by 20%. In this case, the rapid fracture closure and the low primary fracture conductivity harms the reservoir fluid production.

Table 6.2: Comparison between the scenarios with secondary fractures, horizontal bedding plane fractures, and the reference case (only vertical hydraulic fractures) when the scenario with horizontal bedding plane fractures considers 90% reduction in the vertical hydraulic fracture permeability.

Parameter	3 Vertical HF + 8 Secondary Fractures	3 Vertical HF + 2 Horizontal Fractures
Water Rate Peak [%]	29	**-84**
Oil Rate Peak [%]	10	**-55**
Gas Rate Peak [%]	10	**-55**
Ultimate Water Production [%]	**-13**	**-32**
Ultimate Oil Production [%]	**-8**	**-20**
Ultimate Gas Production [%]	**-8**	**-20**

In summary, the reactivation of perpendicular natural fractures and the generation of horizontal fractures negatively impact the cumulative fluid production. Compared to the reference scenario, the generation of perpendicular secondary fractures increases the initial hydrocarbon production by 10%, while the horizontal bedding plane fractures reduce hydrocarbon production by 55%. It is important to consider the reduction in primary fracture conductivity during reservoir simulation when the fracture geometry comprises horizontal fractures. The generation of these fractures reduces the primary fracture aperture and produces poor proppant placement.

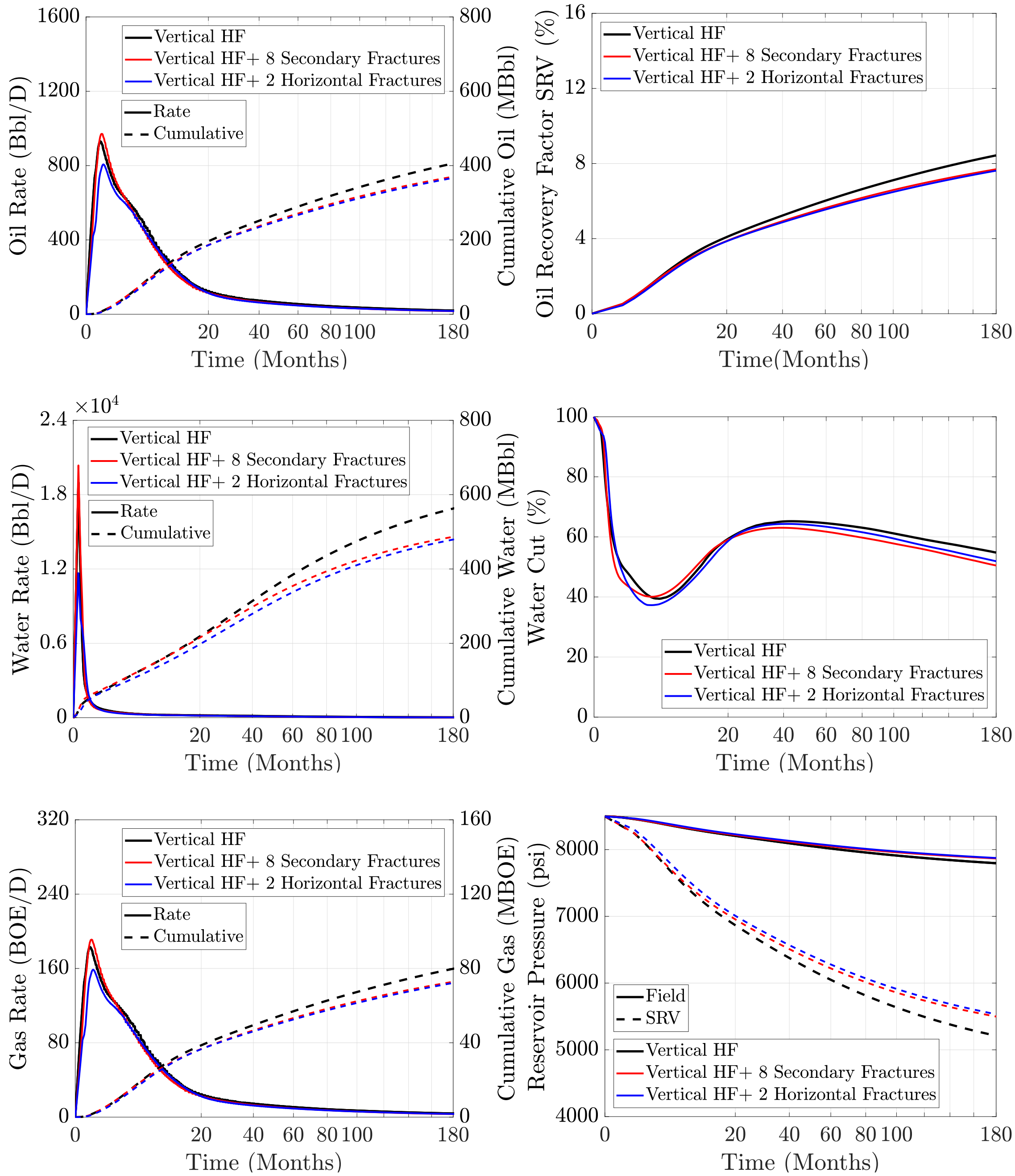

Figure 6.2: 15 years of reservoir fluid production obtained by varying the hydraulic fracture geometry. The first scenario is the reference case, which only has three vertical hydraulic fractures (black line). The second scenario has three vertical hydraulic fractures and eight perpendicular secondary fractures (red line). The last scenario has three vertical hydraulic fractures and two horizontal bedding plane fractures (blue line). All the scenarios have equal vertical hydraulic fracture permeability (2000 mD).

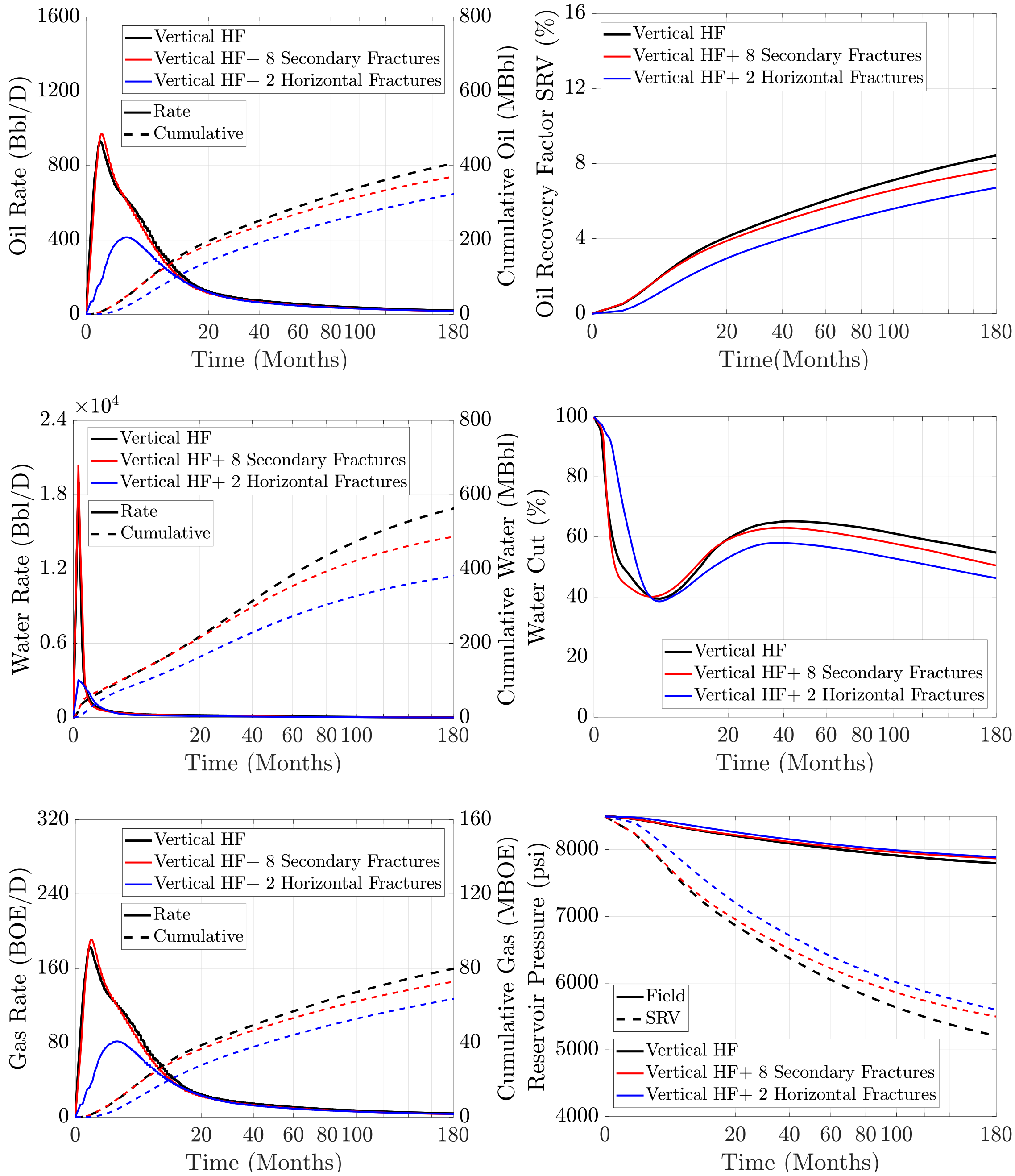

Figure 6.3: 15 years of reservoir fluid production obtained by varying the hydraulic fracture geometry. The first scenario is the reference case, which only has three vertical hydraulic fractures (black line). The second scenario has three vertical hydraulic fractures and eight perpendicular secondary fractures (red line). The last scenario has three vertical hydraulic fractures and two horizontal bedding plane fractures (blue line). The scenario with only vertical hydraulic fractures and the scenario with additional reactivated natural fractures have a vertical hydraulic fracture permeability of 2000 mD. The scenario with horizontal fractures has a vertical hydraulic fracture permeability reduced by 90% (200 mD).

This thesis presents the importance of understanding the possible hydraulic fracture geometry generation based on reservoir conditions, especially in reservoirs with high pore pressure and small differential stress. These reservoirs favor the generation of complex hydraulic fracture systems due to the interaction between the primary hydraulic fractures and reservoir discontinuities. The results illustrate that the assumption of vertical and planar hydraulic fracture geometry in these reservoirs overestimates the hydrocarbon production.

Chapter 7

Conclusions

This section summarizes the key results obtained in this study. Our study was performed in three stages. First, we conducted a literature review of stimulation jobs in shale oil reservoirs focusing on the interactions between hydrofractures and discontinuities (bedding planes and natural fractures) and the complexity of hydrofracture geometry. Second, we investigated the effect of different natural fractures and hydrofractures parameters on wellbore flow performance. Third, we evaluated the impact of hydrofracture geometry on reservoir fluid production. The analysis was performed using a commercial reservoir simulator (CMG IMEX).

The main conclusions derived from this study are as follows:

- A single-stage model is a valid simplification to model hydraulically fractured shale oil reservoirs when the analysis includes the stimulated reservoir volume (SRV) concept. This concept assumes uniform hydrofracture distribution along the wellbore and equal hydrofracture properties that result in identical fracture stage behavior. Our results show less than 5% difference between the cumulative hydrocarbon production at 15 years using the single-stage model and the multi-stage model (22 stages). The single-stage model reduces the computational time from an hour to a few minutes in reservoir model construction.
- We attempt to evaluate the effect of natural fracture spacing and orientation on wellbore flow performance. These analyses enable us to select realistic values for our simulation models. The first study evaluated three scenarios with natural fracture spacing of 6 m (20 ft), 9 m (30 ft), and 12 m (40 ft). Our

results show that the reduction of natural fracture spacing enhances reservoir fluid production. It results in more flow conduits per reservoir volume that enhance reservoir permeability. The reduction of fracture spacing by 3 m (10 ft) increases the cumulative water production by 20% and the cumulative hydrocarbon production at 15 years by 4%. Incremental production was observed, especially during the initial stages, before natural fracture closure. Initial hydrocarbon production increases by about 100% when natural fracture spacing varies from 12 m (40 ft) to 6 m (20 ft). The second study evaluated three scenarios with different natural fracture orientation. Our results reveal that natural fractures, oriented parallel to the wellbore, enhance the connectivity between reservoir matrix and hydrofractures. Consequently, they increase the initial hydrocarbon production by 40% compared to the scenario with natural fractures oriented perpendicular to the wellbore.

- We evaluated the closure-mechanism of natural fractures and hydraulic fractures by varying the compaction curves on the simulation model. Our results show that natural fracture closure impacts reservoir fluid production. The cumulative hydrocarbon production at 15 years increases by 15% with the reduction of natural fracture compressibility from 3×10^{-8} Pa^{-1} (2×10^{-4} psi^{-1}) to 1×10^{-9} Pa^{-1} (9×10^{-6} psi^{-1}). In contrast, hydraulic fracture closure-mechanism plays an important role in wellbore flow performance, when hydrofractures are partially propped. The lack of proppant in hydrofracture tips generates a rapid closure and reduces the effective (propped) hydrofracture length. It reduces the initial hydrocarbon production by 20% and the cumulative hydrocarbon production at 15 years by 30% compared to the scenario with fully propped hydrofractures.
- The increase in the number of clusters per stage during stimulation jobs enhances the initial hydrocarbon production, but it may harm the long-term pro-

duction. We studied three scenarios with two, three, and five clusters per stage. Our results reveal that the scenarios with five and three clusters per stage generate an ultimate oil recovery factor at 15 years of 8.5%. The scenario with two clusters per stage produces an ultimate oil recovery factor of 6.1%. In contrast, the initial hydrocarbon production significantly increases with the number of clusters per stage. The initial hydrocarbon production increases by about 70% when the wellbore completion varies from three to five clusters per stage. Currently, operators opt for wellbore completions with a higher number of clusters per stage to produce higher initial hydrocarbon rates. This methodology recovers the initial investment in the first few years of production.

- The interaction between primary hydrofractures and perpendicular natural fractures may initiate and hydraulically open secondary fractures. Our results show that those fractures improve reservoir permeability and contribute to the initial hydrocarbon production when they reach similar primary hydrofracture conductivity. The increase in the number of secondary fractures from 6 to 14 enhances the initial hydrocarbon production by about 13%. The generation of secondary fractures reduces the primary hydrofracture length and aperture. The shortened primary fracture length, combined with the closure of secondary fractures, harms long-term production. Thus, they reduce the cumulative hydrocarbon production at 15 years by about 8% compared to the scenario with only vertical hydrofractures.
- The generation of horizontal fractures reduces the primary hydrofracture length and aperture. This may produce premature proppant screen-out and inefficient proppant placement into primary hydrofractures. The lowered primary fracture conductivity combined with rapid horizontal fracture closure harm wellbore flow performance. Our results show that horizontal fractures reduce cumulative hydrocarbon production at 15 years by about 20% and the initial hydrocarbon

production by 55% compared to the scenario with only vertical hydraulic fractures. This fracture geometry is a particular scenario that may occur in shale plays with high pore pressure and small differential stress. Such conditions often exist in reservoir environments with transitional strike-slip to reverse faulting regime. These conditions favor the interaction between hydrofractures and horizontal bedding planes, which may result in massive stimulation jobs and undesirable reservoir fluid production.

- It is crucial to consider hydrofracture geometry complexity in shale oil reservoir simulation to obtain more realistic hydrocarbon forecasting. The assumption of vertical, symmetrical, and ideal fractures may lead to an overestimation of hydrocarbon production, especially if the modeled formation is characterized by high pore pressure and small differential stress. These conditions enhance the interaction between primary hydrofractures and natural fractures or horizontal bedding planes. Thus, stimulation jobs may create vertical secondary fractures or horizontal fractures. The generation of unpropped horizontal fractures harms hydrocarbon productivity, while secondary fractures may improve initial fluid production.

REFERENCES

[1] K. Liao, S. Zhang, X. Ma, and Z. Yushi, “Numerical Investigation of Fracture Compressibility and Uncertainty on Water-Loss and Production Performance in Tight Oil Reservoirs,” *Energies*, vol. 12, p. 1189, 2019.

[2] Y. Su, L. Ren, F. Meng, C. Xu, and W. Wang, “Theoretical Analysis of the Mechanism of Fracture Network Propagation with Stimulated Reservoir Volume (SRV) Fracturing in Tight Oil Reservoirs,” *PLOS ONE*, vol. 10, no. 5, p. e0125319, 2015. [Online]. Available: https://doi.org/10.1371/journal.pone.0125319

[3] L. Ren, J. Zhao, and Y. Hu, “Hydraulic Fracture Extending into Network in Shale: Reviewing Influence Factors and Their Mechanism,” *TheScientificWorldJournal*, vol. 2014, p. 847107, 2014.

[4] R. D. Barree, M. W. Conway, J. V. Gilbert, and R. A. Woodroof, “Evidence of Strong Fracture Height Containment Based on Complex Shear Failure and Formation Anisotropy,” Florence, Italy, p. 20, 2010. [Online]. Available: https://doi.org/10.2118/134142-MS

[5] T. L. Blanton, “An Experimental Study of Interaction Between Hydraulically Induced and Pre-Existing Fractures,” Pittsburgh, Pennsylvania, p. 13, 1982. [Online]. Available: https://doi.org/10.2118/10847-MS

[6] ——, “Propagation of Hydraulically and Dynamically Induced Fractures in Naturally Fractured Reservoirs,” Louisville, Kentucky, p. 15, 1986. [Online]. Available: https://doi.org/10.2118/15261-MS

[7] J. Zhou, M. Chen, Y. Jin, and Z. Guangqing, “Analysis of fracture propagation behavior and fracture geometry using a tri-axial fracturing system in naturally fractured reservoirs,” *International Journal of Rock Mechanics and Mining Sciences*, vol. 45, pp. 1143–1152, 2008.

[8] Z. Liu, M. Chen, and G. Zhang, “Analysis of the Influence of a Natural Fracture Network on Hydraulic Fracture Propagation in Carbonate Formations,” *Rock Mechanics and Rock Engineering*, vol. 47, no. 2, pp. 575–587, 2014. [Online]. Available: https://doi.org/10.1007/s00603-013-0414-7

[9] J. Zhou, Y. Jin, and M. Chen, “Experimental investigation of hydraulic fracturing in random naturally fractured blocks,” *International Journal of Rock Mechanics and Mining Sciences - INT J ROCK MECH MINING SCI*, vol. 47, pp. 1193–1199, 2010.

[10] L. J. L. Beugelsdijk, C. J. de Pater, and K. Sato, “Experimental Hydraulic Fracture Propagation in a Multi-Fractured Medium,” Yokohama, Japan, p. 8, 2000. [Online]. Available: https://doi.org/10.2118/59419-MS

[11] N. R. Warpinski, “Hydraulic Fracturing in Tight, Fissured Media,” *Journal of Petroleum Technology*, vol. 43, no. 02, pp. 146–209, 1991. [Online]. Available: https://doi.org/10.2118/20154-PA

[12] C. J. de Pater and L. J. L. Beugelsdijk, “Experiments and numerical simulation of hydraulic fracturing in naturally fractured rock,” Anchorage, Alaska, p. 12, 2005. [Online]. Available: https://doi.org/

[13] Z. Yushi, Z. Shicheng, T. Zhou, Z. Xiang, and T. Guo, “Experimental Investigation into Hydraulic Fracture Network Propagation in Gas Shales Using CT Scanning Technology,” *Rock Mechanics and Rock Engineering*, vol. 49, 2015.

[14] C. E. Renshaw and D. D. Pollard, “Are large differential stresses required for straight fracture propagation paths?” *Journal of Structural Geology*, vol. 16, no. 6, pp. 817–822, 1994. [Online]. Available: http://www.sciencedirect.com/science/article/pii/0191814194901473

[15] P. Tan, Y. Jin, K. Han, B. Hou, M. Chen, X. Guo, and J. Gao, “Analysis of hydraulic fracture initiation and vertical propagation behavior in laminated shale formation,” *Fuel*, vol. 206, pp. 482–493, 2017. [Online]. Available: http://www.sciencedirect.com/science/article/pii/S0016236117306026

[16] B. Huang and J. Liu, “Fully three-dimensional propagation model of horizontal borehole hydraulic fractures in strata under the effect of bedding planes,” *Energy Exploration & Exploitation*, vol. 36, no. 5, pp. 1189–1209, 2018. [Online]. Available: https://doi.org/10.1177/0144598717754101

[17] J. Tang, L. Zuo, L. Xiao, K. Wu, B. Qian, C. Yin, C. Ehlig-Economides, and X. You, “A 3-D Hydraulic Fracture Propagation Model Applied for Multiple-Layered Formation,” Beijing, China, p. 20, 2019. [Online]. Available: https://doi.org/10.2523/IPTC-19238-MS

[18] G. Izadi, D. Moos, L. Cruz, M. Gaither, L. Chiaramonte, and S. Johnson, “Fully Coupled 3-D Hydraulic Fracture Growth in the Presence of Weak

Horizontal Interfaces," The Woodlands, Texas, USA, p. 15, 2017. [Online]. Available: https://doi.org/10.2118/184854-MS

[19] B. Hou, R. Zhang, Y. Zeng, W. Fu, Y. Muhadasi, and M. Chen, "Analysis of hydraulic fracture initiation and propagation in deep shale formation with high horizontal stress difference," *Journal of Petroleum Science and Engineering*, vol. 170, pp. 231–243, 2018. [Online]. Available: http://www.sciencedirect.com/science/article/pii/S0920410518305497

[20] Y. Guo, C. Yang, L. Wang, and F. Xu, "Study on the Influence of Bedding Density on Hydraulic Fracturing in Shale," *Arabian Journal for Science and Engineering*, vol. 43, no. 11, pp. 6493–6508, 2018. [Online]. Available: https://doi.org/10.1007/s13369-018-3263-6

[21] A. Alalli and M. Zoback, "Microseismic evidence for horizontal hydraulic fractures in the Marcellus Shale, southeastern West Virginia," *The Leading Edge*, vol. 37, pp. 356–361, 2018.

[22] H. M. Celleri, M. F. Castez, S. Serebrinsky, M. Sánchez, J. P. Álvarez, E. A. Winograd, and M. Vitolo, "Hydraulic Fracture Propagation in Strike-Slip Regime With Weak Interfaces," New York City, New York, p. 9, 2019. [Online]. Available: https://doi.org/

[23] A. K. Nicholson, R. V. Hawkes, and R. C. Bachman, "Close Encounters in the 3rd Dimension: Using Diagnostic Fracture Injection Tests DFITs from the Alberta Duvernay Shale Formation to Quantify Simultaneous Horizontal- & Vertical-Plane Hydraulic Fracture Growth," The Woodlands, Texas, USA, p. 21, 2019. [Online]. Available: https://doi.org/10.2118/194316-MS

[24] W. Saputra, W. Kirati, D. Hughes, and T. Patzek, "Generalized Extreme Value Statistics, Physical Scaling, and Forecasts of Gas Production in Marcellus Shale," *Journal of Natural Gas Science and Engineering*, 2020.

[25] A. Al-Momin, M. Kurdi, S. Baki, K. Mechkak, and A. Al-Saihati, "Proving the Concept of Unconventional Gas Reservoirs in Saudi Arabia Through Multistage Fractured Horizontal Wells," Brisbane, Australia, p. 18, 2015. [Online]. Available: https://doi.org/10.2118/176844-MS

[26] A. Hakami and S. nan, "A basin modeling study of the Jafurah Sub-Basin, Saudi Arabia: Implications for unconventional hydrocarbon potential of the Jurassic Tuwaiq Mountain Formation," *International*

Journal of Coal Geology, vol. 165, pp. 201–222, 2016. [Online]. Available: http://www.sciencedirect.com/science/article/pii/S0166516216303032

[27] B. Abaza, S. Baki, A. Sadykov, K. Mechkak, and J. Rueda, "Determining the Magnitude of Interference Among Adjacent Wells in a Saudi Arabian Unconventoinal Formation," Dhahran, Kingdom of Saudi Arabia, p. 13, 2020. [Online]. Available: https://doi.org/10.2523/IPTC-19711-MS

[28] N. I. Al-Mulhim, M. Korosa, A. Ahmed, A. Hakami, A. Sadykov, S. Baki, K. S. Asiri, and A. Al Ruwaished, "Saudi Arabia's Emerging Unconventional Carbonate Shale Resources: Moving to Horizontals with an Integrated Engineering and Geosciences Approach," Brisbane, Australia, p. 15, 2015. [Online]. Available: https://doi.org/10.2118/176936-MS

[29] M. Ameen, "Borehole Imaging of Natural Fractures and Stress Indicators in the Jurassic Carbonate Shale Plays, Eastern Saudi Arabia. Invited Key Note at the Sixth EAGE Shale Workshop, Bordeaux , France. 28 April, 2019, EAGE Earthdoc," 2019.

[30] K. M. Bartko, I. H. Arnaout, K. S. Asiri, K. M. McClelland, N. I. Mulhim, R. Tineo, M. N. Gurmen, Z. Al-Jalal, D. Pantsurkin, and D. Y. Emelyanov, "From the Backyard Dune to Fracturing a Highly Tectonically Complex Formation in Saudi Arabia," The Woodlands, Texas, USA, p. 18, 2017. [Online]. Available: https://doi.org/10.2118/184823-MS

[31] M. D. Zoback and A. H. Kohli, "Introduction," in *Unconventional Reservoir Geomechanics: Shale Gas, Tight Oil, and Induced Seismicity*. Cambridge: Cambridge University Press, 2019, pp. 3–30. [Online]. Available: https://www.cambridge.org/core/books/unconventional-reservoir-geomechanics/introduction/1948FFCEC74258BAABF71F4D692FC157

[32] Z. Jiang, W. Zhang, C. Liang, Y. Wang, H. Liu, and X. Chen, "Basic characteristics and evaluation of shale oil reservoirs," *Petroleum Research*, vol. 1, no. 2, pp. 149–163, 2016. [Online]. Available: http://www.sciencedirect.com/science/article/pii/S209624951730039X

[33] W. Yu and K. Sepehrnoori, "Chapter 2 - Numerical Model for Shale Gas and Tight Oil Simulation," in *Shale Gas and Tight Oil Reservoir Simulation*, W. Yu and K. Sepehrnoori, Eds. Gulf Professional Publishing, 2018, pp. 11–70. [Online]. Available: http://www.sciencedirect.com/science/article/pii/B978012813868700002X

[34] H. Belyadi, E. Fathi, and F. Belyadi, "Chapter One - Introduction to unconventional reservoirs," in *Hydraulic Fracturing in Unconventional Reservoirs (Second Edition)*, H. Belyadi, E. Fathi, and F. Belyadi, Eds. Gulf Professional Publishing, 2019, pp. 1–12. [Online]. Available: http://www.sciencedirect.com/science/article/pii/B9780128176658000011

[35] H. Wang, "What Factors Control Shale-Gas Production and Production-Decline Trend in Fractured Systems: A Comprehensive Analysis and Investigation," *SPE Journal*, vol. 22, no. 02, pp. 562–581, 2017. [Online]. Available: https://doi.org/10.2118/179967-PA

[36] J. Gale, R. Reed, and J. Holder, "Natural fractures in the Barnett Shale and their importance for hydraulic fracture treatments," *Aapg Bulletin - AAPG BULL*, vol. 91, pp. 603–622, 2007.

[37] M. D. Zoback and A. H. Kohli, "Composition, Fabric, Elastic Properties and Anisotropy," in *Unconventional Reservoir Geomechanics: Shale Gas, Tight Oil, and Induced Seismicity*. Cambridge: Cambridge University Press, 2019, pp. 31–64. [Online]. Available: https://www.cambridge.org/core/books/unconventional-reservoir-geomechanics/composition-fabric-elastic-properties-and-anisotropy/3F31D61FF00934F608B84F5301853E9E

[38] K. Smye, H. Hamlin, R. Eastwood, and G. McDaid, "Variability of Geologic Properties of Shale Gas and Tight Oil Plays," *Gulf Coast Association of Geological Societies*, vol. 8, pp. 191–209, 2019.

[39] M. D. Zoback and A. H. Kohli, "Pore Networks and Pore Fluids," in *Unconventional Reservoir Geomechanics: Shale Gas, Tight Oil, and Induced Seismicity*. Cambridge: Cambridge University Press, 2019, pp. 115–148. [Online]. Available: https://www.cambridge.org/core/books/unconventional-reservoir-geomechanics/pore-networks-and-pore-fluids/793F9AB24303C092E4A594DAA9F625C1

[40] Y. Zhang, D. Shao, J. Yan, X. Jia, Y. Li, P. Yu, and T. Zhang, "The pore size distribution and its relationship with shale gas capacity in organic-rich mudstone of Wufeng-Longmaxi Formations, Sichuan Basin, China," *Journal of Natural Gas Geoscience*, vol. 1, no. 3, pp. 213–220, 2016. [Online]. Available: http://www.sciencedirect.com/science/article/pii/S2468256X16300438

[41] M. Dernaika, O. Al Jallad, S. Koronfol, M. Suhrer, W. J. Teh, J. Walls, S. Matar, N. Murthy, and M. Zekraoui, "Petrophysical and Fluid Flow Properties of a Tight Carbonate Source Rock Using Digital Rock Physics," San Antonio, Texas, USA, p. 18, 2015. [Online]. Available: https://doi.org/10.15530/URTEC-2015-2154815

[42] A. S. Chaudhary, C. A. Ehlig-Economides, and R. A. Wattenbarger, "Shale Oil Production Performance from a Stimulated Reservoir Volume," Denver, Colorado, USA, p. 21, 2011. [Online]. Available: https://doi.org/10.2118/147596-MS

[43] M. D. Zoback and A. H. Kohli, "Horizontal Drilling and Multi-Stage Hydraulic Fracturing," in *Unconventional Reservoir Geomechanics: Shale Gas, Tight Oil, and Induced Seismicity*. Cambridge: Cambridge University Press, 2019, pp. 233–262. [Online]. Available: https://www.cambridge.org/core/books/unconventional-reservoir-geomechanics/horizontal-drilling-and-multistage-hydraulic-fracturing/578E4B6ED34ABBB10DA8FF52A3075EE6

[44] H. Belyadi, E. Fathi, and F. Belyadi, "Chapter Eleven - Horizontal well multistage completion techniques," in *Hydraulic Fracturing in Unconventional Reservoirs (Second Edition)*, H. Belyadi, E. Fathi, and F. Belyadi, Eds. Gulf Professional Publishing, 2019, pp. 177–189. [Online]. Available: http://www.sciencedirect.com/science/article/pii/B9780128176658000114

[45] B. Guo, X. Liu, and X. Tan, "Chapter 14 - Hydraulic Fracturing," in *Petroleum Production Engineering (Second Edition)*, B. Guo, X. Liu, and X. Tan, Eds. Boston: Gulf Professional Publishing, 2017, pp. 389–501. [Online]. Available: http://www.sciencedirect.com/science/article/pii/B9780128093740000143

[46] H. Belyadi, E. Fathi, and F. Belyadi, "Chapter Five - Hydraulic fracturing fluid systems," in *Hydraulic Fracturing in Unconventional Reservoirs (Second Edition)*, H. Belyadi, E. Fathi, and F. Belyadi, Eds. Gulf Professional Publishing, 2019, pp. 47–69. [Online]. Available: http://www.sciencedirect.com/science/article/pii/B9780128176658000059

[47] J. G. Speight, "Shale Oil and Gas Production Processes," in *Shale Oil and Gas Production Processes*, J. Speight, Ed. United States: Gulf Professional Publishing, 2020, pp. xi–xiii. [Online]. Available: http://www.sciencedirect.com/science/article/pii/B9780128133156050016

[48] L. K. Britt, "Keys to successful multi-fractured horizontal wells in tight and unconventional reservoirs," Tech. Rep., 2011.

[49] M. Soliman, L. East, and J. Augustine, "Fracturing design aimed at enhancing fracture complexity," 06 2010.

[50] T. Patzek, F. Male, and M. Marder, "A simple model of gas production from hydrofractured horizontal wells in shales," *AAPG Bulletin*, vol. 98, pp. 2507–2529, 2014.

[51] H. Belyadi, E. Fathi, and F. Belyadi, "Chapter Six - Proppant Characteristics and Application Design," in *Hydraulic Fracturing in Unconventional Reservoirs*, H. Belyadi, E. Fathi, and F. Belyadi, Eds. Boston: Gulf Professional Publishing, 2017, pp. 73–96. [Online]. Available: http://www.sciencedirect.com/science/article/pii/B978012849871200006X

[52] F. Liang, M. Sayed, G. A. Al-Muntasheri, F. F. Chang, and L. Li, "A comprehensive review on proppant technologies," *Petroleum*, vol. 2, no. 1, pp. 26–39, 2016. [Online]. Available: http://www.sciencedirect.com/science/article/pii/S2405656115000693

[53] H. Li, Y. Zou, P. P. Valko, and C. Ehlig-Economides, "Hydraulic Fracture Height Predictions in Laminated Shale Formations Using Finite Element Discrete Element Method," The Woodlands, Texas, USA, p. 17, 2016. [Online]. Available: https://doi.org/10.2118/179129-MS

[54] R. Jeffrey, X. Zhang, and Z. Chen, "Hydraulic fracture growth in naturally fractured rock," 2017, pp. 93–116.

[55] C. E. Renshaw and D. D. Pollard, "An experimentally verified criterion for propagation across unbounded frictional interfaces in brittle, linear elastic materials," *International Journal of Rock Mechanics and Mining Sciences & Geomechanics Abstracts*, vol. 32, no. 3, pp. 237–249, 1995. [Online]. Available: http://www.sciencedirect.com/science/article/pii/0148906294000374

[56] L. W. Teufel and J. A. Clark, "Hydraulic Fracture Propagation in Layered Rock: Experimental Studies of Fracture Containment," *Society of Petroleum Engineers Journal*, vol. 24, no. 01, pp. 19–32, 1984. [Online]. Available: https://doi.org/10.2118/9878-PA

[57] X. Zhang, R. G. Jeffrey, and M. Thiercelin, "Deflection and propagation of fluid-driven fractures at frictional bedding interfaces: A numerical investigation," *Journal of Structural Geology*, vol. 29, no. 3, pp. 396–410,

2007. [Online]. Available: http://www.sciencedirect.com/science/article/pii/S0191814106002185

[58] X. Weng, O. Kresse, C. E. Cohen, R. Wu, and H. Gu, "Modeling of Hydraulic Fracture Network Propagation in a Naturally Fractured Formation," The Woodlands, Texas, USA, p. 18, 2011. [Online]. Available: https://doi.org/10.2118/140253-MS

[59] T. Gong, B. Xia, L. Liu, Z. Peng, and Y. Gao, "Propagation of hydraulic fracture under the joint impact of bedding planes and natural fractures in shale reservoirs," *Energy Science & Engineering*, vol. 7, 2019.

[60] A. Gudmundsson and S. Brenner, "How hydrofractures become arrested," *Terra Nova*, vol. 13, pp. 456–462, 2002.

[61] N. R. Warpinski, M. J. Mayerhofer, M. C. Vincent, C. L. Cipolla, and E. P. Lolon, "Stimulating Unconventional Reservoirs: Maximizing Network Growth While Optimizing Fracture Conductivity," *Journal of Canadian Petroleum Technology*, vol. 48, no. 10, pp. 39–51, 2009. [Online]. Available: https://doi.org/10.2118/114173-PA

[62] P. Tan, Y. Jin, Y. Zhou, B. Hou, R. Zhang, Z. Chang, and M. Fan, "Laboratory investigation of shale rock to identify fracture propagation in vertical direction to bedding," *Journal of Geophysics and Engineering*, vol. 15, 2018.

[63] J. Tang, K. Wu, B. Zeng, H. Huang, X. Hu, X. Guo, and L. Zuo, "Investigate effects of weak bedding interfaces on fracture geometry in unconventional reservoirs," *Journal of Petroleum Science and Engineering*, vol. 165, pp. 992–1009, 2018. [Online]. Available: http://www.sciencedirect.com/science/article/pii/S0920410517309269

[64] M. Lin, S. Chen, W. Ding, Z. Chen, and J. Xu, "Effect of Fracture Geometry on Well Production in Hydraulic-Fractured Tight Oil Reservoirs," *Journal of Canadian Petroleum Technology*, vol. 54, no. 03, pp. 183–194, 2015. [Online]. Available: https://doi.org/10.2118/167761-PA

[65] R. Yuan, L. Jin, C. Zhu, M. Zhou, and S. Vitthal, "Vertical or Horizontal? Hydraulic Fracture Geometry as a Make or Break to a Tight Gas Field in the Western Sichuan Basin," Beijing, China, p. 15, 2013. [Online]. Available: https://doi.org/10.2523/IPTC-16757-MS

[66] S. C. Maxwell, U. Zimmer, R. W. Gusek, and D. J. Quirk, "Evidence of a Horizontal Hydraulic Fracture From Stress Rotations Across a Thrust Fault,"

SPE Production & Operations, vol. 24, no. 02, pp. 312–319, 2009. [Online]. Available: https://doi.org/10.2118/110696-PA

[67] B. Abell, P. Xing, A. Bunger, E. Dontsov, and R. Suarez-Rivera, "Laboratory Investigation of Leak-Off During Hydraulic Fracturing into Bedding Interfaces," Denver, Colorado, USA, p. 17, 2019. [Online]. Available: https://doi.org/10.15530/urtec-2019-900

[68] M. M. Rahman, M. A. Aghighi, S. S. Rahman, and S. A. Ravoof, "Interaction Between Induced Hydraulic Fracture and Pre-Existing Natural Fracture in a Poro-Elastic Environment: Effect of Pore Pressure Change and the Orientation of Natural Fractures," Jakarta, Indonesia, p. 8, 2009. [Online]. Available: https://doi.org/10.2118/122574-MS

[69] H. Lee, J. Olson, J. Holder, J. Gale, and R. Myers, "The interaction of propagating opening mode fractures with preexisting discontinuities in shale: SHALE VEIN-FRACTURE INTERACTION," *Journal of Geophysical Research: Solid Earth*, vol. 120, 2014.

[70] G. Izadi, R. Guises, C. Barton, S. Randazzo, S. Mahrooqi, M. Shaibani, and A. Dobroskok, "Advanced Integrated Subsurface 3D Reservoir Model for Multistage Full-Physics Hydraulic Fracturing Simulation," Dhahran, Kingdom of Saudi Arabia, p. 13, 2020. [Online]. Available: https://doi.org/10.2523/IPTC-20064-Abstract

[71] Y. Zou, S. Zhang, X. Ma, T. Zhou, and B. Zeng, "Numerical investigation of hydraulic fracture network propagation in naturally fractured shale formations," *Journal of Structural Geology*, vol. 84, pp. 1–13, 2016. [Online]. Available: http://www.sciencedirect.com/science/article/pii/S0191814116300049

[72] M. L. Cooke and C. A. Underwood, "Fracture termination and step-over at bedding interfaces due to frictional slip and interface opening," *Journal of Structural Geology*, vol. 23, no. 2, pp. 223–238, 2001. [Online]. Available: http://www.sciencedirect.com/science/article/pii/S0191814100000924

[73] H. Gu, E. Siebrits, and A. Sabourov, "Hydraulic Fracture Modeling With Bedding Plane Interfacial Slip," Pittsburgh, Pennsylvania, USA, p. 8, 2008. [Online]. Available: https://doi.org/10.2118/117445-MS

[74] J. Wang, Y. Guo, K. Zhang, G. Ren, and J. Ni, "Experimental Investigation on Hydraulic Fractures in the Layered Shale Formation," *Geofluids*, vol. 2019, pp. 1–14, 2019.

[75] B. Huang and J. Liu, "Experimental Investigation of the Effect of Bedding Planes on Hydraulic Fracturing Under True Triaxial Stress," *Rock Mechanics and Rock Engineering*, vol. 50, no. 10, pp. 2627–2643, 2017. [Online]. Available: https://doi.org/10.1007/s00603-017-1261-8

[76] S. Jalili and K. Ahangari, "Effects of different stress regimes on hydraulic fracture geometry: a particle flow code approach," *Innovative Infrastructure Solutions*, vol. 2, 2017.

[77] S.-C. Zhang, X. Lei, Y.-S. Zhou, and G.-Q. Xu, "Numerical simulation of hydraulic fracture propagation in tight oil reservoirs by volumetric fracturing," *Petroleum Science*, vol. 12, no. 4, pp. 674–682, 2015. [Online]. Available: https://doi.org/10.1007/s12182-015-0055-4

[78] C. Meng and H. J. De Pater, "Hydraulic Fracture Propagation in Pre-Fractured Natural Rocks," The Woodlands, Texas, USA, p. 16, 2011. [Online]. Available: https://doi.org/10.2118/140429-MS

[79] T. Chun, Z. Zhang, S. Mao, and K. Wu, "Experimental Study of Proppant Transport in Complex Fractures with Horizontal Bedding Planes for Slickwater Fracturing," Denver, Colorado, USA, p. 19, 2019. [Online]. Available: https://doi.org/10.15530/urtec-2019-547

[80] J. Speight, *Handbook of Hydraulic Fracturing.* Wiley, 2016. [Online]. Available: https://books.google.com.sa/books?id=g4rACwAAQBAJ

[81] T. Guo, S. Zhang, Y. Zou, and B. Xiao, "Numerical simulation of hydraulic fracture propagation in shale gas reservoir," *Journal of Natural Gas Science and Engineering*, vol. 26, pp. 847–856, 2015. [Online]. Available: http://www.sciencedirect.com/science/article/pii/S1875510015300457

[82] T. N. Olsen, T. R. Bratton, and M. J. Thiercelin, "Quantifying Proppant Transport for Complex Fractures in Unconventional Formations," The Woodlands, Texas, p. 12, 2009. [Online]. Available: https://doi.org/10.2118/119300-MS

[83] R. Sahai and R. G. Moghanloo, "Proppant transport in complex fracture networks A review," *Journal of Petroleum Science and Engineering*, vol. 182, p. 106199, 2019. [Online]. Available: http://www.sciencedirect.com/science/article/pii/S0920410519306114

[84] R. Sahai, J. L. Miskimins, and K. E. Olson, "Laboratory Results of Proppant Transport in Complex Fracture Systems," The Woodlands, Texas, USA, p. 26, 2014. [Online]. Available: https://doi.org/10.2118/168579-MS

[85] M. A. Alotaibi and J. L. Miskimins, "Slickwater Proppant Transport in Complex Fractures: New Experimental Findings & Scalable Correlation," Houston, Texas, USA, p. 26, 2015. [Online]. Available: https://doi.org/10.2118/174828-MS

[86] C. L. Cipolla, E. Lolon, M. J. Mayerhofer, and N. R. Warpinski, "The Effect of Proppant Distribution and Un-Propped Fracture Conductivity on Well Performance in Unconventional Gas Reservoirs," The Woodlands, Texas, p. 10, 2009. [Online]. Available: https://doi.org/10.2118/119368-MS

[87] R. Keshavarzi, S. Mohammadi, and H. Bayesteh, "Hydraulic Fracture Propagation In Unconventional Reservoirs: The Role of Natural Fractures," Chicago, Illinois, p. 8, 2012. [Online]. Available: https://doi.org/

[88] C. L. Cipolla, N. R. Warpinski, M. J. Mayerhofer, E. Lolon, and M. C. Vincent, "The Relationship Between Fracture Complexity, Reservoir Properties, and Fracture Treatment Design," Denver, Colorado, USA, p. 25, 2008. [Online]. Available: https://doi.org/10.2118/115769-MS

[89] M. M. Sharma and R. Manchanda, "The Role of Induced Un-propped (IU) Fractures in Unconventional Oil and Gas Wells," Houston, Texas, USA, p. 14, 2015. [Online]. Available: https://doi.org/10.2118/174946-MS

[90] A. Moinfar, W. Narr, M.-H. Hui, B. T. Mallison, and S. H. Lee, "Comparison of Discrete-Fracture and Dual-Permeability Models for Multiphase Flow in Naturally Fractured Reservoirs," The Woodlands, Texas, USA, p. 17, 2011. [Online]. Available: https://doi.org/10.2118/142295-MS

[91] H. Kazemi, L. S. Merrill Jr., K. L. Porterfield, and P. R. Zeman, "Numerical Simulation of Water-Oil Flow in Naturally Fractured Reservoirs," *Society of Petroleum Engineers Journal*, vol. 16, no. 06, pp. 317–326, 1976. [Online]. Available: https://doi.org/10.2118/5719-PA

[92] J. E. Warren and P. J. Root, "The Behavior of Naturally Fractured Reservoirs," *Society of Petroleum Engineers Journal*, vol. 3, no. 03, pp. 245–255, 1963. [Online]. Available: https://doi.org/10.2118/426-PA

[93] B. Rubin, "Accurate Simulation of Non Darcy Flow in Stimulated Fractured Shale Reservoirs," Anaheim, California, USA, p. 16, 2010. [Online]. Available: https://doi.org/10.2118/132093-MS

[94] Y.-l. Zhao, L.-f. Liu, L.-h. Zhang, X.-Y. Zhang, and B. Li, "Simulation of a multistage fractured horizontal well in a tight oil reservoir using an embedded discrete fracture model," *Energy Science & Engineering*, vol. 7, no. 5, pp. 1485–1503, 2019. [Online]. Available: https://doi.org/10.1002/ese3.379

[95] F. T. Blaskovich, G. M. Cain, F. Sonier, D. Waldren, and S. J. Webb, "A Multicomponent Isothermal System for Efficient Reservoir Simulation," Manama, Bahrain, p. 18, 1983. [Online]. Available: https://doi.org/10.2118/11480-MS

[96] CMG, "IMEX User's guide. Three-phase, Black-oil Reservoir Simulator," 2016.

[97] A. C. Hill and G. W. Thomas, "A New Approach for Simulating Complex Fractured Reservoirs," Bahrain, p. 12, 1985. [Online]. Available: https://doi.org/10.2118/13537-MS

[98] N. Kasiri and A. Bashiri, "Status of Dual-Continuum Models for Naturally Fractured Reservoir Simulation," *Petroleum Science and Technology*, vol. 29, pp. 1236–1248, 2011.

[99] J. M. DeGraff, M. E. Meurer, L. H. Landis, and S. L. Lyons, "Fracture Network Modeling and Dual-Permeability Simulation of Carbonate Reservoirs," Doha, Qatar, p. 7, 2005. [Online]. Available: https://doi.org/10.2523/IPTC-10954-MS

[100] H. Hoteit and A. Firoozabadi, "Compositional Modeling of Discrete-Fractured Media Without Transfer Functions by the Discontinuous Galerkin and Mixed Methods," *SPE Journal*, vol. 11, no. 03, pp. 341–352, 2006. [Online]. Available: https://doi.org/10.2118/90277-PA

[101] I. Berre, F. Doster, and E. Keilegavlen, *Flow in fractured porous media: A review of conceptual models and discretization approaches*, 2018.

[102] S. D. Mohaghegh, "Reservoir modeling of shale formations," *Journal of Natural Gas Science and Engineering*, vol. 12, pp. 22–33, 2013. [Online]. Available: http://www.sciencedirect.com/science/article/pii/S1875510013000048

[103] U. Aybar, W. Yu, M. O. Eshkalak, K. Sepehrnoori, and T. Patzek, "Evaluation of production losses from unconventional shale reservoirs," *Journal of Natural Gas Science and Engineering*, vol. 23, pp. 509 – 516, 2015. [Online]. Available: http://www.sciencedirect.com/science/article/pii/S1875510015000888

[104] T. W. Patzek, W. Saputra, and W. Kirati, "A Simple Physics-Based Model Predicts Oil Production from Thousands of Horizontal Wells in Shales," San Antonio, Texas, USA, p. 26, 2017. [Online]. Available: https://doi.org/10.2118/187226-MS

[105] W. Saputra, W. Kirati, and T. Patzek, "Generalized Extreme Value Statistics, Physical Scaling and Forecasts of Oil Production in the Bakken Shale," *Energies*, vol. 12 no.19, p. 3641, 2019. [Online]. Available: https://doi.org/10.3390/en12193641

[106] T. Tran, P. D. Sinurat, and B. A. Wattenbarger, "Production Characteristics of the Bakken Shale Oil," Denver, Colorado, USA, p. 14, 2011. [Online]. Available: https://doi.org/10.2118/145684-MS

[107] A. Ivanova, N. Mitiurev, A. Cheremisin, A. Orekhov, R. Kamyshinsky, and A. Vasiliev, "Characterization of Organic Layer in Oil Carbonate Reservoir Rocks and its Effect on Microscale Wetting Properties," *Scientific Reports*, vol. 9, no. 1, p. 10667, 2019. [Online]. Available: https://doi.org/10.1038/s41598-019-47139-y

[108] S. P. Ojha, S. Misra, A. Sinha, S. Dang, A. Tinni, C. Sondergeld, and C. Rai, "Relative Permeability and Residual Saturation Estimates for Organic-Rich Shale Samples From Bakken, Wolfcamp, Eagle Ford and Woodford Formations," San Antonio, Texas, USA, p. 17, 2017. [Online]. Available: https://doi.org/10.2118/187398-MS

[109] R. Velasco, P. Panja, and M. Deo, "Simplification workflow for hydraulically fractured reservoirs," *Petroleum*, vol. 4, no. 2, pp. 134–147, 2018. [Online]. Available: http://www.sciencedirect.com/science/article/pii/S240565611730072X

[110] K. Terzaghi, "Theoretical Soil Mechanics," 2007, pp. i–xvii.

[111] W. Xiao, T. Li, M. Li, J. Zhao, L. Zheng, and L. Li, "Evaluation of the stress sensitivity in tight reservoirs," *Petroleum Exploration and Development*, vol. 43, no. 1, pp. 115–123, 2016. [Online]. Available: http://www.sciencedirect.com/science/article/pii/S1876380416300131

[112] H. Dou, H. Zhang, S. Yao, D. Zhu, T. Sun, S. Ma, and X. Wang, "Measurement and evaluation of the stress sensitivity in tight reservoirs," *Petroleum Exploration and Development*, vol. 43, no. 6, pp. 1116–1123, 2016. [Online]. Available: http://www.sciencedirect.com/science/article/pii/S1876380416301306

[113] M. Mokhtari, A. A. Alqahtani, A. N. Tutuncu, and X. Yin, “Stress-Dependent Permeability Anisotropy and Wettability of Shale Resources,” Denver, Colorado, USA, p. 16, 2013. [Online]. Available: https://doi.org/10.1190/urtec2013-283

[114] B. J. Huan Wang, L. Z. Chengyuan Lv, C. C. Xiaofeng Li, and J. N. Hongmin Yu, “The stress sensitivity of permeability in tight oil reservoirs,” *Energy Exploration & Exploitation*, vol. 37, no. 4, pp. 1364–1376, 2019. [Online]. Available: https://doi.org/10.1177/0144598719855819

[115] R. Aguilera, “Effect of Fracture Compressibility on Gas-in-Place Calculations of Stress-Sensitive Naturally Fractured Reservoirs,” Calgary, Alberta, Canada, p. 5, 2006. [Online]. Available: https://doi.org/10.2118/100451-MS

[116] J. Zhou and C. Xue, “Experimental Investigation of Fracture Interaction between Natural Fractures and Hydraulic Fracture in Naturally Fractured Reservoirs,” Vienna, Austria, p. 12, 2011. [Online]. Available: https://doi.org/10.2118/142890-MS

[117] Y. Cho, O. G. Apaydin, and E. Ozkan, “Pressure-Dependent Natural-Fracture Permeability in Shale and its Effect on Shale-Gas Well Production,” San Antonio, Texas, USA, p. 18, 2012. [Online]. Available: https://doi.org/10.2118/159801-MS

[118] R. Aguilera, “Recovery Factors And Reserves In Naturally Fractured Reservoirs,” *Journal of Canadian Petroleum Technology*, vol. 38, no. 07, p. 4, 1999. [Online]. Available: https://doi.org/10.2118/99-07-DA

[119] Y. Tan, Z. Pan, X.-T. Feng, D. Zhang, L. D. Connell, and S. Li, “Laboratory characterisation of fracture compressibility for coal and shale gas reservoir rocks: A review,” *International Journal of Coal Geology*, vol. 204, pp. 1–17, 2019. [Online]. Available: http://www.sciencedirect.com/science/article/pii/S0166516218308863

[120] M. J. Kaiser, “Haynesville shale play economic analysis,” *Journal of Petroleum Science and Engineering*, vol. 82-83, pp. 75–89, 2012. [Online]. Available: http://www.sciencedirect.com/science/article/pii/S0920410512000034

[121] EIA, “Trends in U.S. Oil and Natural Gas Upstream Costs,” 2016.

[122] R. Weijermars, N. Sorek, D. Sen, and W. B. Ayers, “Eagle Ford Shale play economics: U.S. versus Mexico,” *Journal of Natural Gas*

Science and Engineering, vol. 38, pp. 345–372, 2017. [Online]. Available: http://www.sciencedirect.com/science/article/pii/S187551001630909X

[123] J. Browning, S. Ikonnikova, G. Gülen, and S. Tinker, "Barnett Shale Production Outlook," *SPE Economics & Management*, vol. 5, no. 03, pp. 89–104, 2013. [Online]. Available: https://doi.org/10.2118/165585-PA

[124] Q. Darugar, D. Heinisch, B. J. Lundy, P. Witte, W. Wu, and S. Zhou, "Estimating Ultimate Recovery and Economic Analysis of Shale Oil Wells in Eagle Ford and Bakken," Abu Dhabi, UAE, p. 18, 2016. [Online]. Available: https://doi.org/10.2118/183396-MS

[125] S. Haider, W. Saputra, and T. Patzek, "The key factors that determine the economically viable, horizontal hydrofractured gas wells in mudrocks," 2020. [Online]. Available: http://hdl.handle.net/10754/662819

[126] M. Zoback and A. Kohli, "Stress, Pore Pressure, Fractures and Faults," in *Unconventional Reservoir Geomechanics: Shale Gas, Tight Oil, and Induced Seismicity.* Cambridge: Cambridge University Press, 2019, pp. 181–230.

[127] W. Saputra, W. Kirati, and T. Patzek, "Generalized extreme value statistics, physical scaling and forecasts of gas production in the Haynesville shale," 2020.

APPENDICES

A Appendix A Economic model

In order to calculate the net present value (NPV), it is necessary to calculate the net cash flow, which reproduces the cash flows in the project over the life time. Then, the net cash flow is the earnings minus the cost of the project. The net cash flow (NCF) in the year-x is calculated by the following equation [120]:

$$\mathrm{NCF_x} = \mathrm{GR_x} - \mathrm{CAPEX_x} - \mathrm{OPEX_x} - \mathrm{ROY_x} - \mathrm{TAX_x} \tag{A.1}$$

Where,

- $\mathrm{GR_x}$, Gross revenue in year-x, [$ Million].
- $\mathrm{CAPEX_x}$, Capital expenditures in year-x, [$ Million].
- $\mathrm{OPEX_x}$, Operating expenditure in year-x, [$ Million].
- $\mathrm{ROY_x}$, Royalty in year-x, [$ Million].
- $\mathrm{TAX_x}$, Taxation in year-x, [$ Million].

The Gross revenue (GR) is the multiplication of the average oil price by the annual oil production rate [120, 127].

$$\mathrm{GR_x} = \mathrm{P_x} \times \mathrm{Q_x} \tag{A.2}$$

Where,

- $\mathrm{P_x}$, Oil price in year-x, [$/bbl].
- $\mathrm{Q_x}$, net production in year- x, [bbls/year].

The capital expenditure (CAPEX) is the total investment made during the first year to do the project. Then, the CAPEX comprises mainly the drilling cost, completion cost and the land cost. Additionally, the operating expenditure (OPEX) are the expenses related to the operations in the field. Then, it comprises the surface facilities, the type of wellbores, the reservoir fluids storage, the water disposal and other services required in the well [120]. Then, the operating expenditure can be calculate by the following equation [120, 127]:

$$\mathrm{OPEX_x} = \mathrm{OPECOST} \times \mathrm{Q_x} \tag{A.3}$$

Where,

– OPECOST, operating cost, [$/Mbbl].

The royalty is the cost per unit of production. Then, it is calculated by multiplying the royalty rate (R) by the gross revenue (GR) [120].

$$\mathrm{ROY_x} = \mathrm{R} \times \mathrm{GR_x} \tag{A.4}$$

Where,

– R, royalty rate, [fraction/year]. This rate is the company ownership of a part of the hydrocarbon produced.

The taxation (TAX) is the money paid to the government. This can be calculated by the difference between the net revenue (NR) and the operating expenditure. The equation to calculate the taxation is [120, 127]:

$$\mathrm{TAX_x} = \mathrm{CORPTAX}(\mathrm{GR_x} - \mathrm{ROY_x} - \mathrm{OPEX_x} - \mathrm{INTANEX_x} - \mathrm{DEP_x}) \times \mathrm{SEVTAX}(\mathrm{Q_x} \times \mathrm{P_x}) \tag{A.5}$$

Where,

– CORPTAX, federal or corporate tax, [fraction/year]. The corporate tax is the tax paid to the Internal Revenue Service (IRS).

– SEVTAX, severance or production, [fraction/year]. This value is the percentage of the market value of oil produced that is taken by the state.

– $\mathrm{INTANEX_x}$, intangible capital expenditures in year x, [$ Million].

– $\mathrm{DEP_x}$, depreciation in year x, [$ Million].

The intangible capital expenditures ($\mathrm{INTANEX_x}$) or intangible drilling cost can be calculated by the following equation [120]:

$$\mathrm{INTANEX_x} = \mathrm{INTAN} \times \mathrm{CAPEX_0} \left(\frac{\mathrm{Q_x}}{\sum_{\mathrm{i=0}}^{\mathrm{Total\ years}} \mathrm{Q_x}} \right) \tag{A.6}$$

The depreciation, depletion and amortization ($\mathrm{DEP_x}$) is the cost of the tangible evaluation over the useful life. It is calculated by the following equation [127]:

$$\mathrm{DEP_x} = \frac{\mathrm{DB}}{\mathrm{t}} \times \left[(1 - \mathrm{INTAN}) \times \mathrm{CAPEX_0} \sum_{\mathrm{i=0}}^{\mathrm{x-1}} \mathrm{DEP_x} \right] \tag{A.7}$$

Where,

– DB, declining balance. This is the percentage assigned to tangible expenditures.

– t, time period in which the equipment is amortized [120].

Finally, the present value (PV) is calculated by the following equation [120]:

$$\mathrm{PV_x} = \frac{\mathrm{NCF_x}}{(1 + \mathrm{DR})^{\mathrm{x}}} \tag{A.8}$$

Where,

– DR, discount rate, [fraction/year].

Then, the net present value is the summation of all the present value calculated by the total years of production [120]:

$$\mathrm{NPV} = \sum_{\mathrm{i=0}}^{\mathrm{Total\ years}} \mathrm{PV_x} \tag{A.9}$$